Synthesis, characterization and evaluation of Ru(II) and Co(II) complexes of some nitrogen chelating ligands as sensitizers for dye sensitized solar cells (DSSCs)

MOTAUNG Mathato Petronella

Department of Chemistry

Faculty of Science and Agriculture

University of Fort Hare

Together in Excellence

January 2015

Synthesis, characterization and evaluation of Ru(II) and Co(II) complexes of some nitrogen chelating ligands as sensitizers for dye sensitized solar cells (DSSCs)

By

MOTAUNG Mathato Petronella (201109105)
B. Sc., B. Sc. (Honours) Chemistry (UFH)

Being a dissertation submitted to the Faculty of Science and Agriculture **in fulfilment of the requirements for the award of the degree of**

Master of Science in chemistry

of the

University of Fort Hare,

Supervisor: Professor P. A. Ajibade

January 2015

DECLARATION BY CANDIDATE

"I hereby declare that this dissertation submitted for MSc degree in Chemistry, at the University of Fort Hare, is my own original work and has not been previously submitted to any other institution of higher learning. I further declare that all sources cited or quoted are indicated and acknowledged by means of a comprehensive list of references".

_____ _____

Date M. P. Motaung

CERTIFICATION

This is to certify that this research is a record of original work carried out by Motaung Mathato Petronella under my supervision in the Inorganic Materials Research laboratory of the Department of Chemistry, University of Fort Hare in fulfilment of the requirements for the award of Master of Science degree in Chemistry.

_____ _____

Date Supervisor

P. A. Ajibade
Professor of Inorganic Materials Chemistry
B.Sc (Hons), MSc (Ibadan);
PhD (UniZul); MRSC (London)

DEDICATION

This work is dedicated to my family for their support and encouragement

ACKNOWLEDGEMENT

I would like to thank God Almighty, the giver of life, because without Him, all this would be impossible. I wish to thank my supervisor, Professor P. A. Ajibade, for his guidance and support during the course of this research. I thank members of my family especially my mother and friends for their support, love and encouragement. I would also like to thank Inorganic Materials Research Group and my laboratory colleagues for their assistance in this project.

I take this opportunity to thank, Mr. T. Mcako for the technical assistance provided with FTIR, UV-Vis and PL spectroscopy. Mr. M. Manamela and Dr Siswana at WSU for giving me the opportunity to conduct analysis on electrochemistry and for their assistance during the experiment. I acknowledge the Department of Chemistry, University of Fort Hare for facilities. National Research Foundation (NRF) and Sasol Inzalo Foundation for their funding.

ABSTRACT

The demand for fossil fuels has resulted in decrease in natural resources and created negative impacts on the environment. These negative impacts require the development of alternative sources of energy that are environmentally friendly. Dye sensitized solar cells (DSSCs) is a new class of renewable source of clean energy that is environmentally friendly with relatively low-cost. DSSC is one of the most promising solar cell devices with incident to power conversion efficiency of up to 13%. The highest efficiency of DSSC has been obtained by using a sintered TiO_2 semiconductor with Zn based porphyrin dye (**SM315**) as sensitizers.

Five nitrogen chelating ligands containing 2,6-bis-(benzimidazolyl)pyridine (**L_1**), 2,6-bis-(butylbenzimidazolyl)pyridine (**L_2**), 2,6-bis-(benzylbenzimidazolyl)pyridine (**L_3**), 2,6-bis-(pyrazolyl)pyridine (**L_4**), 2,6-bis-(3,5-dimethylpyrazolyl)pyridine (**L_5**), and their corresponding ruthenium(II) and cobalt(II) complexes have been synthesized and characterized by elemental analysis, conductivity measurements, melting point, FTIR and NMR spectroscopy. The photophysical and electrochemical studies of the metal complexes were carried out by UV-Vis, photoluminescence and cyclic voltammetry.

The FTIR spectroscopic studies confirmed the coordination of the ligands to the Ru(II) and Co(II) metal ions. The results of the electronic spectra studies show that the complexes are coordinated to the ligands in six coordinate octahedral geometry and the

complexes exhibited some photoluminescence properties of suitable for application in dye sensitizers. The cyclic voltammogram of complexes containing 2,6-bis-(benzimidazolyl)pyridine have more reduction potentials which could be ascribed to the increased π conjugation in the ligands used for the synthesis of the complexes. The solar cell efficiencies of the complexes was calculated from the I-V curves of fabricated solar cells. The solar cell fabricated from complex **C_5** (ruthenium complex of 2,6-bis-(3,5-dimethylpyrazolyl)pyridine) on TiO_2 semiconductor produced the highest open-circuit photovoltage of 87.3×10^{-3} mV, short-circuit photocurrent of 0.022 mA/cm^{-2} and the solar conversion efficiency was 1.01×10^{-3} %

CONTENTS

LIST OF FIGURES

List of schemes

List of Tables

ABREVIATIONS AND SYMBOLS

CH_3CN	Acetonitrile
a.u.	Arbitrary units
^{13}C NMR	Carbon nuclear magnetic resonance
cm	Centimeter
δ	Chemical shift
I-V	Current-Voltage
°C	Degrees Celsius
DMF	Dimethylformamide
DMSO	Dimethyl sulfoxide
DSSCs	Dye sensitized solar cells
η	Energy conversion efficiency
HOMO	High occupied molecular orbital
h	Hour
FF	Fill factor
FTIR	Fourier transition infrared
I^-	Iodide
P	Incident light
ITO	Indium tin oxide
T	Intensity
λ	Lambda
LUMO	Low unoccupied molecular orbital
MLCT	Metal-to-ligand charge transfer

M	Molarity
m	meter
mg	milligram
µs	microsecond
mL	milliliter
mV	millivolts
NMR	Nuclear Magnetic Resonance
π	pi
PL	Photoluminescence
PBS	Phosphate buffer solution
Pyr	Pyrazole
Py	Pyridine
J_{sc}	Short circuit current
THF	Tetrahydrofuran
SnO_2	Tin Oxide
TiO_2	Titanium dioxide
I^-_3	Triiodide
UV-Vis	Ultra violet-visible
V_{oc}	Open-circuit voltage
W	Watt
ZnO	Zinc Oxide

CHAPTER 1

1.0 INTRODUCTION AND LITERATURE REVIEW

1.1 Introduction

The increase in demand for energy is one of the many challenges the world is facing today. This causes an increase in consumption of fossil fuels and thus decreases in the amount of fossil fuels and also results in negative impact on the environment. The increase exploitation of fossil fuels led to the development of alternative sources of energy that are environmentally friendly [1-6].

Progress has been made in the development of alternative energy sources such as biomass [7], solar [8], nuclear [9] and wind [10]. The conversion of power from solar energy may be accomplished by solar cells, a class of electrical devices that generate electric power through a photovoltaic effect [4, 11]. Crystalline silicon and compound semiconductor thin films were developed for use in solar cells [12, 13]. Single crystalline silicon solar cells operate on the principle of p-n junctions formed by joining p-type and n-type semiconductors [14]. The electrons and holes are photo generated at the interface of p-n junctions, separated by an electrical field across the p-n junction, and collected through the external circuits [1, 15, 16]. Silicon based solar cells have high efficiency for solar energy conversion with efficiency of up to 25% [6]. However, such devices still possess the disadvantage of high production cost [12]. Since the 1950s, several new types of solar cells have been studied and developed [17]. Among the solar cells, dye sensitized solar cells (DSSCs) are very attractive choices for utilizing the solar

energy [16, 17], due to their potentially low production cost. DSSCs are among the promising solar cell with incident to power conversion efficiency of up to 13% of photovoltaic characteristic [18].

In 1960s it was discovered that electricity can be generated at oxide electrode from clear organic dyes in an electrochemical cell, but the instability of this solar cell was found to be the main change in developing solar cells. Fine thin oxides were used to improve its efficiency and stability but the problem of instability remains and hinders further development [19]. Gratzel and O'Regan in 1991 developed a new type of solar cell (known as DSSC or Gratzel cell) the third generation of solar cells [20]. DSSCs are sensitized by nanoparticle titanium oxide films with ruthenium bipyridyl complex [21, 22]. These DSSCs contain carboxylic group as anchoring ligands that are attached to the surface of TiO_2 thin film semiconductor and transfer electrons to the conduction band. TiO_2 (anatase) has a wide band gap of 3.2 eV that comprises valence band and conduction band [23, 24]. In DSSCs the separation of the charge by kinetic energy is similar to photosynthesis in plants while charge separation on solar cells takes place by movement of current with efficiency of 7.1 -7.9 % [25].

1.2 Structure and operation principle of dye sensitized solar cells

A dye sensitized solar cell consist of a conducting glass substrate, dye sensitizer, an electrolyte, a mesoporous oxide layer (TiO_2), and counter electrode as shown in Figure 1 [26].

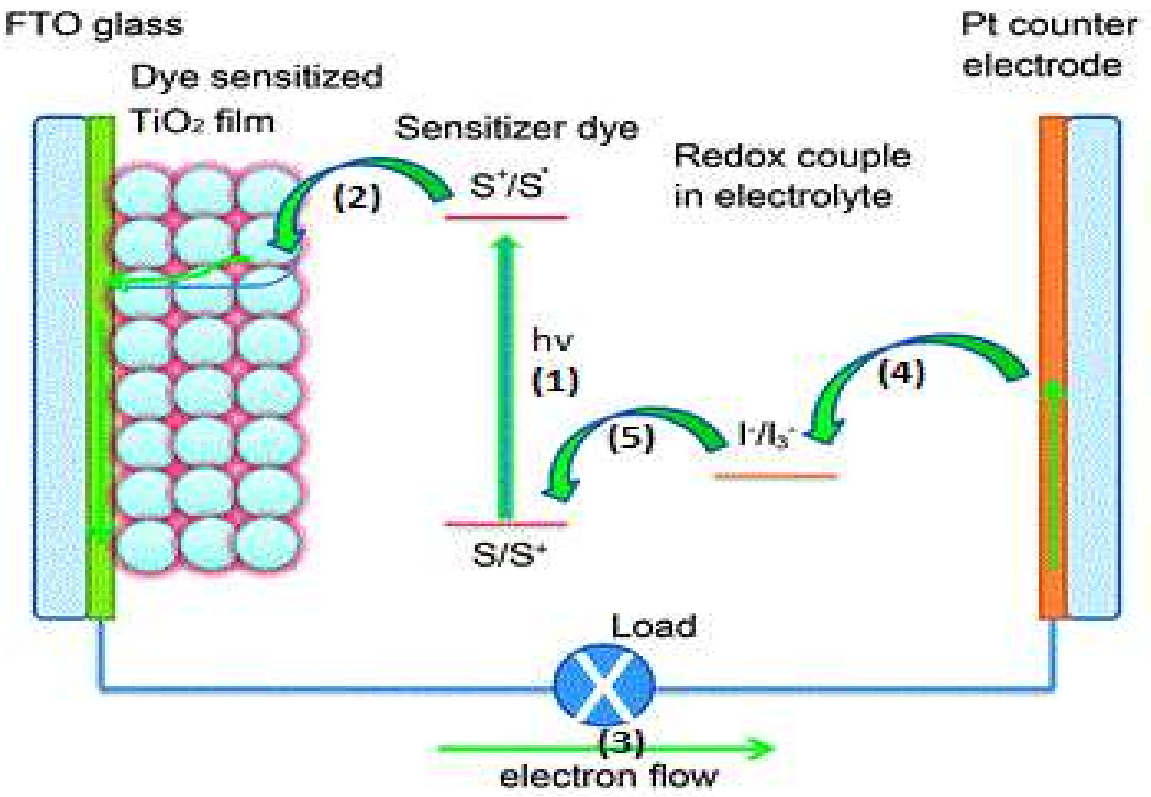

Figure 1. Operation principle of DSSC [27]

Dye sensitized solar cells are composed of four different components:

1.2.1 Working electrode

Working electrode consists of anode made up of transparent glass sheet that allows the light to pass through the solar cell, the glass is treated with mesoporous thin film conductive layer such as TiO_2, ZnO and SnO_2. The thin film is situated on the anode to improve electronic conduction [28, 29].

1.2.2 Sensitizer

A monolayer charge transfer of a sensitized dye is covalently bonded to the surface of mesoporous thin film conductive layer to increase the absorption of light and provide electron passage through the cell. The function of sensitizer in solar cells is to absorb light and convert photons into excited electrons and cause current to flow [30].

1.2.3 Counter electrode

A counter electrode consists of cathode made up of a glass or plastic substrate coated with a catalyst (graphite or platinum) to ease the collection of electrons [30, 31].

1.2.4 Electrolytes

An electrolyte containing a redox intermediate (usually CH_3CN) and I^-/I^-_3 as the prepared electrolyte. Electrons in sensitized dye are balanced by electrolytes [19, 20, 32]. The electrolyte is situated between counter electrode and TiO_2 thin film layer. Electrolytes are responsible for the flow of electron in the circuit. In this case iodine is oxidized into triiodide after the dye has lost an electron and this reduces chances of a solar cell to have short circuit, the dye is reduced to its oxidation state by the oxidized I^-_3 and the electric conversion is repeated [33].

In a DSSC, sunlight is absorbed in a form of light energy into a dye sensitizer, the absorption of light makes the dye electrons to travel from the highest occupied molecular orbital (HOMO) in the ground state to the lowest unoccupied molecular orbital (LUMO) **(1)** (Figure 1) in the excited state [22, 34]. Then the excited electron travels

through a conduction band of TiO_2 thin film leaving the dye in its oxidized state **(2)** (Figure 1). The electrons start traveling through an external circuit **(3)** (Figure 1) [35]. The electrons present in the electrolyte are collected from external circuit by counter electrode and the circuit is closed by the reduction of the dye by electron transfer from the electrolyte or hole-conductor [36], in this step **(4)** (Figure 1). A catalyst is required such as platinum. The catalyst is fixed on the conducting TiO_2 layer of counter electrode, catalysts assists the flow of electrons. Then the electrons travel through catalyst to reach the electrolyte solution positioned in between the working and counter electrodes [23, 37]. Electrolyte solution contains a large number of charged ions that are decomposed and provide electrons to the dye sensitizer [38]. The charged ions transport electrons to their original position through the nanoparticle TiO_2 thin film to the dye molecules where they regain their original positions. In step **(5)** (Figure 1) the circuit closes and recharged dye, the DSSC capable of repeating the process of changing light energy into electrical energy. In this way electrical circuit is complete [21, 39].

$$S + photon \longrightarrow S^* \quad \text{.....(1)}$$

$$S^* + TiO_2 \longrightarrow 3/2I^- + CE \quad \text{.....(2)}$$

$$e^-(TiO_2) + CE \longrightarrow TiO_2 + e^-_{CE} + \text{electric charge} \quad \text{.....(3)}$$

$$S^+ + 3/2I^- \longrightarrow S + 1/2I^-_3 \quad \text{.....(4)}$$

$$1/2I^-_3 + e^-_{CE} \longrightarrow 3/2I^- + CE \quad \text{.....(5)}$$

The stability of DSSCs depends on four components discussed about (dye sensitizer, counter electrode, electrolyte and semiconducting oxides). For instance sensitizers stabilized with phosphonic or carboxylic are capable to perform many redox cycles

without decomposition [31]. Gratzel developed a DSSC sensitizer material that can sustain redox cycle with a remarkable continuous performance in light for 20 years [40]. In ruthenium complexes the transfer of injected electron through the thin film occurs at a faster rate than the reverse reaction causes the electron to combine the oxidized dye molecule instead of flowing through the circuit and produce electric power [41,42]. The structure of a dye sensitizers strongly affect the stability, performance and efficiency of DSSC. The stability of a solar cell is also affected by the light absorption and intensity of a dye sensitizer. In natural dyes, the solvent used to extract dyes from plants affect the performance of DSSC [1, 43].

1.3 Sensitizer

Semiconductor oxides with wide band gaps are used in DSSC, but these semiconductors do not absorb in the visible region. Dye sensitizers attached to the surface of a solar cell play an important role in absorption of light and conversion of solar to electrical energy [44-46]. Researchers have focused on the study of dye sensitizers such as natural, organic and metal-organic dyes (Figure 2) [48]. In the case of metal-organic compounds, ruthenium complexes are mostly used as charge transfer in solar cells with efficiency up to 11% and they are the most effective sensitizers due to their high efficiency, great charge transfer absorption in the visible region, chemical stability and they possess photochemical properties [43, 49, 50].

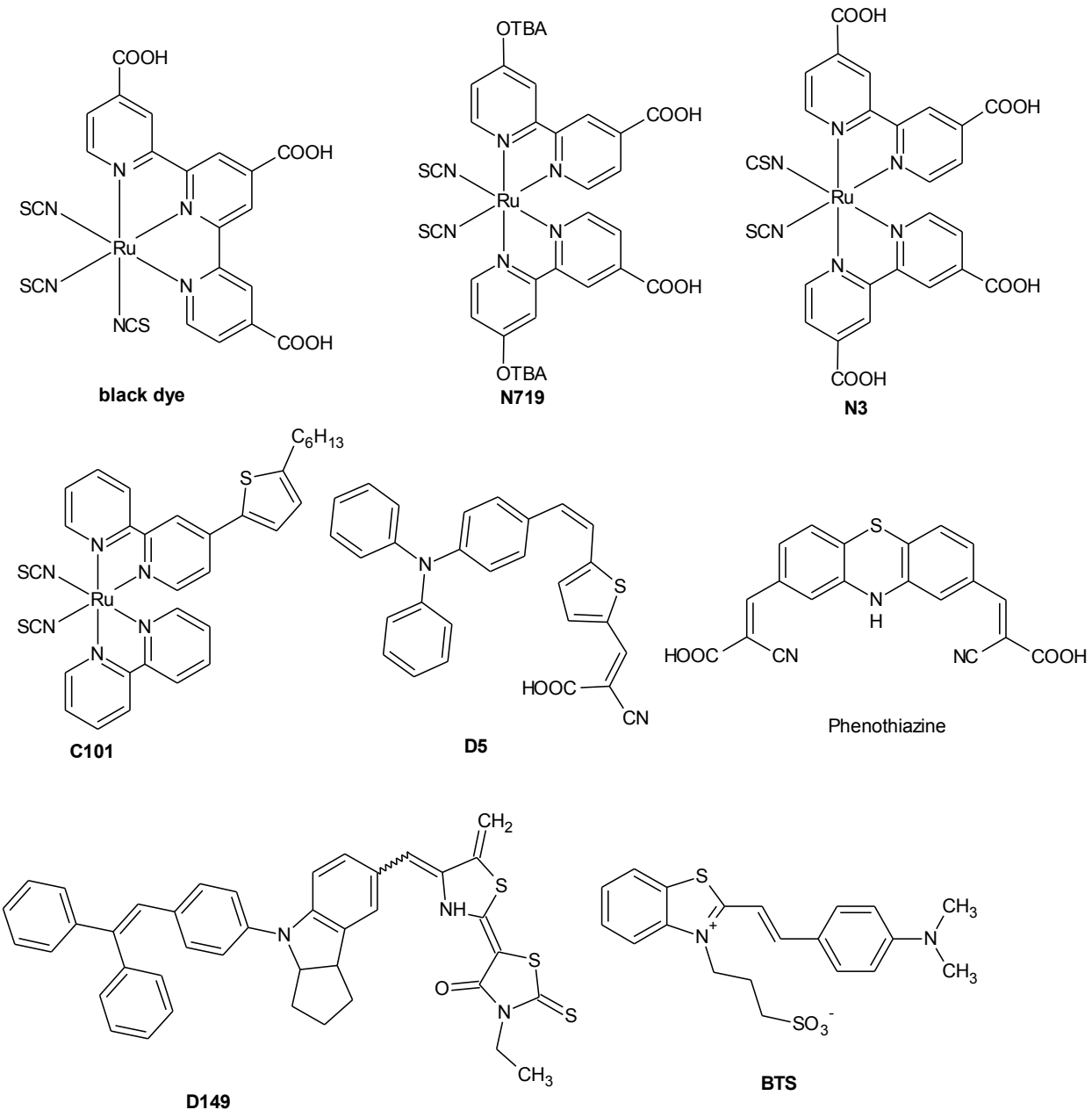

Figure 2. Structures of some dye sensitizers.

According to Wu et al and Feldt et al [49, 50] these are several factors to be considered when synthesizing a dye sensitizer they:

- The dye should have a broad absorption spectrum, preferably all the way into the near-IR wavelength (approximately at 920 nm) in order to collect as many incident photons as possible.
- Low toxicity and possibility to recycle.
- High photo-stability to sustain at least 20 years of use.
- It must consist of oxygen or hydrogen group to be stable on the surface of the semiconductor.
- The energy levels should match the conduction band of the semiconductor and the redox potential of the hole-conductor.

1.4 Solar energy to electricity conversion efficiency (η)

The overall solar energy to electricity conversion efficiency of a solar cell is defined as the ratio of the maximum output of the cell divided by the power of the incident light [1, 53]. The overall conversion efficiency (η) can be determined by the photocurrent density measured at short circuit (J_{sc}), the open circuit photovoltage (V_{oc}), the fill factor of the cell (FF), and the intensity of the incident light (P_{in}) as follows [51-53] :

$$\eta = \frac{(Voc\ Jsc\ FF)}{Pin} 100\ \% \ldots\ldots\ldots\ldots\ldots\ldots\ldots\ldots\ldots\ldots\ldots (6)$$

$$FF = \frac{Vmax\ Jmax}{Voc\ Jsc} \ldots\ldots\ldots\ldots\ldots\ldots\ldots\ldots\ldots\ldots\ldots\ldots\ldots\ldots (7)$$

Conversion efficiency is dependent on all the first three factors which are J_{sc}, V_{oc} and FF as shown presented in Table 1. Under standard conditions it is importance to use each factor for high overall efficiency [55, 56].

Table 1. Dye sensitizers with efficiencies over 5%

Dye	J_{sc} (mA/cm^{-2})	V_{oc}(V)	FF	(η) %	Ref.
D5	11.9	0.66	0.68	5.1	[43]
BTS	13.9	0.52	0.57	5.2	[44]
Phenothiazine	17.76	0.80	0.57	5.73	[45]
D149	17.76	0.60	0.74	6.1	[46]
N3	11.5	0.74	0.74	10.3	[47]
black dye	20.53	0.72	0.70	10.4	[47]
N719	17.73	0.84	0.74	11.2	[47]
C101	5.42	0.74	0.83	11.3	[48]

J_{sc} =short-circuit current density, η = cell efficiency, V_{oc} = open-circuit voltage and FF= fill factor.

1.5 LITERATURE REVIEW

1.5.1 Nitrogen chelating ligands

Bis-(imino)pyridine ligands (Figure 2) are derived from pyridine with imine on position 2 and 6. These ligands are of great importance due to their electronic modularity, ease of synthesis and ability to stabilize transition and alkali metal ions. Chelate of this type that is tridentate ligands are, now well established that they are both chemically and redox active and accepts up to three electrons [57-59]. Bis-(imino)pyridine has the ability to act as an electron reservoir as such, it is popular for application in catalysis or as reagent for activation of small molecules [60]. In bis-(imino)pyridine ligands (Figure 3) *cis* conformation is enforced allowing faster complexation with metals to promote catalytic activity [61].

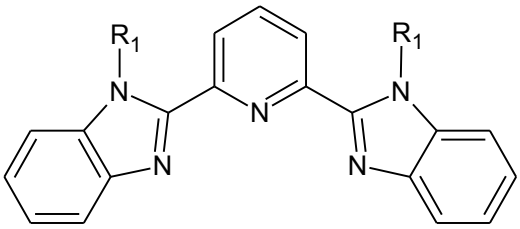

Ligand	R_1
L_1	H
L_2	CH_3
L_3	BZ

Figure 3. Structure of bis-(2-benzimidozoyly) pyridine base compounds.

The late transition metals are less oxophilic than the early transition metals, and are therefore supposed to be more tolerant toward Lewis bases [62, 63]. The late transition metals combined with tridentate ligands (Figure 4), since the reports of 2,6-bis-(imino)pyridine new ones have been synthesized that includes complexes with ligands such as 2,5-bis-(imino)thiophene, 2,5-bis-(imino)-furan, 2,5-bis-(imino)pyrrole, 2,6-bis-(amine)pyridine, 2,6-bis-(2-benzimidazolyl)pyridine, 2,6-bis-(hydrazone)pyridine, 2,6-bis-(aryliminophosphoranyl)pyridine and 2,6-bis-(pyrrolyl)pyridine [64].

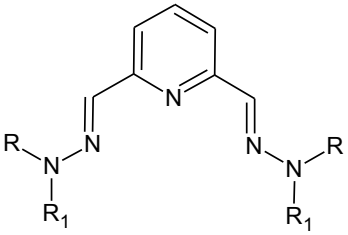

R= Ph, Me, H and R $_1$= Me, H
2,6-bis-(hydrazone)pyridine

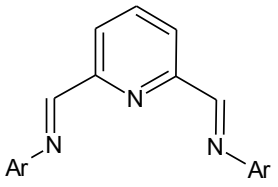

2,6-bis-(imino)pyridine

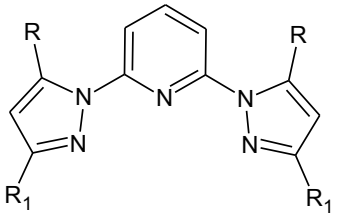

R= Ph, Me, H and R $_1$= Me, H
2,6-bis-(pyrazolyl)pyridine

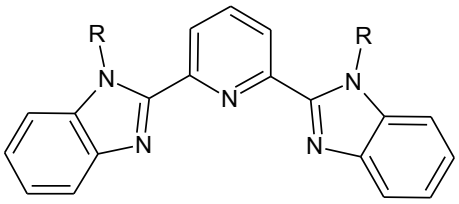

R= Ph, Me and H
2,6-bis(2-benzimidozolyl)pyridine

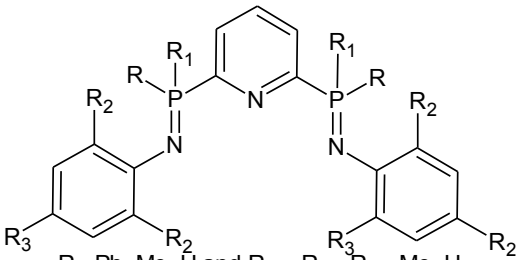

R= Ph, Me, H and R $_1$= R$_2$= R$_3$= Me, H
2,6-bis-(aryliminophosphoranyl)pyridine

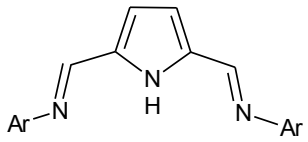

2,5-bis-(amino)pyrrole

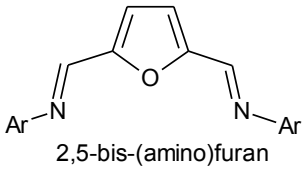

2,5-bis-(amino)furan

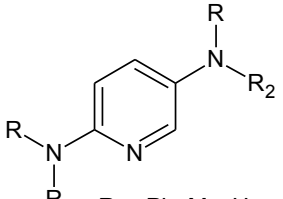

R$_1$= Ph, Me, H and R $_2$= Me, H
2,5-bis-(amino)pyridine

Figure 4. Structures of some bis-(amino)pyridine ligand

Bis-(imino)pyridine is known to be a redox-active ligand, also called redox non-innocent ligands, and can interact with the metal center to facilitate chemical transformations. These redox-active ligands can be easily oxidized or reduced due to the energies of their frontier orbital. The redox non-innocence of the bis-(imino)pyridine ligand (Scheme 1) in the complex which is formulated as an intermediate spin metal center with a doubly reduced bis-(imino)pyridine dianion [66-69].

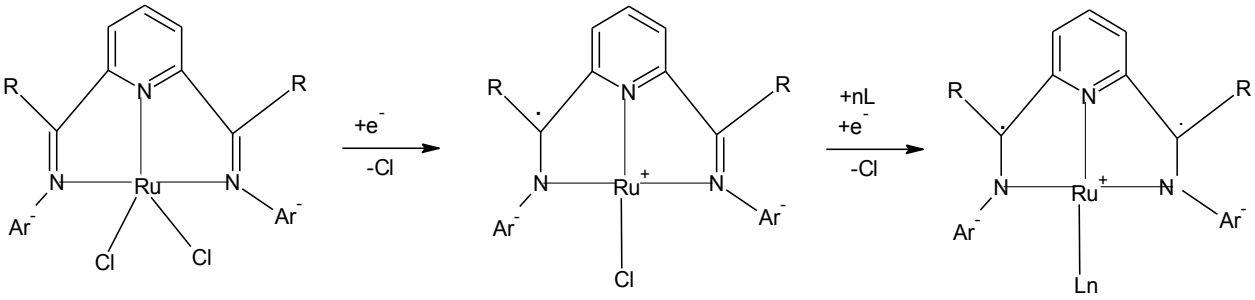

Scheme 1. Redox activity of 2,6-bis-(imino)pyridine ligands in Ru coordination compound (R = Me, Ph)

The stability and catalytic activity of a metal complex depends on the capacity of the ligand to accept up to three electrons from the metal center through conjugated π-acidic nitrogen atoms to mitigate the one electron to metal ion [70].

Pyrazolyl base ligand consists of three possible substituting positions on the pyrazole ring which allows the functionalization of the ligand in order to influence the electronic and steric properties this will depend on the substituent chosen. Jamson *et al,* synthesized and characterized 2,6-bis-(pyrazol)pyridine ligand by combining pyrozolyl and pyridyl to enable the synthesis of tridentate [65] as shown in Scheme 2.

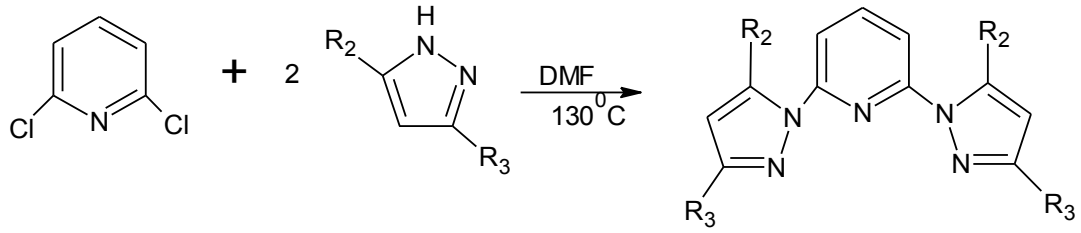

Ligand	R_2	R_3
L_4	H	H
L_5	H	Me
L_6	Me	Me

Scheme 2. Synthesis of Bis-(pyrazolyl)pyridine ligands.

1.5.2 Coordination of metal complexes.

Ruthenium complexes that contains bis-bidentate or tridentate ligands have recently received considerable attention in molecular electronic devices [71]. Bis-(imino)pyridine ligands interact with the *d* orbitals of transition metals through both σ–donor located on the nitrogen atoms and the π–acceptor conjugated aromatic system [72]. Deng *et al*. [73] designed and synthesized a ruthenium complex, $RuCl_2(PPh_3)(Me_4BPPy)$, from the 2,6-bis-(3,5-dimethylpyrazol-1-yl)pyridine (Me_4BPPy) in 2-propanol at 80 °C. The structure was characterized using XRD and showed good crystalline structure.

In 2008, Singh *et al.* [74] synthesized and characterized ruthenium complexes with tridentate 2,6-bis-(benzimidazol-2-yl)pyridine ligand. Ruthenium(II) complex was observed to exhibit strong metal-to-ligand charge transfer (MLCT) band near 475 nm

and intra-ligand π-π* transitions appear at 347 and 314 nm at pH 5. The MLCT band position was found to increase as the pH was increased indicating that the MLCT of 2,6-bis(benzimidazol-2-yl)pyridine ligand was dependent on pH [74]. These electronic properties have raised a lot of interest especially in the solar cell industry and in catalysis.

1.5.3 Application of ruthenium complexes in DSSCs

Ruthenium(II) complexes containing pyridine are the most successful complexes as dyes in DSSCs. The application of ruthenium complexes (**N3** and **N719**) (Figure 5) was first reported by Nazeeruddin *et al*, in 1993 [75].

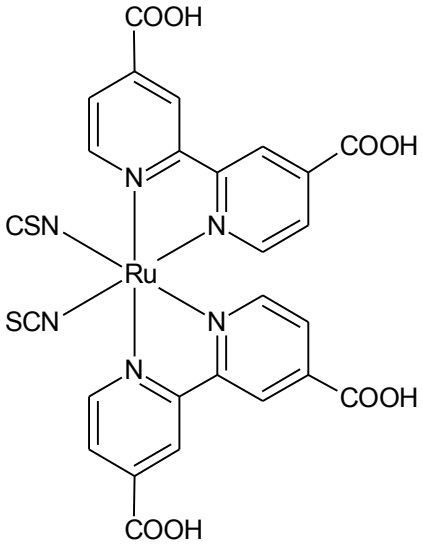

N3

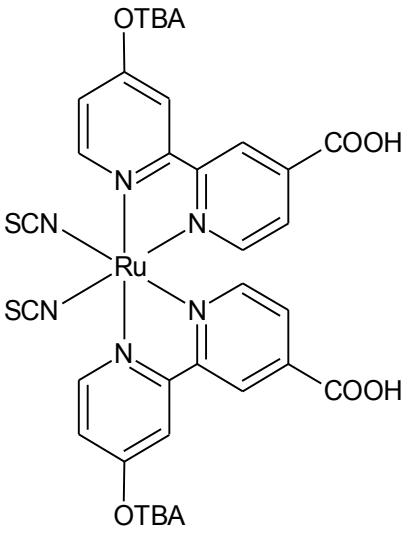

N719

Figure 5. Structure of **N3** and **N719** Ruthenium complex.

Compounds **N3** and **N719** where **N719** are analogous and only differ in their substituents where **N719** contains tetrabutyl ammonium (TBA) in the para position of pyridines **N3** contain two anchoring carboxylic group (-COOH) in the same positions [76]. Several studies in DSSCs have been carried out using *cis*-[$Ru(dcbH_2)_2LL'$] as dyes. This is because these complexes contain good anchoring ligand that allow an efficient absorption onto the surface of the semiconductor, which can be TiO_2 or ZnO and their properties can be enhanced by using different ancillary ligands [77].

In the work reported by Adeloye and Ajibade (2010) the synthesis of ruthenium complexes with general formula [$Ru(L_1)(L_2)(NCS)_2$] where L_1=4-(9-dianthracenly-10-(2,3-dimethylacrylic acid)-7-(9-anthracenly-10-(2,3-dimethylacrylic acid)-1,10-phenthrolline and L_2=4,7-bis-(1-methoxyl-1-butane-3-enye)-1,10-phenothrolline utilizing anthracene derivatives and 1-methoxy-1-butene-3-enyl moiety were introduced to the Ru(II) complex to increase the π-conjugate to enhance the photophysical properties (light-harvesting and electronic transfer) [78].

In the work of pyazolypyridine and terpyridine Ru(II) sensitizers Wu *et al.* (2012) reported a series novel heteroleptic bis-tridentate Ru(II) sensitizers with dicarboxyterpyridine and 2,6-bis(5-pyrazolyl)pyridine, the complexes were denoted as TF 11-14 (Figure 6) Bis-tridentate (terpyridine) sensitizer showed a remarkable performance in dye sensitized solar cells when compared to a DSSC with **N749** (ruthenium polypyridine) sensitizer. The short-circuit photocurrent (J_{sc}) of TF-12

sensitizer found to be 19.0 mA cm^{-2}, an open-circuit voltage (V_{oc}) of 0.71 V, and a fill factor (FF) of 0.68 and an overall conversion efficiency (η) of 9.21%. The π-conjugated pendant group was introduced to TF dyes sensitizer to increase both light-harvesting and photovoltaic energy conversion capability of TF. The carboxyl anchoring group increased the efficiency Ru(II) sensitizer [79].

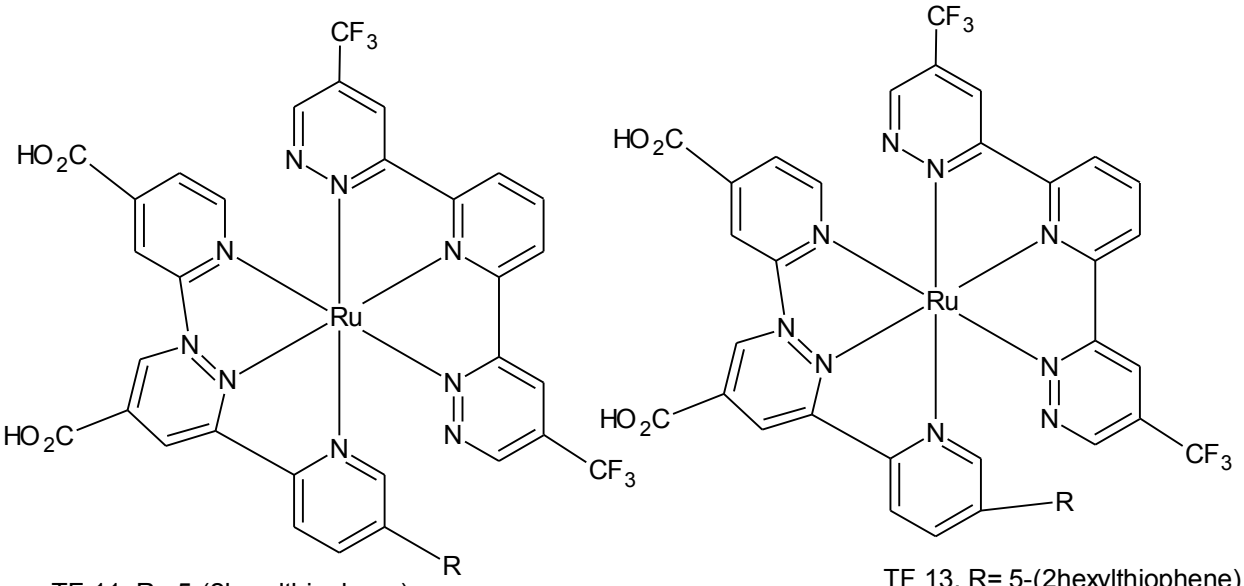

Figure 6. Structure of TF 11-14

Recent publications of Lobello *et al*. (2014) [80] describe the design of a new ruthenium(II) sensitizer, [Ru(L_1)(L_2) $(NCS)_2$] where L1 = (4-(5-hexylthiophen-2-yl)-4'(4-carboxyl-phenyl 2,2'-bipyridine) and L2 = (4,4'-dicarboxy-2,2'-bipyridine), (Figure 7) based on a dissymmetric bipyridine ligand was synthesized and used in DSCs. The observed photovoltaic efficiencies were found to be 7.6 %. The binding of bipyridyne

ligands occurred through three anchoring carboxylic groups its physical properties are similar to that of **N719** (Figure 5) dye [80].

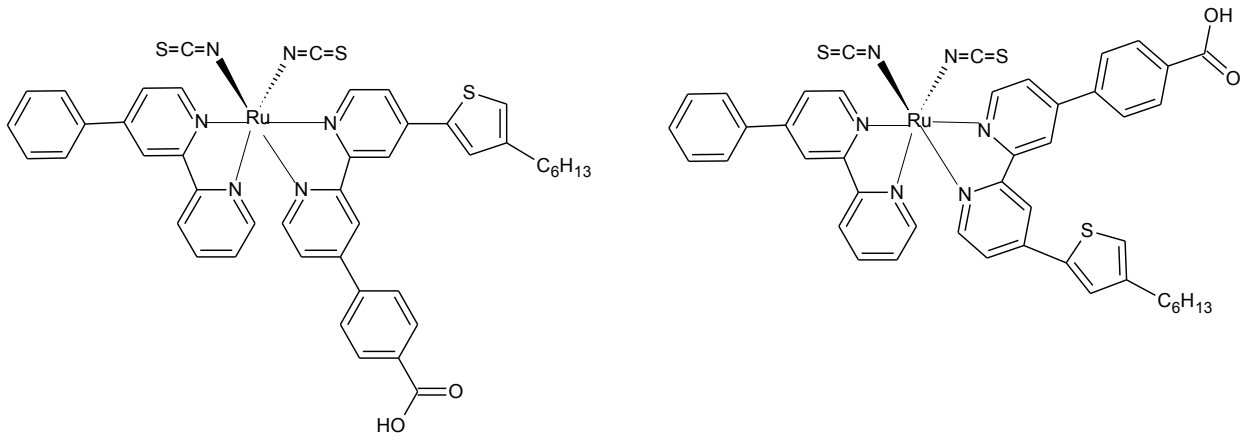

Figure 7. Structures of $[Ru(L_1)(L_2)(NCS)_2]$ [80]

In work reported of Adeloye *et al.* [81] a new homoleptic ruthenium(II) complex, with a general formula $[Ru(L_1)_2(PF6)_2]$, where L_1 = bis-4'-(*trans*-2-methyl-2-butenoic acid)-terpyridyl was designed. Bis-hexafluorophosphate enhances the stability, photophysical and redox properties and also increased the length of π-conjugation to enhance MLCT of the complex, which was found to be far better compared to $[Ru(tpy)_2]^{2+}$. The main drawback was that the electronic spectra exhibit lower wavelength compared to **N3** and **N719** (Figure 5) [81].

1.5.4 Application of cobalt complexes in DSSCs

Large amount of energy can be lost during the regeneration reaction of I^-_3/I^- system. The energy is due to corrosiveness of I^-_3/I^- and absorption of light by triiodide [82].

Researchers have recently developed new redox compound that have higher redox potentials than iodide ions [83]. In order to overcome the loss of energy and increase conversion efficiency of DSSCs, researchers have recently developed a new redox compounds that hence higher redox potentials that I^- ions. Such compounds include cobalt, iron, copper based complexes [84]. Of these compounds, cobalt (II)/(III) bipyridine complexes show interesting performance in DSSCs [85]. The use of cobalt complexes has not been reported to date, these compounds are only employed as redox mediators for DSSCs.

The absorption of light in the visible region of the solar spectrum in cobalt complexes is insignificant, and their redox properties can be adapted to use donor/acceptor substituents on the ligand [86]. For example, cobalt complexes can be used as alternate of I_3^-/I^- used in dye-sensitized solar cells [87]. In 2001 Nusbaumer *et al*. [88] showed that DSSCs containing cobalt complex of 2,6-bis(1-butylbenzimidazol-2-yl)pyridine (Figure 8), as an electron and redox mediator and had the power conversion efficiencies at about 5.2 %. The kinetic behavior of cobalt complexes redox mediator was found to be similar with that of I_3^-/I^- redox couple. These results show that cobalt complex can be used as mediator and as alternative to commonly use I_3^-/I^-redox couple used system in DSSC [88].

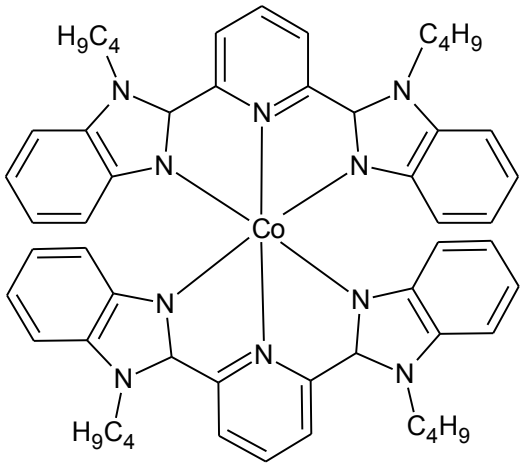

Figure 8. Cobalt(II) complex of 2,6-bis(1-butylbenzimidazol-2-yl)pyridine.

In another study, Feldt *et al*. [89] synthesized cobalt complexes of bipyridine and phenanthroline (Figure 9) These compounds were their redox potential and the proportionality of the driving force for recombination and the regeneration of dye on DSSCs. Photovoltaic current was found to be inversely proportion to the redox potential of cobalt complexes. It was found that the half-life of cobalt tribipyridine complexes was about 20μs for regeneration of dye on a photovoltaic performance, which was found to be similar to that of I^-_3/I^- redox couple.

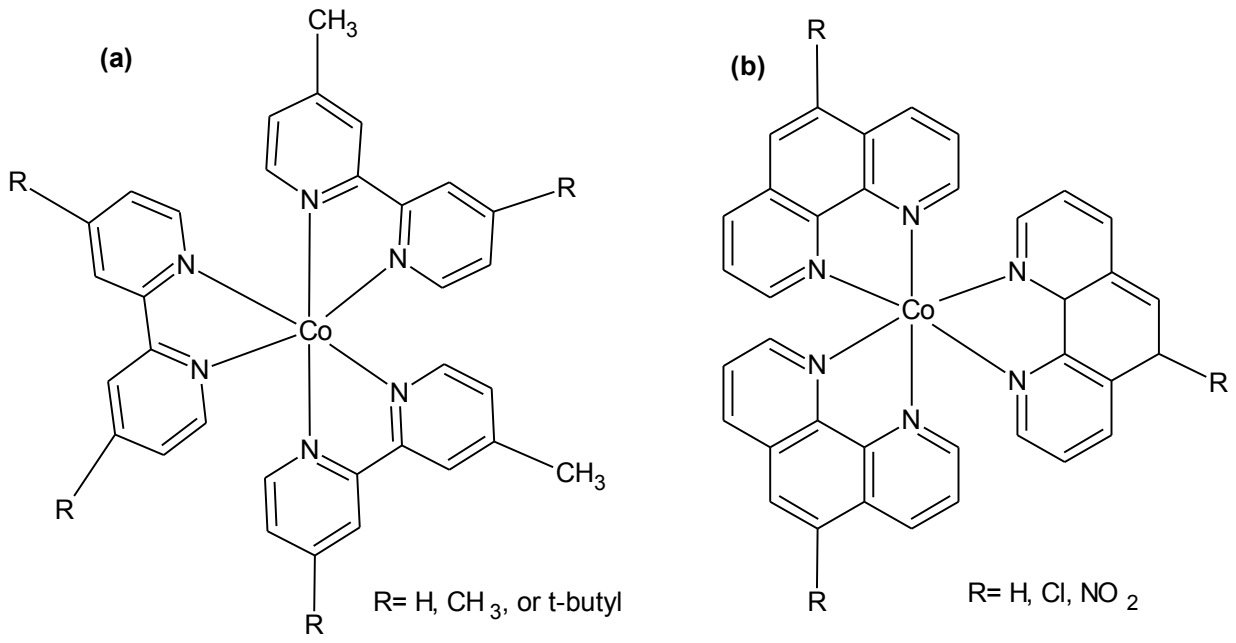

Figure 9. Structure of cobalt(II) complexes of (a) bipyridine and (b) phenanthroline.

Cobalt(II/III) tris(5-chloro-1,10-phenanthroline) was found to have a driving force of 390 mV for regeneration of dye which was enough to regenerate more than 80% of the **D35** (Figure 10) dye molecules, causing generation of electric current from incident photon to be above 80%. The only drawback was when cobalt phenanthroline complexes were used, the photocurrent of the **D35** dye sensitized DSCs decreased [89].

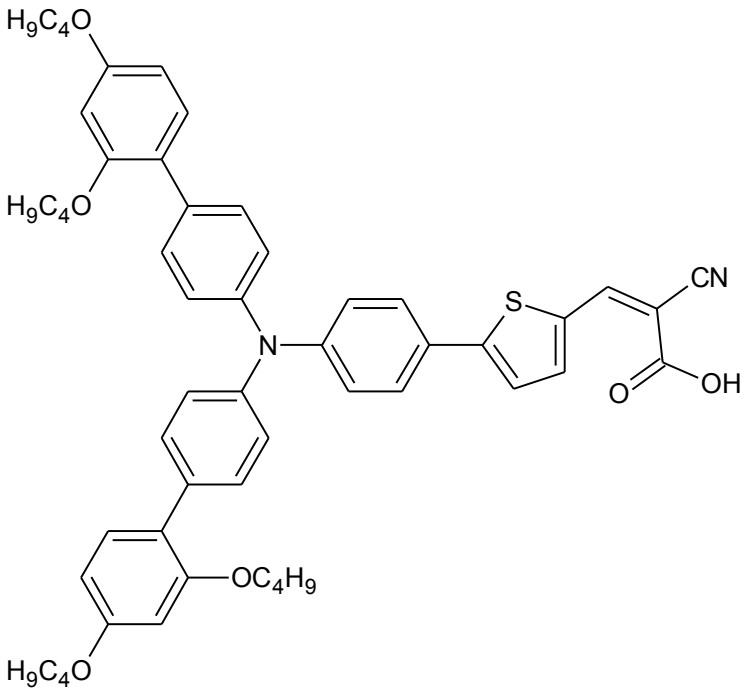

Figure 10. Structure of **D35** dye [90]

In the pioneering work of cobalt redox mediators used in DSSCs, Yum *et al*. designed a cobalt complex of tridendate ligands $[Co(bpypz)_2]^{3/2+}(PF_6)^{3/2}$ in photovoltaic performance as redox mediator with **Y123** dye (Figure 11) the power conversion efficiency was found to be over 10% at 100mWcm^{-2}. It was concluded that cobalt redox couple is a promising alternative to the commonly used I_3^-/I^-redox couple [91].

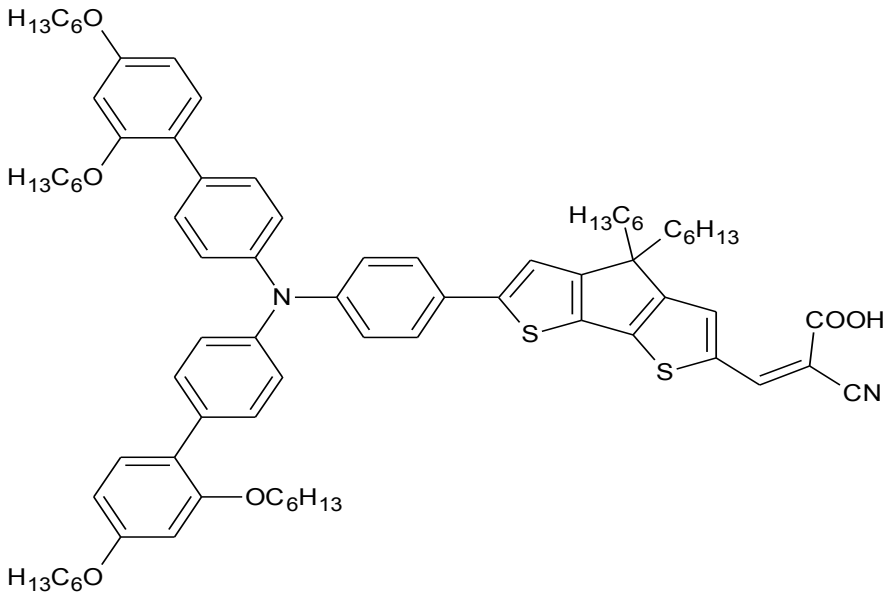

Figure 11. Structure of **Y123** dye [92]

1.6 Motivation and rationale

Fossil fuels are non-renewable source of energy and their use depletes natural resources and cause an increase in greenhouse gases such as, carbon monoxide and carbon dioxide in the atmosphere and consequently global warming [2]. The use of dye sensitized solar cells as a source of electric energy can provide clean and renewable energy. Crystalline silicon solar cell being used at present is very expensive and they require a dopant for them to operate [12]. Such devices are not desirable because of still possess the disadvantage of high production cost. Recent reports [18] show that cobalt(II/III) complexes have interesting promising efficiency compared to natural dyes. Furthermore, ruthenium complexes as dyes can sustain the performance of DSSC for up to 20 years.

1.7 Problem Statement

Researchers are still trying to develop new solar cell technologies that could generate electric energy at low cost that are competitive with energy generated from fossil fuels [5]. At present, most of our energy is from fossil fuels, is it possible to get a DSSC as good as fossil fuel?

Renewable energies such as solar cells have attracted most researchers because it directly converts solar energy into electric energy without affecting the environment [2]. Can a problem related to depletion of natural resources be resolved by using DSSC as a source of electrical energy?

Silicon based solar cells have solar energy conversion efficiency of 25% [12]. However, such devices are associated with high production cost [4]. Is it possible to overcome the disadvantage of high production cost of silicon solar cells by developing DSSCs with comparable or better efficiency?

1.8 Aims and objectives

Aim: To synthesize, characterize and evaluate Ru(II) and Co(II) complexes of nitrogen chelating ligands as sensitizers for DSSCs

Objectives:

- To synthesize bis-(imino)pyridine and bis-(pyrazolyl)pyridine based ligands.
- To synthesize ruthenium(II) and Co(II) complexes of these ligands.
- To characterize the ligands, Ru(II) and Co(II) complexes using elemental analysis and spectroscopic techniques.
- To carry out photophysical and electrochemical studies of the Ru(II) and Co(II) complexes.
- To fabricate solar cells using the Ru(II) and Co(II) complexes.
- To evaluate the conversion efficiency of the fabricated solar cells.

References

[1] Gong, J.; Liang, J.; Sumathy, K. Review on dye-sensitized solar cells (DSSCs): Fundamental concepts and novel material. *Renewable and Sustainable Energy Review,* **2012**, *16*, 5848-5860.

[2] Ludin, N. A.; Mahmoud, A. M. A.; Mohamad, A. B.; Kadhum, A. A. M.; Sopian, K.; Karim, N. S. A. The review on the development of natural dye photosensitizers for dye sensitizerd solar cells. *Renewable and Sustainable Energy Review,* **2014**, *31*, 386-396.

[3] Ito, S.; Murakami, T. N.; Comte, P.; Liska, P.; Gratzel, C.; Nazeeruddin, M. K.; Gratzel, M. Fabrication of thin film dye sensitized solar cells with solar to electric power conversion efficiency over 10%,*Thin Solid Films*, **2008**, *516*, 4613-4619.

[4] Ding, J.; Li, Y.; Hu, H.; Bai, L.; Zhang, S.; Yuan, N. The influence of anatase-rutile mixed phase and ZnO blocking layer on dye-sensitized solar cells based on TiO_2 nanofiber photoanodes*. Nanoscale Research Letters, **2013***, *8*, 1-9.

[5] Cheng M. H.; Hsieh, W. F. High-efficiency metal-free organic-dye-sensitized solar cells with hierarchical ZnO photoelectrode, *Energy and Environmental Sciences*, **2010**, *3*, 442-447.

[6] Adeloye, A. O.; Ajibade, P. A.; Cummings, F. R.; Le Roux, L. J.; Mamphweli, S. N.; Meyer E. L. Synthesis, photophysical and preliminary investigation of the dye-sensitized solar cells properties of functionalized anthracenyl-based bipyridyl and phenanthrolyl Ru(II) complexes. *Journal of Chemical Sciences,* **2013**, *125*, 17-27.

[7] Bajpai, R.; Roy, S.; Koratkar, N.; Misra, D. S. NiO nanoparticles deposited on graphene platelets as a cost-effective counter electrode in a dye sensitized solar cell, *Carbon*, **2013,** *5*, 56-63.

[8] Odobel, F.; Pellegrin, Y.; Gibson, E. A.; Hagfeldt, A.; Smeigh, A. L.; Hammarstrom, L. Recent advances and future directions to optimize the performances of p-type dye-sensitized solar cells. *Coordination Chemistry Reviews,* **2012,** *256*, 2414-2423.

[9] Liu, J.; Li, J. Electrochemical analysis of dye adsorption on aligned carbon nanofiber arrays coated with TiO_2 nanoneedles for dye-sensitized solar cell. *Frontier of Optoelectronics in China*, **2011**, *4*, 53-58.

[10] Ashraful, A.; Hironori, A. Molecular design of ruthenium(II) polypyridyl photosensitizer for efficient nanocrastalline TiO_2 solar cells. *Journal of Photochemistry and Photobiology A: Chemistry*, **2003**, *158*, 131-138.

[11] Menzies, D. B.; Cervini, R.; Cheng, Y. B.; Simon, G. P. Nanostructured ZrO_2-coated TiO_2 electrodes for dye-sensitised solar cells. *Journal of Sol-Gel Sciences and Technology*, **2004**, *32*, 363-366.

[12] Gratzel, M. Recent advances in sensitized mesoscopic solar cells. *Accounts of Chemical Research,* **2009**, *42*, 1788-1798.

[13] Umar, A. A.; Rahman, M. Y. A.; Taslim, R.; Salleh, M. M. Dye-sensitized solar cell utilizing quasi one-dimensional of highly compact vertical array ZnO nanorod. *International Journal of Electrochemical Science*, **2012**, *7*, 7253-7260.

[14] Kuang, D.; Ito, S.; Wenger, B.; Klein, C.; Moser, J. E.; Humphry-Baker, R.; Zakeeruddin, S. M.; Gratzel, M. High molar extinction coefficient heteroleptic ruthenium

complexes for thin film dye-sensitized solar cells. *Journal of the American Chemistry Society*, **2006**, *128*, 4146-4154.

[15] Zhang, Q.; Dandeneau, C. S.; Zhou, X.; Cao, G. ZnO nanostructures for dye-sensitized solar cells. *Advanced Materials*, **2009**, *21*, 4087-4108.

[16] Wang, P.; Zakeeruddin, S. M.; Comte, P.; Charvet, R.; Humphry-Baker, R.; Gratzel, M. Enhance the performance of dye-sensitized solar cells by co-grafting amphiphilic sensitizer and hexadecylmalonic acid on TiO_2 nanocrystal. *Journal of Physical Chemistry B,* **2003**, *107,* 14336-14341.

[17] Lee, K. H.; Suryanarayanan, V.; Ho, K. C; Thomas, K. R. J.; Lin, J. T.; Effects of co-adsorbate and additive on the performance of dye-sensitized solar cells: A photophysical study. *Solar Energy Materials and Solar Cells*, **2007**, *91*, 1426-1431.

[18] Matthew, S.; Yella, A.; Gao, P.; Humphry-Baker, R.; Curchod, B. F. E.; Ashari-Astani, N.; Travernelli, I.; Rothlisberger, U.; Nazeeruddin, M. K.; Gratzel, M. Dye sensitized solar cells with 13% efficiency achieved through the molecular engineering of porphyrin sensitizers. *Nature Chemistry*, **2014**, *6*, 242-247.

[19] Iliopoulos, K.; Guezguez, I.; Kerasidou, A. P.; El-Ghayoury, A.; Branzea, D.; Nita, G.; Avarvari, N.; Belmabrouk, H.; Couris, S.; Sahraoui,B. Effect of metal cation complexation on the nonlinear optical response of an electroactive bisiminopyridine ligand. *Dyes and Pigments*, **2014**, *101*, 229-233.

[20] O'Regan, B.; Gratzel, M. A low-cost, high-efficiency solar cell based on dye sensitized colloidal TiO_2 films. *Nature*, **1991**, *353*, 737-740.

[21] Lu, X., Wei, S.; Wu, C. M. L.; Guo, W.; Zhao, L. Theoretical characterization of ruthenium complexes containing functionalized bithiophene ligands for dye-sensitized solar cells. *Journal of Organic Chemistry*, **2011**, *696*, 1632-1639.

[22] Bajpai, R.; Roy, S.; Koratkar, N.; Misra, D. S. NiO nanoparticles deposited on graphene platelets as a cost-effective counter electrode in a dye sensitized solar cell, *Carbon*, **2013**, *5*, 56-63.

[23] Karlsson K. M., Jiang, X.; Eriksson, S. K.; Gabrielsson, E.; Rensom, H.; Hangfeldt, A. Penoxazine dye for dye-sensitized solar cells: Relationship between molar structure. *Chemistry European Journal*, **2011**, *17*, 6415-6424.

[24] Jamson, D. L.; Goldsby, K. A. 6-bis(N-pyrazolyl)pyridines: The convenient synthesis of a family of planar tridentate N3 ligands that are terpyridine analogs. *Journal of Organic Chemistry*, **1990**, *55*, 4992-4994.

[25] Ondersma, J. W.; Hamann, T. W. Recombination and redox couples in dye-sensitized solar cells. *Coordination Chemistry Reviews*, **2013**, *257*, 1533-1543.

[26] Buchalska, M.; Kuncewicz, J.; Swietek, E.; Labuz, P.; Baran, T.; Stochel, G.; Macyk, W. Photoinduced hole injection in semiconductor-coordination compound systems. *Coordination Chemistry Reviews,* **2013**, *257*, 767-775.

[27] Wu, Y.; Zhu, W. Organic dye sensitizers from D-π-A to D-A-π-A: Effects of internal electron–withdrawing units on molecular absorption, energy level and photovoltaic performance. *Chemical Society Reviews*, **2013**, *12*, 2039-2058.

[28]. Zhou, H.; Wu, L.; Gao, Y.; Ma, T. Dye-sensitized solar cells using 20 natural dyes as sensitizers. *Journal of Photochemistry and Photobiology A: Chem*istry, **2011**, *219*, 188-194.

[29]. Pellegrin, Y.; Pleux, L. L.; Blart, L.; Renaud, A.; Chavillon, B.; Szuwarski, N.; Boujtita, M.; Cario, L.; Jobic, S.; Jacquemin, D.; Odobel, F. Ruthenium polypyridine complexes as sensitizers in NiO based p-type dye-sensitized solar cells: Effects of the anchoring groups. *Journal Photochemistry and Photobiology A: Chemistry*, **2011**, *219*, 235-242.

[30] Hocevar, M.; Krasovec, U. O.; Berginc, M.; Drazic, G.; Hauptman, N.; Topic, M. Development of TiO_2 pastes modified with Pechini sol-gel method for high efficiency dye-sensitized solar cell. *Journal of Sol-Gel Science Technology*, **2008**, *48*, 156-162.

[31] Peiris, T. A. N.; Alessa; H.; Sagu, J. S.; Bhatti, I. A.; Isherwood, P.; Wijayantha, K.G.U. Effect of ZnO seed layer thickness on hierarchical ZnO nanorod growth on flexible substrates for application in dye sensitised solar cells. *Journal of Nanoparticle Res*earch, **2013**, *15*, 2115-2124.

[32] Gong, H. H.; Hong, S. B.; Hong, S. C. Dispersion controlled platinum/multi-walled carbon nanotube hybrid for counter electrodes of dye-sensitized solar cells. *Macromolecule Research*, **2014**, *22*, 397-404.

[33] Joshi, P. H.; Korfiatis, D. P.; Potamianou, S. F.; Thoma, K. A. T. Oxide thickness and roughness factor as parameters for TiO_2 dye sensitized solar cells performance. *Russian Journal of Electrochemistry,* **2011**, *47*, 517-521.

[34] Lobello, M. G.; Wu, K. L.; Reddy, A. M.; Marotta, G.; Grätzel, M.; Nazeeruddin. M. K., Chi, Y.; Chandrasekharam, M.; Vitillaro, G.; De Angelis, F. Engineering of Ru(II) dyes for interfacial and light-harvesting optimization. *Dalton Transactions*, **2014**, *43*, 2726-2732.

[35] Moehl, T.; Tsao, N. H.; Wu, K.L.; Hsu, H. C.; Chi, Y. L.; Ronca, E.; De Angelis, F.; Nazeeruddin, M. K.; Gratzel, M. High open-circuit voltages: Evidence for a sensitizer-induced TiO_2 conduction band shift in Ru(II)-dye sensitized solar cells. *Chemistry of Materials*, **2013**, *25*, 4497−4502.

[36] Ole, A. F.; Santos, G. N. C, Quiroga, R. V. Fabrication and characterization of dye sensitized solar cells using nanostructured TiO_2 photoelectrode. *International Journal of Scientific and Engineering Research*, **2012**, *8*, 1-7.

[37] Mamidi, T.; Mandha, S. B.; Mishra, A. Effects of lithium ions on dye-sensitized ZnO aggregate solar cells. *International Journal of Modern Engineering and Research Technology*, **2012**, *2*, 3597-3601.

[38] Zhang, X.; Chen, L.; Li, L.; Mao, J.; Wu, W.; Agren, H.; Hua, J. Photovoltaic properties of bis-(octyloxy)benzo-[c][1,2,5]thiadiazole sensitizers based on *N*,*N*-diphenylthiophen-2-amine donor. *Journal of Materials Chemistry,* **2014**, *2*, 4063-4072.

[39] Kim, J. J.; Yoon, J. A new ruthenium containing dipyridylamine ligand for effective nanocrystalline dye-sensitized solar cells. *Inorganic Chimica Acta,* **2013***, 394,* 506-511.

[40] Appleyard, S. Assessing the use of simple dye-sensitized solar cells for drinking water chrorinarion by communities with limited resources. *Renewable Energy*, **2009**, *34*, 1651-1654.

[41] Martinez Diaz, M.V.; de la Torre, G.; Torres, T. Lighting porphyrins and phthalocyanines for molecular photovoltaics. *Chemical Communications,* **2010**, *46*, 7090-7108.

[42] Yella, A.; Lee, H. W.; Tsao, W. H. N.; Yi, C.; Chandiran, K. A.; Nazeeruddin, M. D.; Diau, E. W. G.; Yeh, C. Y.; Zakeeruddin, S. M. Z.; Gratzel, M. Porphyrin-sensitized solar cells with cobalt (II/III)–based redox electrolyte exceed 12 percent efficiency. *Science,* **2011**, *334*, 629-629.

[43] Zhang; C. R.; Liu Z. J.; Chen, Y. H.; Chen H. S.; Wu Y. Z.; Yuan L. H. DFT and TDDFT study on organic dye sensitizers D5, DST and DSS for solar cells. *Journal of Molecular Structure: Theochem*, **2009**, *899*, 86-93.

[44] Stathatos, E.; Lianos, P. Synthesis of a hemicyanine dye bearing two carboxylic groups and its use as a photosensitizer in dye-sensitized photoelectrochemical cells. *Chemistry of Materials*, **2001**, *13*, 3888-3892.

[45] Gratzel, M. Conversion of sunlight to electric power by nanocrystalline dye-sensitized solar cells. *Journal of Photochemistry and Photobiology A: Chemistry,* **2004**, *164*, 3-14.

[46] Burdzinski, G.; Karolczak, J.; Ziolek, M. Dynamics of local Stark effect observed for a complete D149 dye-sensitized solar cell. *Physical Chemistry Chemical Physics*, **2013**, *15*, 3889-3896

[47] Ryan, M. PGM Highlights. Progress in ruthenium complexes for dye sensitized solar cells. *Platinum Metals Review*, **2009**, *53*, 216-218.

[48] Reynal, A.; Forneli, A.; Palomares, E. Dye structure–charge transfer process relationship in efficient ruthenium-dye based dye sensitized solar cells. *Energy and Environmental Science*, **2010**, *3*, 805-812.

[49] Wu, W.; Yang, J.; Hua, J.; Tang, J.; Zhang, L.; Long, L.; Tian, H. Efficient and stable dye-sensitized solar cells based on phenothiazine sensitizers with thiophene units. *Journal of Materials Chemistry*, **2010**, *20*, 1772-1779.

[50] Feldt, S. M.; Gibson, E. A.; Gabrielsson, E.; Sun, L.; Boschloo, G.; Hagfeldt, A. Design of organic dyes and cobalt polypyridine redox mediators for high-efficiency dye-sensitized solar cells. *Journal of the American Chemical Society*, **2010**,*132*, 16714-16724.

[51] Adeloye, A. O., Ajibade, P. A. A high molar extinction coefficient mono-anthracenyl bipyridyl heteroleptic ruthenium(II) complex: Synthesis, photophysical and electrochemical properties. *Molecules,* **2011**, *16*, 4615-4631.

[52] Baheti, A.; Singh, P.; Lee, P. C.; Thomas, K. R. J.; Ho, K. C. 2,7-Diaminofluorene-based organic dyes for dye-sensitized solar cells: Effect of auxiliary donor on optical and electrochemical properties. *Journal of Organic Chemistry*, **2011**, *76*, 4910-4920.

[53] Gratzel, M. Photovoltaic performance and long-term stability of dye-sensitized meosocopic solar cells. *Comptes Rendus Chimie*, **2006**, *9*, 578-583.

[54] Kong, F. T.; Dai, S. Y.; Wang, K. J. Review of recent progress in dye-sensitized solar cells. *Advances in Optoectronics*, **2007**, *10*, 1-13.

[55] Tigreros, A.; Dhas, V.; Ortiz, A.; Insuasty, B.; Martin, N.; Echegoyen, L. Influence ofacetylene-linked π-spacers ontriphenylamine-fluorene dye sensitized solar cells performance. *Solar Energy Materials and Solar Cells*, **2014**, *121*, 61-68.

[56] Bryliakov, K. P.; Talsi, E. P.; Semikolenova, N. V.; Zakharov, V. A. Formation and nature of the active sites in bis-(imino)pyridine iron-based polymerization catalysts. *Organometallics,* **2009**, *28,* 3225-3232.

[57] Scott, J.; Gambarotta, S.; Korobkov, I.; Budzelaar, P. H. M. Reduction of (diiminopyridine)iron: Evidence for a non-cationic polymerization pathway. *Organometallics,* **2005**, *24,* 6298-6300.

[58] Sugiyama, H.; Gambarotta, S.; Yap, G. P. A.; Wilson, D. R.; Thiele, S. K. H. Preparation of an active neodymium catalyst for regioselective butadiene *cis*-polymerization supported by a dianionic modification of the 2,6-diiminopyridine ligand. *Organometallics,* **2004**, *23,* 5054-5061.

[59] Campora, J.; Perez, C. M.; Rodrıguez-Delgado, A.; Naz, A. M.; Palma, P.; Ivarez, A. E. Selective alkylation of 2,6-diiminopyridine ligands by dialkylmanganese reagents: A “one-pot” synthetic methodology. *Organometallics,* **2007**, *26,* 1104-1107.

[60] Darmon, J. M.; Turner, R. Z.; Lobkovsky, E.; Chirik P. J. Electronic effects in 4-substituted bis-(imino)pyridines and the corresponding reduced iron compounds. *Organometallics,* **2012**, *31*, 2275-2285.

[61] Lappalainen, K.; Yliheikkila, K.; Abu-Surrah, A. S.; Polamo, M.; Leskel, M.; Repo, T. Iron(II)- and cobalt(II) complexes with tridentate bis-(imino)pyridine nitrogen ligands bearing chiral bulky aliphatic and aromatic substituents: Crystal structure of [$CoCl_2${2,6-bis-[R-(bornylimino)methyl]pyridine}]. *Zeitschrift fur anorganische und* allgemeine *Chemie,* **2005**, *631*, 763-768.

[62] Hoogervorst, W. J.; Elsevier, C. J.; Lutz, M.; Spek, A. L. New cis- and trans-arylplatinum(II) acetylide compounds containing a bis-(imino)aryl [NCN] ligand. *Organometallics,* **2001**, *20,* 4437-4440.

[63] Hoyt, J. M.; Sylvester, K. T.; Semproni, S. P.; Chirik, P. J. Synthesis and electronic structure of Bis-(imino)pyridine iron metallacyclic intermediates in iron-catalyzed cyclization reactions. *Journal of the American Chemistry Society*, **2013**, *135*, 4862-4877.

[64] Bouwkamp, M. W.; Lobkovsky, E.; Chirik, P. J. Bis-(imino)pyridine iron(II) alkyl cations for olefin polymerization. *Journal of the American Chemistry Society*, **2005**, *127*, 9660-9661.

[65] Jamson, D. L.; Goldsby, K. A. 6-bis(N-pyrazolyl)pyridines: The convenient synthesis of a family of planar tridentates N3 ligands that are terpyridine analogs. *Journal of Organic Chemistry*, **1990**, *55*, 4992-4994.

[66] Kaul, F. A. R.; Puchta, G. T.; Schneider, H.; Bielert, F.; Mihalios, D.; Herrman, W. A.Immobilization of bis-(imino)pyridyliron(II) complexes on silica. *Organometallics,* **2002**, *21,* 74-82.

[67]. Gong, D.; Jia, X.; Wang, B.; Zhang, X.; Jiang, L. Synthesis, characterization, and butadiene polymerization of iron(III),iron(II) and cobalt(II) chlorides bearing 2,6-bis-(2-benzimidazolyl)pyridylor 2,6-bis-(pyrazol)pyridine ligand. *Journal of Organometallic Chemistry,* **2012**, *702*, 10-18.

[68] Hoogervorst, W. J.; Goubitz, K.; Fraanje, J.; Lutz, M.; Spek, A. L.; Ernsting, J. M.; Elsevier, C. J. Bis-(imino)aryl)rhodium(III) halide and methyl compounds. *Organometallics,* **2004**, *23,* 4550-4563.

[69] Bianchini. C.; Lee, H. M. Cyclopropanation of styrene with ethyl diazoacetate catalyzed by chiral and achiral ruthenium 2,6-bis-(imino)pyridyl complexes *Organometallics,* **2000**, *19,* 1833-1840.

[70] Darmon, J. M.; Stieber, S. C. E.; Sylvester, K. T.; Fernandez, I.; Lobkovsky, E.; Semproni, S. P.; Bill, E.; Wieghardt, K.; DeBeer, S.; Chirik, P. J. Oxidation of carbon-carbon bonds with a redox-active bis-(imino)pyridine iron complex. *Journal of the American Chemistry Society*, **2012**, *134*, 17125-17137.

[71] Chetia, B.; Iyer P. K. 2,6-Bis-(2-benzimidazolyl)pyridine as a chemosensor for fluoride ions. *Tetrahedron Letters,* **2008**, *49*, 94-97.

[72] Chetia, B.; Iyer, P. K. Utilization of 2,6-bis-(2-benzimidazolyl)pyridine to detect toxic benzene metabolites. *Tetrahedron Letters,* **2007**, *48*, 47-50.

[73] Deng, H.; Yu, Z.; Dong, J.; Wu, S. 2,6-Bis(3,5-dimethylpyrazol-1-yl)pyridine: A useful pseudo-N3 ligand in efficient ruthenium(II)-catalyzed transfer hydrogenation of ketones , *Organometallics,* **2005,** *24,* 4110-4112.

[74] Singh, A.; Chetia, B.; Mobin, S. M.; Das, G.; Iyer, P. K.; Mondal, B. Ruthenium monoterpyridine complexes with 2,6-bis-(benzimidazol-2-yl)pyridine: Synthesis, spectral properties and structure. *Polyhedron,* **2008**, *27*, 1983-1988.

[75] Nazeeruddin, M. K.; Kay, A.; Rodicio, I.; Humphry-Baker, R.; Muller, E.; Liska, P.; Vlachopoulos, N.; Gratzel, M. Converversion of light to electicity by cis-X2bis(2,2'-bipyridyl-4,4'-dicarboxylate)ruthenium(II) charge-transfer sensitizers (X= Cl^-, Br^-, I^-, CN^- and SCN^-) on nanocrystalline titanium dioxide electrodes. *Journal of the American Society*, **1993**, 115, 6382-6390.

[76]. Lee, H. J.; Chen, P.; Moon, S. J.; Sauvage, F.; Sivula, K.; Bessho, T.; Gamelin, D. R.; Comte, P.; Zakeeruddin, S. M.; Seok, S.; Gratzel, M.; Nazeeruddin, M. K. CdSe quantum dot (QD) and molecular dye hybrid sensitizers for TiO_2 mesoporous solar cells: working together with a common hole carrier of cobalt complexes. *Chemical Communications,* **2010**, *46*, 8788-8790.

[77] Andre, S. P.; Melina, K. I.; Yukie, M. I. N. Metal complex sensitizers in dye sensitized solar cells. *Coordination Chemistry Reviews*, **2004**, *48*, 1343-1361.

[78] Adeloye, A. O.; Ajibade, P. A. Synthesis and characterization of a Ru(II) complex with functionalized phenanthroline ligands having single-double linked anthracenyl and 1-methoxy-1-buten-3-yne moieties. *Molecules,* **2010**, *15*, 7570-7581.

[79] Wu, K. L.; Li, C. H.; Chi, Y.; Clifford, J. N.; Cabau, L.; Palomares, E.; Cheng, Y. M.; Pan, H. A.; Chou, T. P. Dye molecular structure device open-circuit voltage correlation in Ru(II) sensitizers with heteroleptic tridentate chelates for dye-sensitized solar cells. *Journal of the American Chemical Society*, **2012**, *134*, 7488-7496.

[80] Lobello, M. G.; Wu, K. L.; Reddy, A.M.; Marotta, G.; Gratzel, M.; Nazeeruddin, M. K.; Chi, Y.; Chandrasekharam, M.; Vitillaro, G.; De Angelis, F. Engineering of Ru(II) dyes for interfacial and light-harvesting optimization. *Dalton Transactions*, **2014**, *43*, 2726-2732.

[81] Adeloye, A. O.; Olomola, T. O.; Adebayo, A. I.; Ajibade, P. A. A high molar extinction coefficient bisterpyridyl homoleptic Ru(II) complex with *trans*-2-methyl-2-butenoic acid functionality: Potential dye for dye-sensitized solar cells**,** *International Journal of Molecular Science*, **2012**, *13*, 3511-3526.

[82] Yum, J. H.; Baranoff, E.; Kessler, F.; Moehl, T.; Ahmad, S.; Bessho, T.; Marchioro, A.; Ghadiri, E.; Moser, E. J. E.; Yi, C.; Nazeeruddin, M. K.; Gratzel, M. A cobalt complex redox shuttle for dye-sensitized solar cells with high open-circuit potentials. *Nature,* **2001**, *414*, 338-344.

[83] Kim, H. S.; Lee, C. R.; Im, J. H.; Lee, K. B.; Moehl, T.; Marchioro, A.; Moon, S. J.; Humphry-Baker, R.; Yum, J. H.; Moser, J. E.; Gratzel, M.; Park, N. Lead iodide perovskite sensitized all-solid-state submicron thin film mesoscopic solar cell with efficiency exceeding 9%. *Scientific Reports*, **2012**, *2*, 591-597.

[84] Nusbaumer, H.; Zakeeruddin, S. M.; Moser, J. E.; Gratzel, M. An alternative efficient redox couple for the dye-sensitized solar cells system. *European Journal of Chemistry*, **2003**, *9*, 3756-3763.

[85] Lee, H. J.; Chen, P.; Moon, S. J.; Sauvage, F.; Sivula, K.; Bessho, T.; Gamelin, D. R.; Comte, P.; Zakeeruddin, S. M.; Seok, S.; Nazeeruddin, M. K.; Gratzel, M. Regenerative PbS and CdS quantum dot sensitized solar cells with a cobalt complex as hole mediator. *Langmuir,* **2009**, *25*, 7602-7608.

[86] Klahr, B. M.; Hamann, T. W. Performance enhancement and limitations of cobalt bipyridyl redox shuttles in dye-sensitized solar cells. *Journal of Physical Chemistry C,* **2009**, *113,* 14040-14045.

[87] Nelson, J. J.; Amick, T. J.; Elliott, M. C. Mass transport of polypyridyl cobalt complexes in dye-sensitized solar cells with mesoporous TiO_2 photoanodes. *Journal of Physical Chemistry C,* **2008**, *112,* 18255-18263.

[88] Nusbaumer, H.; Moser, J. E.; Zakeeruddin S. M.; Nazeeruddin, M. K.; Gratzel, M.

$Co(dbbip)_2^{2+}$ complex rivals tri-iodide/Iodide redox mediator in dye-sensitized photovoltaic cells. *Journal of Physical Chemistry B,* **2001**, *105,* 10461-10464.

[89] Feldt, S. M.; Wang, G.; Boschloo, G.; Hagfeldt, A. Effects of driving forces for recombination and regeneration on the photovoltaic performance of dye-sensitized solar cells using cobalt polypyridine redox couples. *Journal of Physical Chemistry C*, **2011**, *115*, 21500-21507.

[90] Pollander, L. E.; Yella, A.; Curchod, B. F. E.; Ashari Asani, N.; Teuscher, J.; Scopelliti, R.; Gao, P.; Mathew, S.; Moser, J. S.; Tavernelli, I.; Rothlisberger, U.; Gratzel, M.; Nazeeruddin, M. K.; Frey. J. Towards compatibility between ruthenium sensitizers and cobalt electrolytes in dye-sensitized solar cells. *Angewandte Chemie*, **2013**, *52*, 8731-8735.

[91] Yum, J. H.; Baranoff, E.; Kessler, F.; Moehl, T.; Ahmad, S.; Bessho, T.; Marchioro, A.; Ghadiri, E.; Moser, J. E.; Yi, C.; Nazeeruddin, M. K.; Gratzel, M. A cobalt complex redox shuttle for dye-sensitized solar cells with high open-circuit potentials. *Nature Communications*, **2012**, *631*, 1655-1662

[92] Clifford, J. N.; Planell, M.; Palomares, E. Advances in high efficiency dye sensitized solar cells based on Ru(II) free sensitizers and a liquid redox electrolyte. *Journal of Materials Chemistry,* **2012**, *22*, 24195-24201.

CHAPTER 2

2.0 EXPERIMENTAL

2.1 Chemicals and solvents

$RuCl_3 \cdot 3H_2O$, $CoCl_2 \cdot 6H_2O$, 1,2-phenylenediamine, polyphosphoric acid, pyridine-2,6-carboxylic acid, ammonium solution, pyrazole, 2,5-dimethylpyrazol, sodium hydrate, 2,6-dichloropyridine-4-carboxylic acid, $MgSO_4$, potassium hydroxide, potassium thiocynate, DMF, DMSO, acetone, ethanol, bromobezene, chlorobut-2-ane, THF, dichloromethane and diethyl ether, all the chemicals were bought from Sigma Aldrich.

2.2 Characterization techniques

2.2.1 FTIR spectroscopy

The FTIR spectra of different nitrogen chelating ligands and complexes (as KBr pellets) were obtained by using Perkin-Elmer Paragon 2000 spectrophotometer at 370 cm^{-1} to 4400 cm^{-1} range.

2.2.2 UV-Vis spectroscopy

Uv-Vis spectra of ligands and complexes were recorded on a 1 cm path length quartz cell on a Perkin-Elmer Lambda 25 UV-Vis spectrophotometer using DMSO as a solvent.

2.2.3 NMR spectroscopy

^{1}H NMR and ^{13}C NMR spectra were recorded on a Buker EMX 400 MHz spectrophometer.

2.2.4 Melting point

The melting point of the compounds was determined using Stuart melting point apparatus.

2.2.5 Electrochemistry

Cyclic voltammetry measurements were obtained using Autolab potentiostat with three electrodes, glassy carbon working electrode, Ag/AgCl reference electrode and Pt counter electrode. The potential range was +1.5 to -1.5 at a scan rate of 100 mVs^{-1}. The three electrode were immersed in 0.5 mM of cobalt(II) and ruthenium(II) solution in water with 0.1 M of phosphate buffer solution (PBS) as a supporting electrolyte. Bubbling nitrogen gas purged through the solution for 15 minutes to remove interfering oxygen gas during the measurements deoxygenated the solutions. After each measurement, the working electrode was cleaned with alumina and water on a felt pad and rinsed with water.

2.2.6 Solar cell fabrication

Scotch tape was put on the conducting side of Indium Tin Oxide (ITO), TiO_2 paste and flattens it with a razor blade on the same side of the ITO glass. The electrode was put

on top of a hot plate and heated at 450 °C for 30 minutes. The concentration of the dye solution was 0.3 mM. TiO_2 electrode was dipped into the dye solution for 10 minutes. Pt plate electrode with a hole was put on top of a hot plate at 450 °C for 10 minutes to activate the electrode. The TiO_2/dye electrode was taken out from the dye solution and washed with fresh ethanol and allowed to dry. The two electrodes were combined and a sealer was placed between the two electrodes and clipped with a blinder then heated at 70 °C for 15 minutes. After cooling, electrode construct was filled with electrolyte and the hole was sealed with a cap sealer. A solar analyzer was used to characterize the cells.

2.3 Preparation of nitrogen chelating ligands

2.3.1 Preparation of 2,6-bis(2-benzimidazolyl)pyridine (L_1).

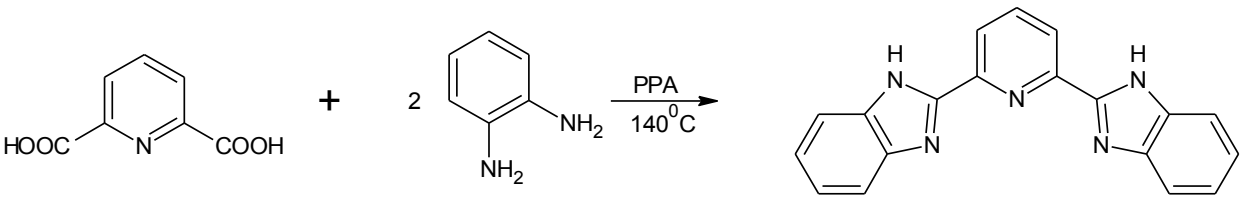

Scheme 3. Synthesis of 2,6-bis(2-benzimidazolyl)pyridine.

The ligand 2,6-bis(2-benzimidazolyl)pyridine (L_1) was synthesized according to Singh and co-workers procedure [1]. Under nitrogen, pyridine-2,6-dicarboxylic acid (1.7 g, 13 mmol) and 1,2-phenylenediamine (2.13 g, 26.4 mmol) were added to 3.9 g of polyphosphoric acid. The mixture was refluxed while stirring at 150 °C for 6 h. The

mixture was cooled to 90°C and poured into 50 mL of water. Subsequently, the mixture was neutralized to pH 8 with ammonium solution. The resultant white solid was collected by filtration and repeatedly washed with methanol. The equation of the reaction is as shown in Scheme 3. Yield: 3.23g, 79%, m.p. 180°C, IR (KBr pellet) υ(cm^{-1}): 3208, 3105, 2822, 2364, 2208, 1945, 1716,1675,1725, 1517,1462, 1206, 1067, 896, 533.

2.3.2 Preparation of 2,6-bis(1-but-2-ylbenzimidazol-2-yl)pyridine (L_2).

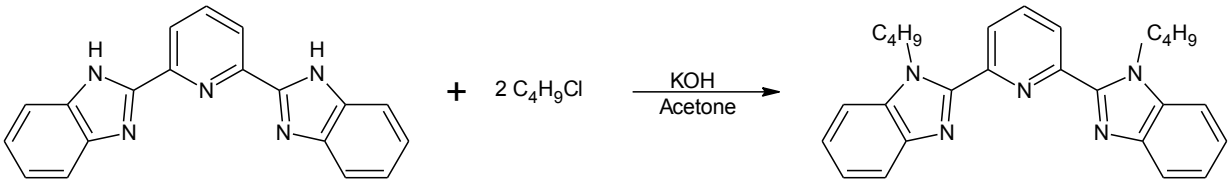

Scheme 4. Synthesis of 2,6-bis(but-2-ylbenzimidazol-2-yl)pyridine.

The synthesis of 2,6-bis(1-but-2-ylbenzimidazol-2-yl)pyridine (**L_2**) (Figure 4) was done using the synthetic route reported by Gong and co-workers [2]. The alkylation of **L_1** was done as shown in Scheme 4. 2-chlorobutane (1.2 g, 7.71 mmol), 2,6-bis-(2-benzimidazolyl)pyridine (**L_1**) (1.2 g, 3.85 mmol) and KOH (0.28 g, 4.98 mmol) were dissolved in 30 mL of acetone and refluxed for 4 h at 35°C. After cooling an equal amount was added to the mixture, which was extracted by dichloromethane, the organic layer was dried over $MgSO_4$ and evaporated to dryness [2]. Yield 1.11g, 68%, m.p. 180°C, IR (KBr pellet) υ(cm^{-1}): 3235, 2370, 2270, 2201, 1937, 1622, 1460, 1091, 791, 618.

2.3.3 Preparation of 2,6-bis(1-benzylbenzimidazol-2-yl)pyridine (L_3).

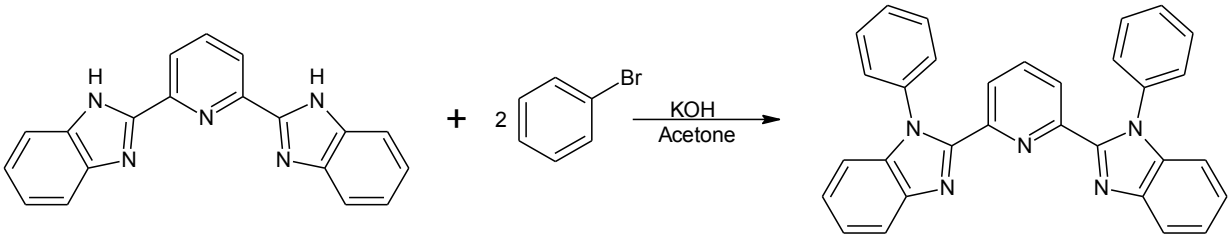

Scheme 5. Synthesis of 2,6-bis(benzylbenzimidazol-2-yl)pyridine.

The preparation of of 2,6-bis(1-benzylbenzimidazol-2-yl)pyridine (**L_3**) (Scheme 5) was similar to the method reported for **L_2** (section 2.3.2). Bromobenzene (0.71 g, 7.71 mmol), 2,6-bis-(2-benzimidazolyl)pyridine (1.2 g, 3.85 mmol) (**L_1**) and KOH (0.28 g, 4.98 mmol) were dissolved in 30 mL of acetone and refluxed for 4 h at 35°C. After cooling the mixture an equal amount was added to the mixture, which was extracted by dichloromethane, the product obtained was dried over $MgSO_4$ and evaporated to dryness [2]. Yield: 1.22g, 68%, m.p. 172°C, IR (KBr pellet) υ(cm^{-1}): 3237, 2983, 2904, 1924, 1623, 1400, 1069, 883, 757, 757, 622, 555.

2.3.4 Preparation of 2,6-bis(pyrazol)pyridine (L_4)

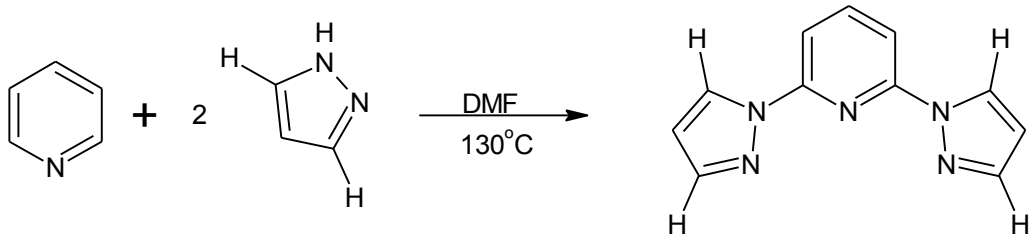

Scheme 6. Preparation of 2,6-bis(pyrazol)pyridine (L_4)

The method used for synthesis 2,6-bis(pyrazol)pyridine (**L_4**) was adopted from Abbo and Titinchi's procedure [3]. Pyrazole (1.2 g, 17.6 mmol) was placed in DMF 30 mL in a 100mL round bottom flask, sodium hydrate (0.422 g, 17.6 mmol) was added to the mixture. The mixture was stirred under nitrogen at 50 °C for 20 minutes. 2,6-dichloropyridine-4-carboxylic acid (1.39 g, 5.86 mmol) was added and refluxed for 24 h at 130°C. The reaction was carried out as presented in (Scheme 6). After cooling the mixture 25 mL of water was added which was extracted with dichloromethane. The organic layer was dried over $MgSO_4$ and evaporated to dryness [3]. Yield: 0.91g, 73 %, m.p. 80°C, IR (KBr pellet) υ(cm^{-1}): 3365, 2976, 2394, 2364,1994, 1664, 1395, 1253, 1043, 831,763, 613.

2.3.5 Preparation of 2,6-bis(3,5-dimethylpyrazol)pyridine (L_5).

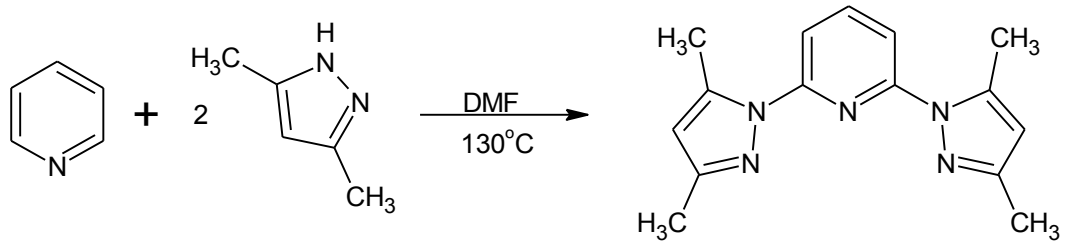

Scheme 7. Synthesis of 2,6-bis(3,5-dimethylpyrazolyl)pyridine.

2,6-bis(3,5-dimethylpyrazol)pyridine, L_5 (Scheme 7) was prepared in a similar method used for **L_4** (section 2.3.4). 3,5-dimethypyrazole (1.3 g, 13.5 mmol) was placed in DMF 30 mL in a 100 mL round bottom flask, sodium hydrate (0.33 g, 13.5 mmol) was added to the mixture. The reaction was carried out under nitrogen at 50 °C for 20 minutes, 2,6-dichloropyridine-4-carboxylic acid (1.07 g, 4.5 mmol) was added and refluxed for 24 h at 130 °C. After cooling the mixture 25mL of water was added to the mixture that was extracted with dichloromethane. The product was dried over $MgSO_4$ and evaporated to dryness [3]. Yield: 0.83g, 69%, m.p. 82°C, IR (KBr pellet) υ(cm^{-1}): 3410, 3198, 2903, 2552, 2366, 1608, 1306, 1161, 1090, 841, 714, 621, 437.

2.4 Preparation of Ruthenium (II) precursor [$RuCl_2(DMSO)_4$].

$$RuCl_3 \cdot 3H_2O \xrightarrow[\text{Reflux, 5 min}]{\text{DMSO}} [RuCl_2(DMSO)_4] \quad \text{.....8}$$

The ruthenium precursor was prepared using Bianchi's method [4]. $RuCl_3 \cdot 3H_2O$ (1g, 1.9 mmol) of was refluxed at 130 °C in DMSO 8 mL for 20 minutes in air. The reaction is as

shown in equation 8. The solution changed from dark to light yellow and bright yellow precipitate was formed during cooling then 30 mL acetone was added and a yellow precipitate was filtered off washed three times with times with acetone.

2.5 Synthesis of ruthenium(II) complexes.

2.5.1 Synthesis of $[RuL_1L_0(NCS)_2]$ (C_1)

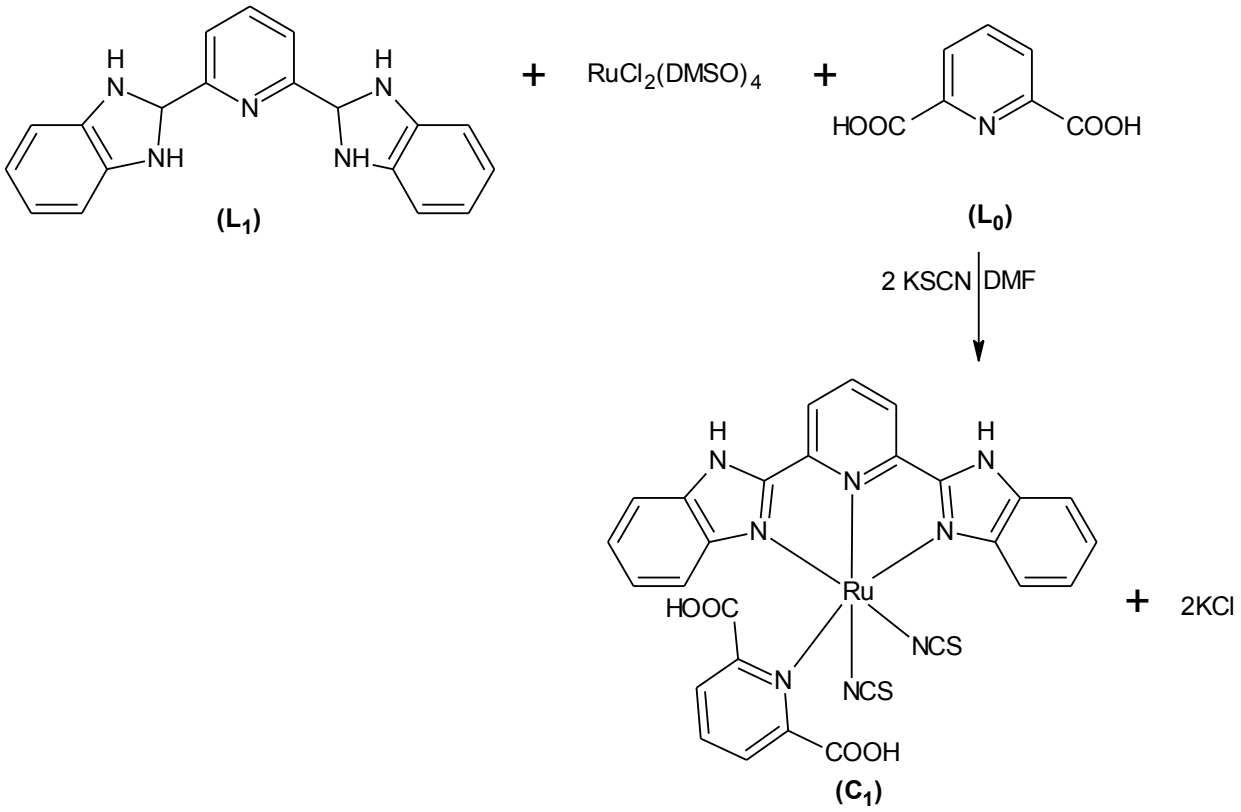

Scheme 8. Synthesis of $[RuL_1L_0(NCS)_2]$

The method used to synthesize **C_1** (Scheme 8) was adopted from Adeloye and Ajibade procedure [5]. Under nitrogen, 2,6-bis-(2-benzimidazolyl)pyridine (**L_1**) (0.12 g, 0.206 mmol) and [$RuCl_2(DMSO)_4$] (0.2 g, 0.206 mmol) were dissolved in 25 mL of DMF. The mixture was refluxed in the dark for 4 h, pyridine-2,6-dicarboxylic acid (0.069 g, 0.206 mmol) was added to the mixture and refluxed for 2 h. After 2h excess potassium thiocynate was added to the mixture and refluxed for 8 h. The reaction mixture was cooled at room temperature, the DMF was evaporated under vacuum. The residue was suspended in diethyl ether, the brown solid was filtered under vacuum, rinsed with diethyl ether and dried under vacuum [5]. Yield: 89 mg, 62%, m.p. 220°C, IR (KBr pellet) υ(cm^{-1}): 3409, 3244, 2839, 2374, 2122, 2084, 1620, 1464, 1400, 1397, 1308, 1109, 1068, 818, 622.

2.5.2 Synthesis of $[RuL_2L_0(NCS)_2]$ (C_2).

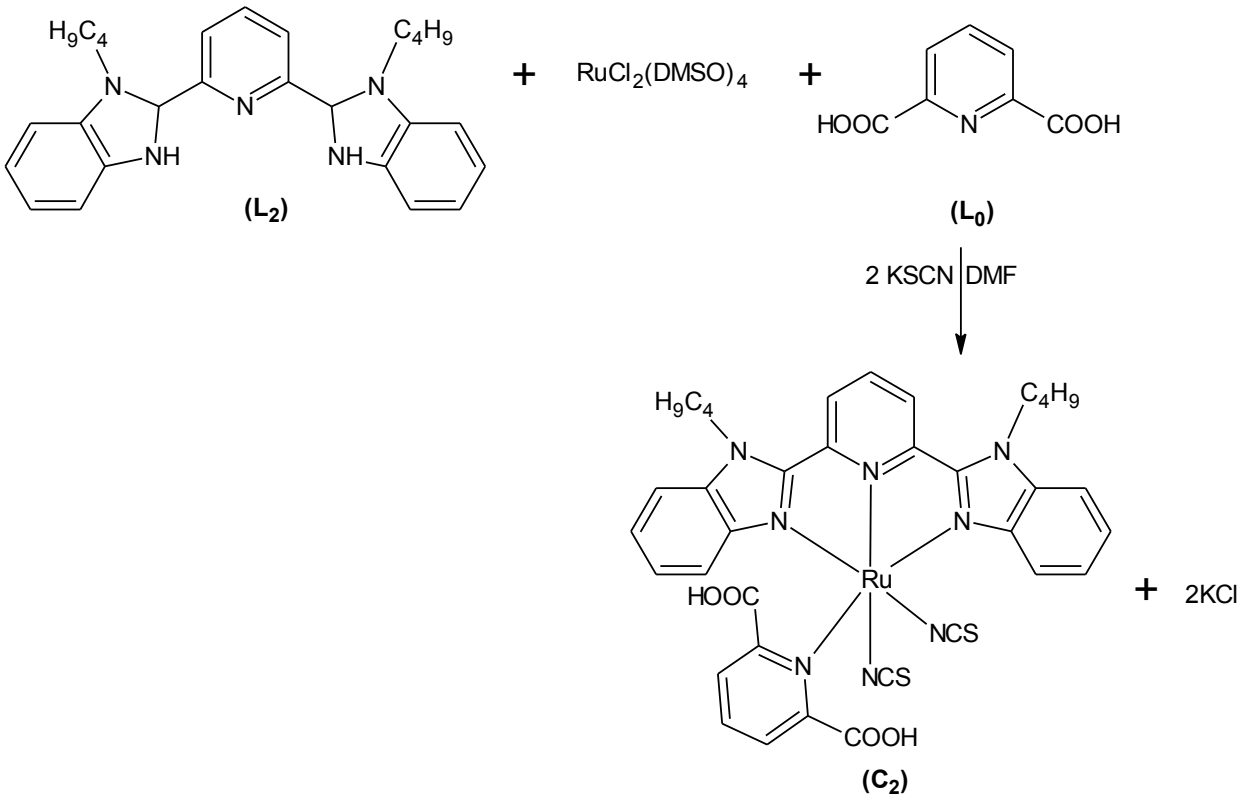

Scheme 9. Synthesis of $[RuL_2L_0(NCS)_2]$

The synthesis of $\mathbf{C_2}$ (Scheme 9) was carried out in a similar method used for $\mathbf{C_1}$ (section 2.5.1). 2,6-bis-(butylbenzimidazolyl)pyridine (0.175 g, 0.206 mmol) and $[RuCl_2(DMSO)_4]$ (0.2 g, 0.206 mmol) were placed in 25 mL of DMF. The mixture was refluxed under nitrogen in the dark, after 4 h pyridine-2,6-dicarboxylic acid (0.069 g, 0.206 mmol) was added to the mixture then excess potassium thiocynate was added after 2 h. The mixture was refluxed for 8 h, after cooling down the reaction medium at room temperature, the DMF was evaporated under vacuum. The product was suspended in diethyl ether, the brown solid was filtered under vacuum, rinsed with diethyl ether and

dried under vacuum [5]. Yield: 106 mg, 64%, m.p. 212°C, IR (KBr pellet) ν(cm^{-1}): 3424, 2821, 2366, 2343, 2068, 1869, 1635, 1400, 1291, 1117, 1015, 839, 758, 618, 536, 472.

2.5.3 Synthesis of [$RuL_3L_0(NCS)_2$] (C_3).

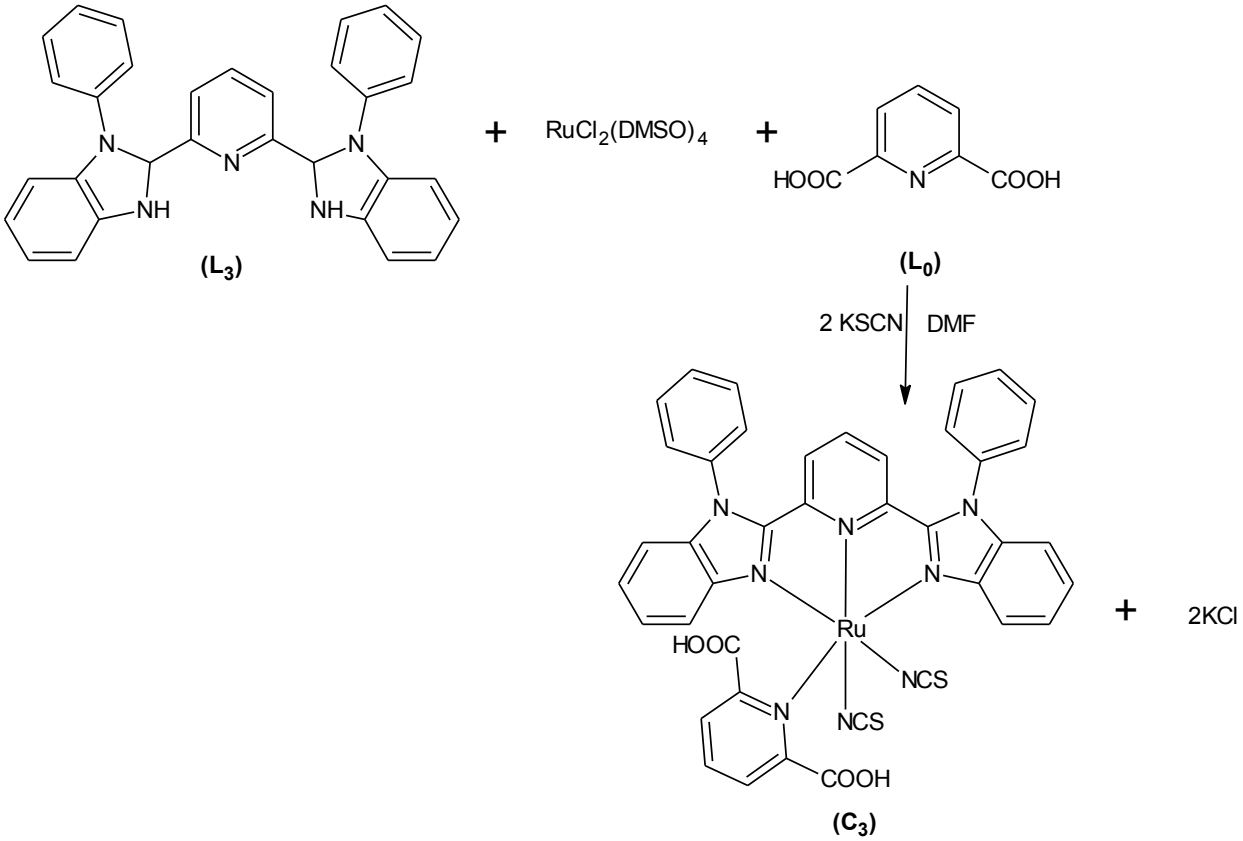

Scheme 10. Synthesis of [$RuL_3L_0(NCS)_2$]

The synthesis of **C_3** (Scheme 10) was carried out using method similar to the one used for **C_1.** 2,6-bis-(benzylbenzimidazolyl)pyridine (0.191 g, 0.206 mmol) and [$RuCl_2(DMSO)_4$] (0.2g, 0.206 mmol) were placed in 25 mL of DMF under nitrogen and

refluxed for 4 h. Pyridine-2,6-dicarboxylic acid (0.069 g, 0.206 mmol) was added to the mixture, after 2 h excess potassium thiocynate was added and refluxed for 8 h. The reaction mixture was allowed to cool at room temperature, the solvent was removed under vacuum. The residue was precipitated in diethyl ether, the final product was filtered under vacuum, rinsed with diethyl ether and dried under vacuum. Yield: 47 mg, 27%, m.p. 210°C, IR (KBr pellet) υ(cm^{-1}): 3429, 2955, 2819, 2359, 2124, 2067, 1978, 1646, 1510, 1377, 1116, 1019, 618, 538.

Synthesis of $[RuL_4L_0(NCS)_2]$ (C_4).

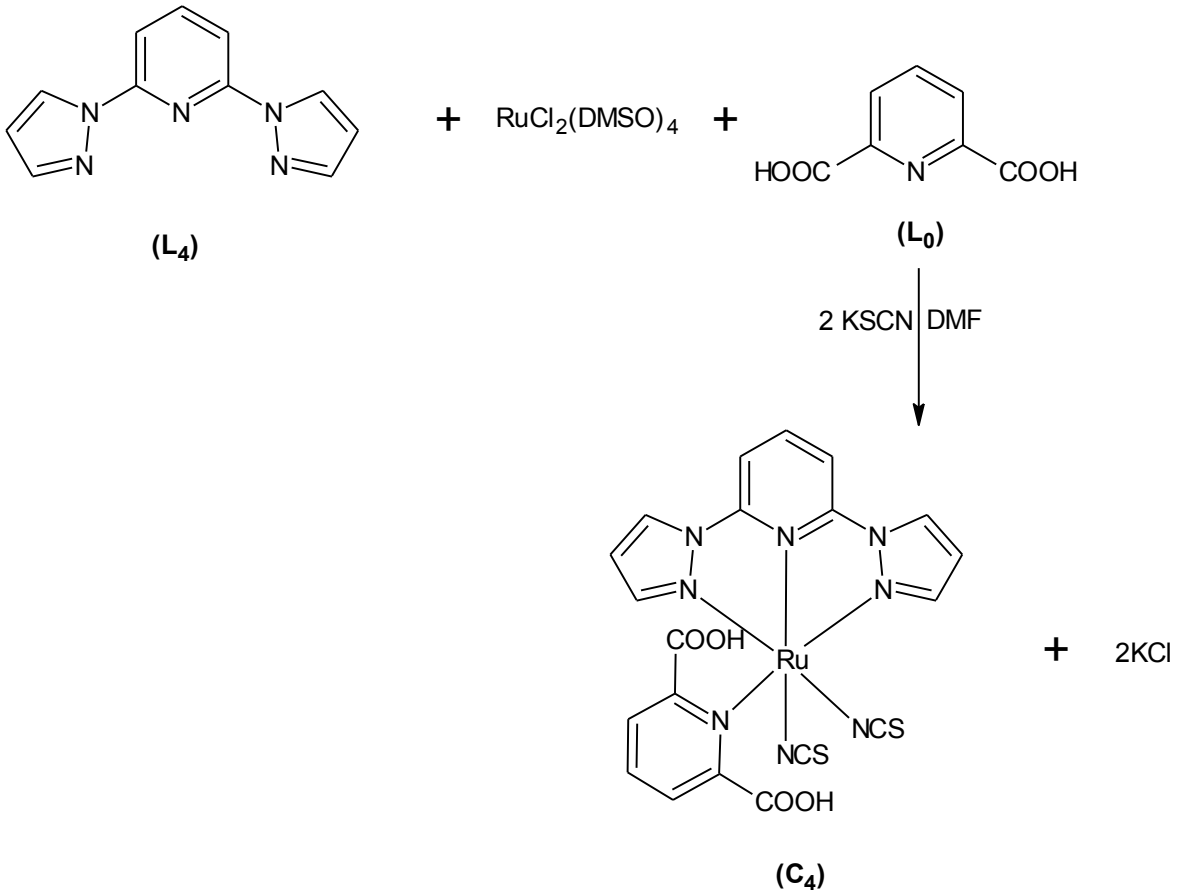

(L_4) (L_0) (C_4)

Scheme 11. Synthesis of $[RuL_4L_0(NCS)_2]$

The synthesis of **C_4** (Scheme 11) was carried out with similar method used for synthesis of **C_1** (section 2.5.4). Under nitrogen, 2,6-bis-(pyrazolyl)pyridine (0.087 g, 0.206 mmol) and $[RuCl_2(DMSO)_4]$ (0.2 g, 0.206 mmol) were dissolved in 25 mL of DMF and refluxed, the reaction was carried out in the dark under nitrogen. After 4 h pyridine-2,6-dicarboxylic acid (0.069g, 0.206 mmol) was added to the mixture, then excess potassium thiocynate was added was added to the mixture and refluxed for 8 h. The

reaction mixture was cooled at room temperature, the DMF was evaporated under vacuum. The product was filtered after precipitation with diethyl ether.

Yield: 63.8 mg, 52%, m.p. 235°C, IR (KBr pellet) υ(cm^{-1}): 3417, 2971, 2971, 2949, 2842, 2368, 2126, 2067, 1869, 1638, 1454, 1397, 1112, 1055, 1016, 619, 477.

2.5.5 Synthesis of $[RuL_5L_0(NCS)_2]$ (C_5).

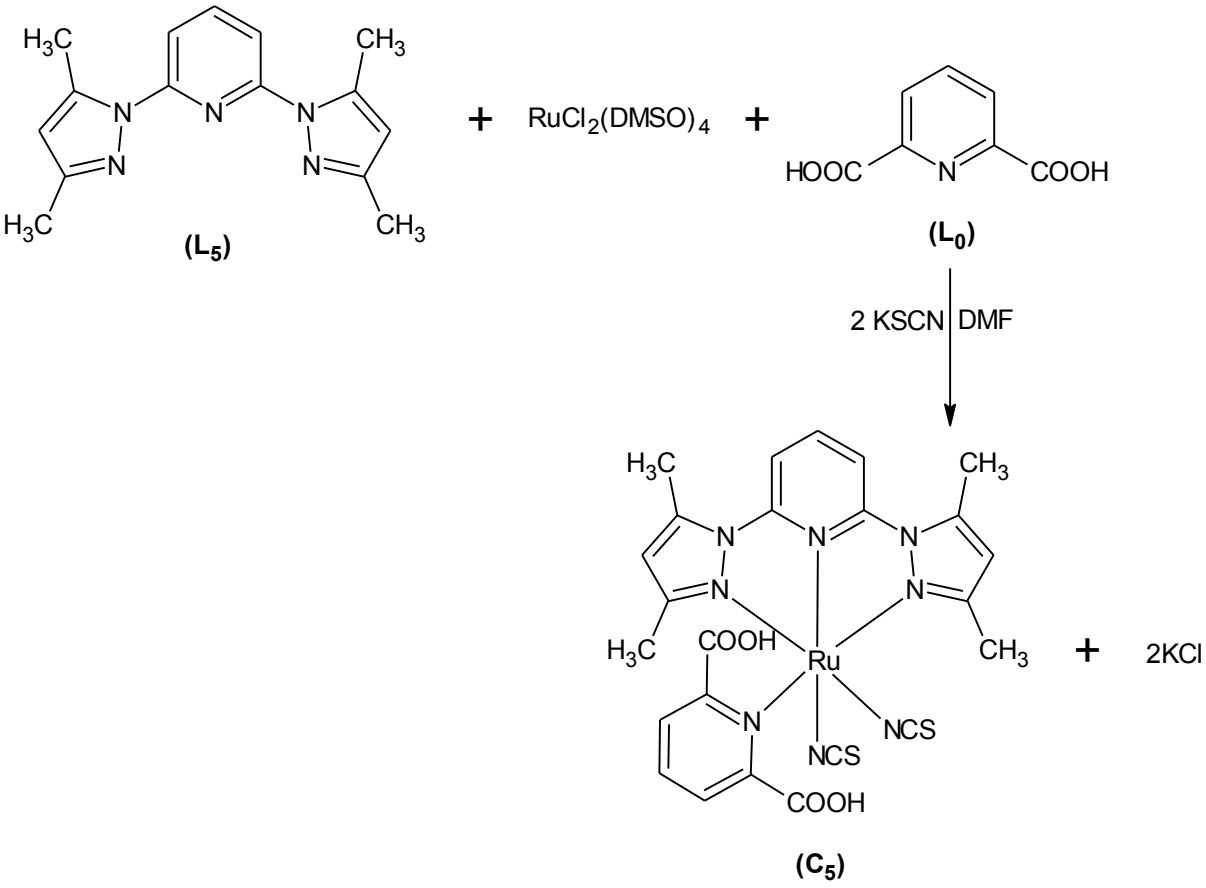

Scheme 12. Synthesis of $[RuL_5L_0(NCS)_2]$

The complex, $\mathbf{C_5}$ was prepared using similar method for the synthesis of $\mathbf{C_1}$ (section 2.5.1). 2,6-bis-(3,5-dimethylzolyl)pyridine (0.11 g, 0.206 mmol) and $[RuCl_2(DMSO)_4]$ (0.2 g, 0.206 mmol) were added and the mixture was refluxed in 25 mL DMF for 4h. Pyridine-2,6-dicarboxylic acid (0.069 g, 0.206 mmol) was added to the reaction mixture then after 2 h excess potassium thiocynate was added and refluxed for 8 h. The equation for synthesis of $\mathbf{C_5}$ is shown in Scheme 12. The mixture was cooled at room

temperature and DMF was evaporated under vacuum. The product was precipitated with diethyl ether, the brown solid finally was filtered and dried under vacuum**.** Yield: 57.7mg, 43%, m.p. 230°C, IR (KBr pellet) ν(cm^{-1}): 3424, 2949, 2839, 2365, 2069, 1870, 1646, 1454, 1398, 1113, 1054, 1020, 619, 539.

2.6 Synthesis of cobalt(II) complexes

2.6.1 Synthesis of $[CoL_1L_0(NCS)_2]$ (C_6).

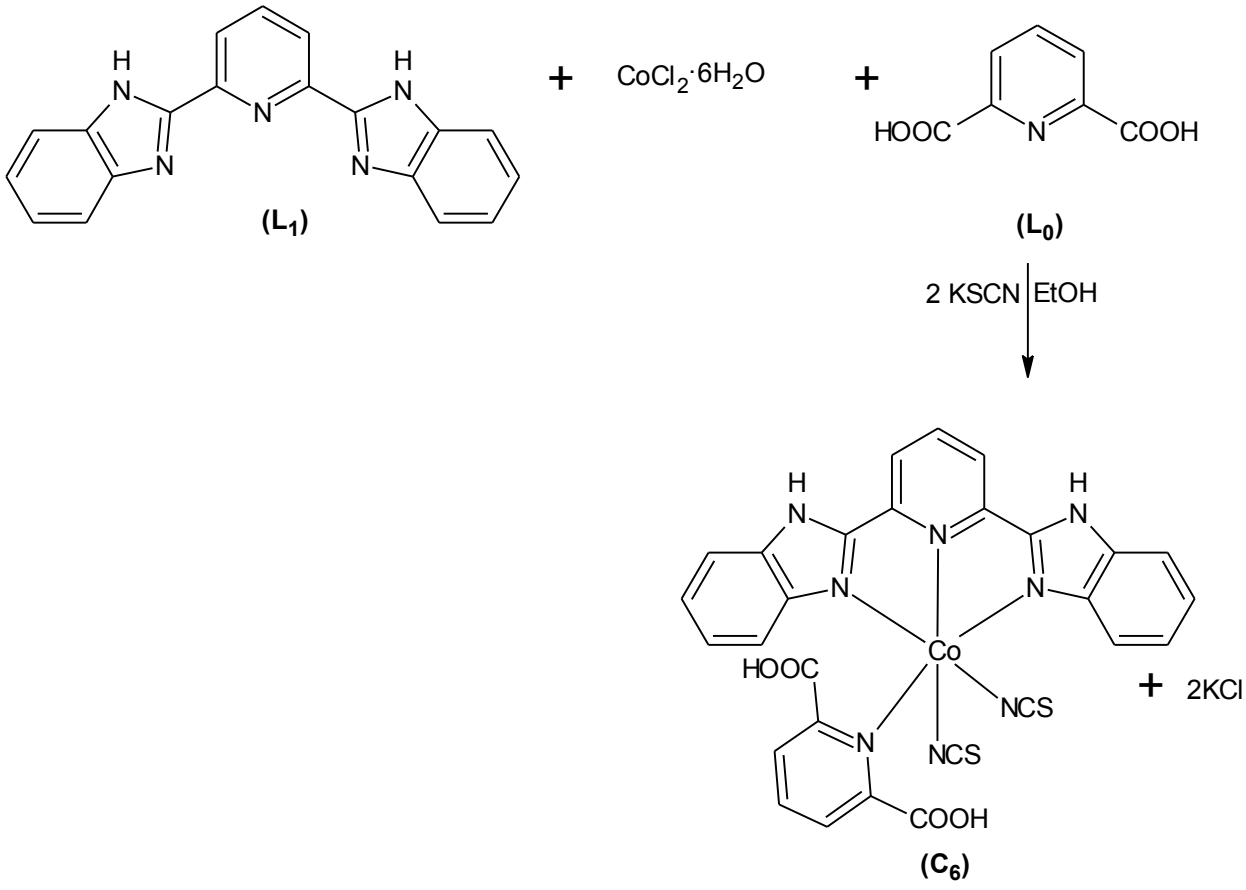

Scheme 13. Synthesis of $[CoL_1L_0(NCS)_2]$

[$CoCl_2 \cdot 6H_2O$] (0.2 g, 0.841 mmol) and 2,6-bis-(benzimidazolyl)pyridine (0.262 g, 0.841 mmol) were dissolved in a minimal amount of ethanol. The solution was left to stir at reflux for 3 h. After 3 h pyridine-2,6-dicarboxylic acid (0.140 g, 0.841 mmol) was added to the mixture then excess potassium thiocynate (0.327 g, 3.364 mmol) was added after 2 h. The mixture was refluxed for 4 h, after cooling down the reaction medium at room temperature, ethanol was evaporated under vacuum diethyl ether was added to the solution to precipitate the compound. The product was then filtered and washed with, ethanol, and diethyl ether; dried under vacuum [6]. Yield: 0.4g, 74%, m.p. 240°C, IR (KBr pellet) υ(cm^{-1}): 3415, 3235, 2839, 2374, 2122, 2067, 1634, 1464, 1398, 1308, 1115, 1058, 1017, 618, 540, 473.

2.6.2 Synthesis of $[CoL_2L_0(NCS)_2]$ (C_7).

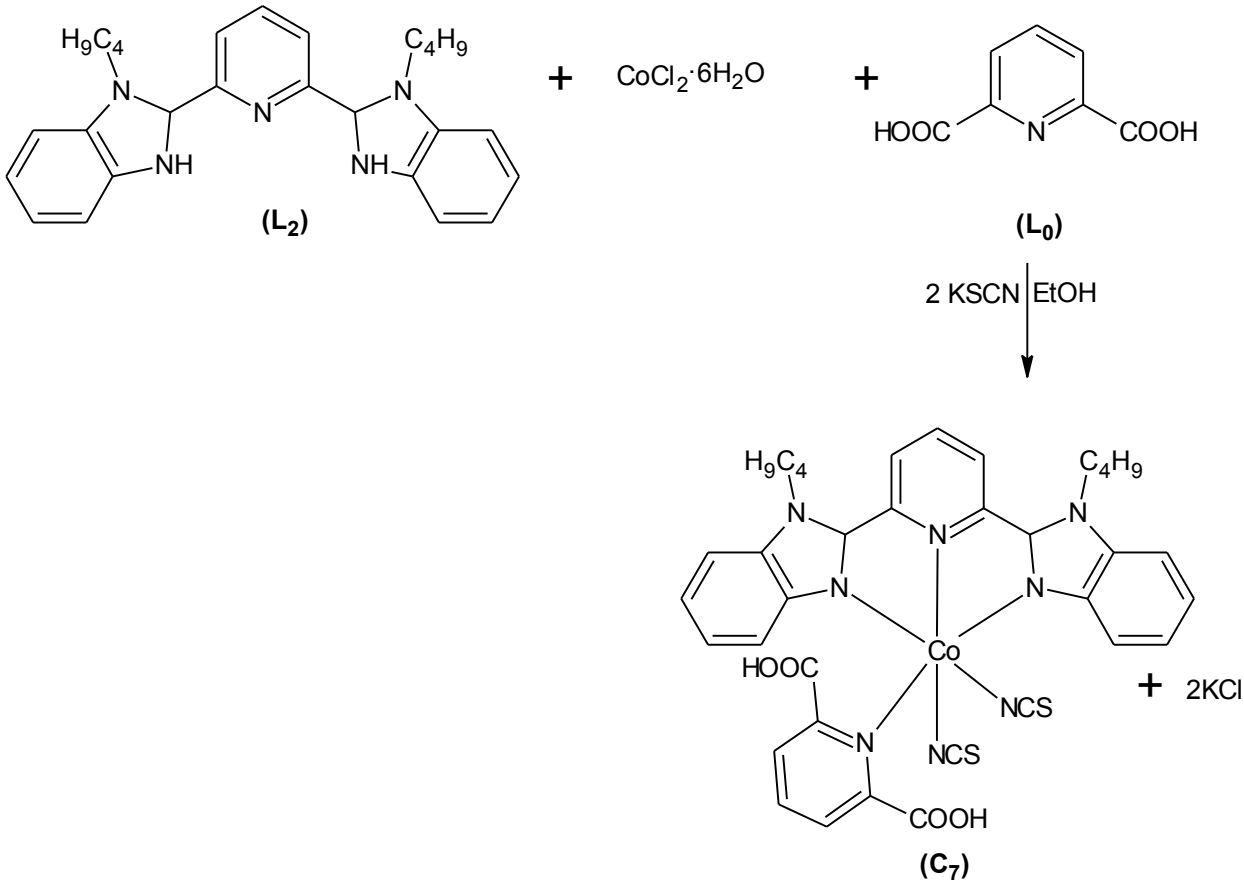

Scheme 14. Synthesis of $[CoL_2L_0(NCS)_2]$

The complex, **C_7** was prepared in a similar method as reported for **C_6** (section 2.6.1) $[CoCl_2·6H_2O]$ (0.2 g, 0.841 mmol) and 2,6-bis-(2-butylmidazolyl)pyridine (0.356 g, 0.841 mmol) were dissolved and refluxed for 3 h. After 3 h pyridine-2,6-dicarboxylic acid (0.140 g, 0.841 mmol) was added and refluxed for 2 h. Excess potassium thiocynate (0.327 g, 3.364 mmol) was added to and reaction mixture and was also added and refluxed for 4 h. The equation for the reaction is as shown in Scheme 14. After cooling

down the reaction medium at room temperature, ethanol removed by rotatory evaporator, diethyl ether was added to the solution to precipitate the compound. The product obtained was filtered, washed with ethanol then diethyl ether and dried under vacuum [6]. Yield: 0.46g, 72%, m.p. 242°C, IR (KBr pellet) ν(cm^{-1}): 3418, 2839, 2374, 2170, 2068, 1869, 1623, 1427, 1304, 1291, 1102, 1015, 839, 750, 618, 536, 422.

2.6.3 Synthesis of $[CoL_3L_0(NCS)_2]$ (C_8).

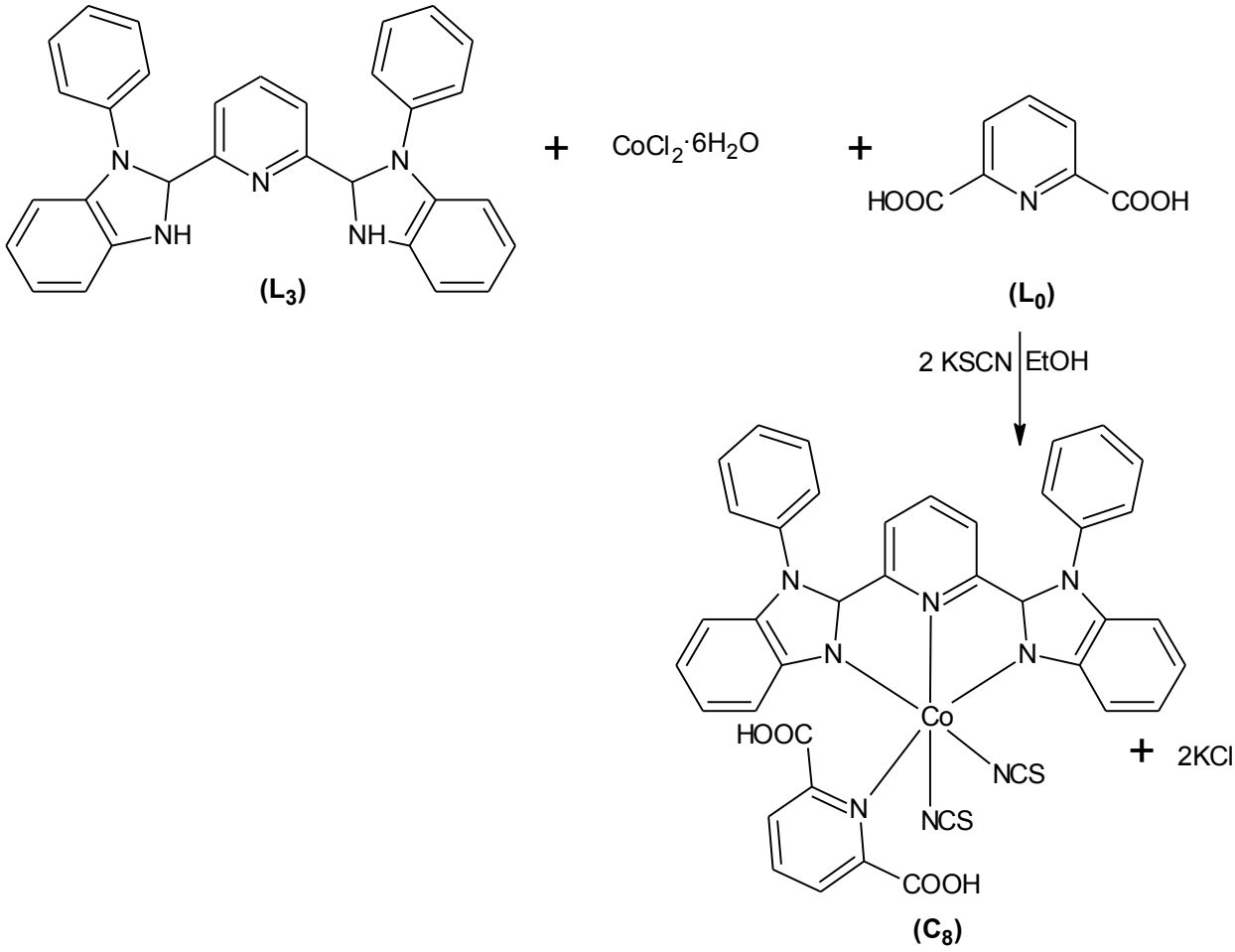

Scheme 15. Synthesis of $[CoL_3L_0(NCS)_2]$

The synthesis of **C_8** (Scheme 15) was carried out using similar method reported for **C_6** (section 2.6.1). [$CoCl_2 \cdot 6H_2O$] (0.2 g, 0.841 mmol) and 2,6-bis-(2-buytlbenzimidazolyl)pyridine (0.389 g, 0.841 mmol) were added and refluxed for 3 h. Pyridine-2,6-dicarboxylic acid (0.140 g, 0.841 mmol) was added to the mixture and refluxed for 2h then excess potassium thiocynate (0.327 g, 3.364 mmol) was added and refluxed for 4h. The reaction was allowed to cool at room temperature then ethanol was evaporated under vacuum. The product obtained after precipitation with diethyl ether was filtered and washed with, ethanol, and diethyl ether; dried under vacuum [6]. Yield: 0.42g, 62%, m.p. 240°C, IR (KBr pellet) υ(cm^{-1}): 3415, 3235, 2496, 2368, 1622, 1394, 1283, 1075, 917, 776, 733, 619, 541.

2.6.4 Synthesis of $[CoL_4L_0(NCS)_2]$ (C_9).

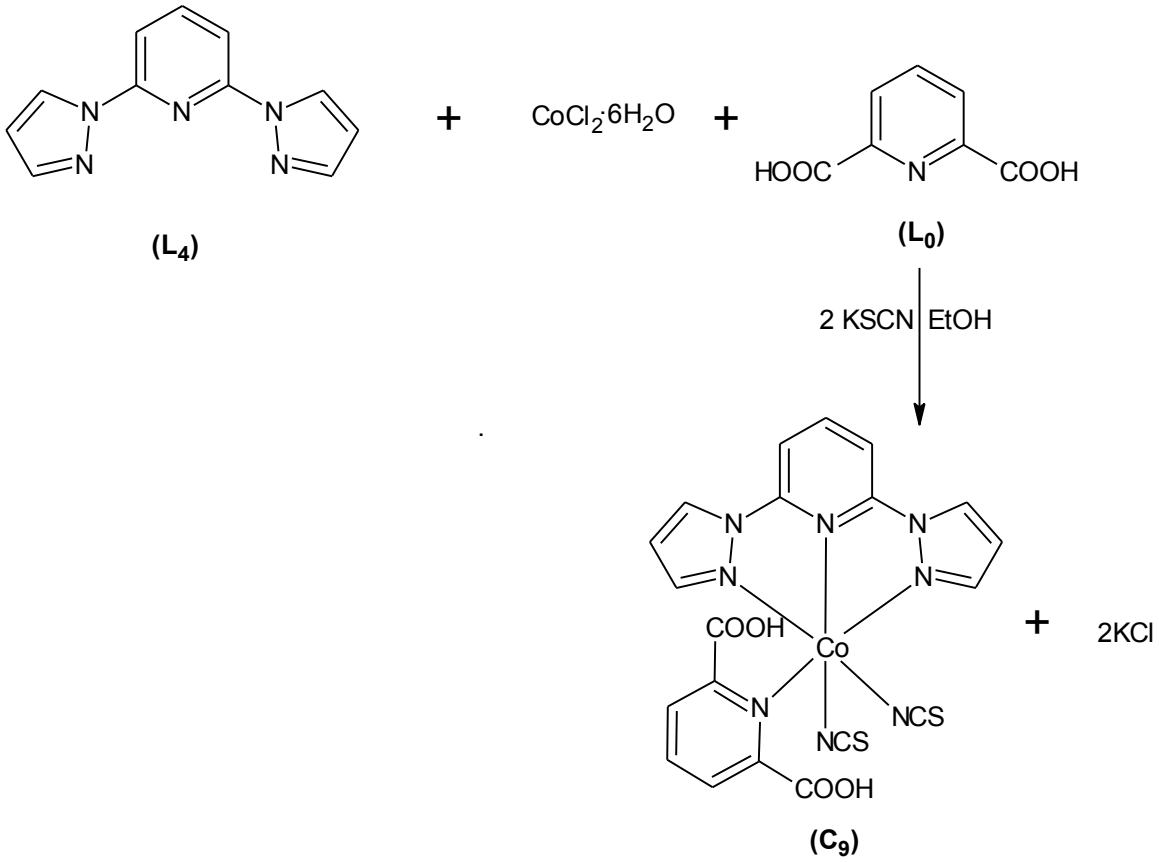

Scheme 16. Synthesis of $[CoL_4L_0(NCS)_2]$

The synthesis of **C_9** (Scheme 16) was carried using similar method used for **C_6** (section 2.6.1). $[CoCl_2{\cdot}6H_2O]$ (0.2 g, 0.841 mmol) and 2,6-bis-(pyrazolyl)pyridine (0.178 g, 0.841 mmol) were dissolved and refluxed. After 3 h pyridine-2,6-dicarboxylic acid (0.140 g, 0.841 mmol) was added to the mixture and refluxed for 2h. Excess potassium thiocynate (0.327 g, 3.364 mmol) was added and refluxed for 4 h. The reaction mixture was cooled and methanol was removed under vacuum. The obtained after precipitation with diethyl ether was filtered and dried [6]. Yield: 0.27g, 58%, m.p. 250°C, IR (KBr

pellet) ν(cm^{-1}): 3409, 3244, 2340, 2043, 1624, 1447, 1396, 1109, 984, 838, 737, 622, 455.

2.6.5 Synthesis of $[CoL_5L_0(NCS)_2]$ (C_{10}).

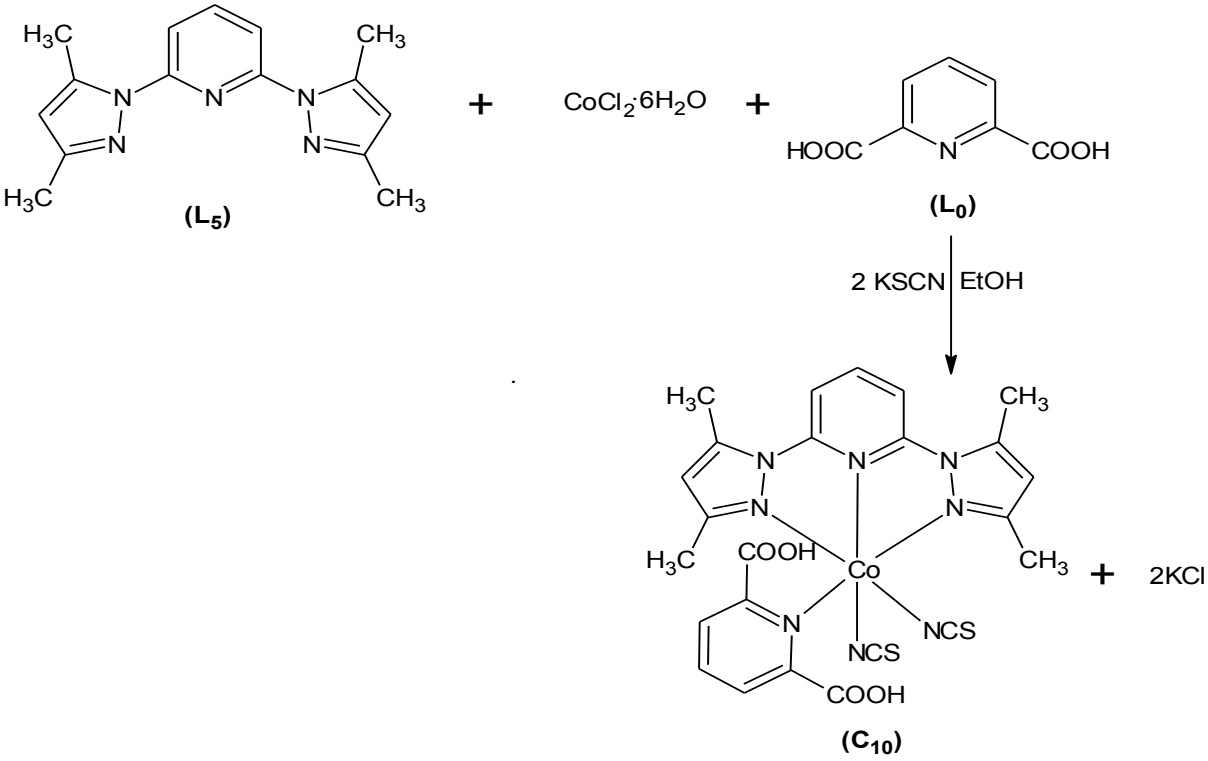

Scheme 17. Synthesis of $[CoL_5L_0(NCS)_2]$

The synthesis of **C_{10}** (Scheme 17) was prepared in a similar method reported for **C_6** (section 2.6.1). $[CoCl_2{\cdot}6H_2O]$ (0.2 g, 0.841 mmol) and 2,6-bis-(benzimidazolyl)pyridine (0.225 g, 0.841 mmol) were dissolved in a minimal amount of ethanol and refluxed for 3h. Then pyridine-2,6-dicarboxylic acid (0.140 g, 0.841 mmol) was added to the mixture then excess potassium thiocynate (0.327 g, 3.364 mmol) was added after 2 h. The

mixture was refluxed for 4 h, after cooling down the reaction mixture at room temperature. Ethanol was evaporated under vacuum, the obtained product after precipitation with diethyl ether was filtered and dried under vacuum [6]. Yield: 0.31g, 61%, m.p. 249°C, IR (KBr pellet) υ(cm^{-1}): 3490, 2949, 2839, 2365, 2067, 1870, 1622, 1433, 1397, 1236, 1112, 1020, 619, 533.

References

[1] Singh, A.; Chetia, B.; Mobin, S. M.; Das, G.; Iyer, P. K.; Mondal, B. Ruthenium monoterpyridine complexes with 2,6-bis-(benzimidazol-2-yl)pyridine: Synthesis, spectral properties and structure. *Polyhedron,* **2008**, *27*, 1983-1988.

[2] Gong, D.; Jia, X.; Wang, B.; Zhang, X.; Jiang, L. Synthesis, characterization, and butadiene polymerization of iron(III),iron(II) and cobalt(II) chlorides bearing 2,6 bis-(2-benzimidazolyl)pyridyl or 2,6-bis-(pyrazol)pyridine ligand. *Journal of Organometallic Chemistry,* **2012**, *702*, 10-18.

[3] Abbo, H. S.; Titinchi, S. J. J. A new vanadium (III) complex of 2,6-bis(3,5-diphenylpyrazol-1-ylmethyl)pyridine as a catalyst for ethylene polymerization. *Molecules,* **2013**, *18*, 4728-4738.

[4] Bianchini. C.; Lee, H. M. Cyclopropanation of styrene with ethyl diazoacetate catalyzed by chiral and achiral ruthenium 2,6-bis-(imino)pyridyl complexes. *Organometallics,* **2000**, *19,* 1833-1840.

[5] Adeloye, A. O.; Ajibade, P. A. Synthesis and characterization of a Ru(II) complex with functionalized phenanthroline ligands having single-double linked anthracenyl and 1-methoxy-1-buten-3-yne moieties. *Molecules,* **2010**, *15*, 7570-7581.

[6] Sapp, S. A .; Elliott, C. M.; Contado, C.; Caramori, S.; Bignozzi, C. A. Substituted polypyridine complexes of cobalt(II/III) as efficient electron-transfer mediators in dye sensitized solar cells. *Journal of the American Chemistry Society,* **2002**, *124*, 11215-11222.

CHAPTER 3

3.0 SPECTROSCOPIC CHARACTERIZATION OF THE LIGANDS AND COMPLEXES.

3.1 Introduction

Tridentate ligands such as bis-(imino)pyridine and bis-(pyrazolyl)pyridine are known as redox-active ligands and also called redox non-innocent ligands. These ligands have the ability to allow redox reactions at the metal center and change their oxidation states due to their energetically accessible levels of frontier orbitals [1, 2]. The redox non-innocence of the bis-(imino)pyridine-based ligand in metal complexes, formulated as an intermediate spin metal center with a doubly reduced bis-(imino)pyridine dianion, is shown in Scheme 18 [3].

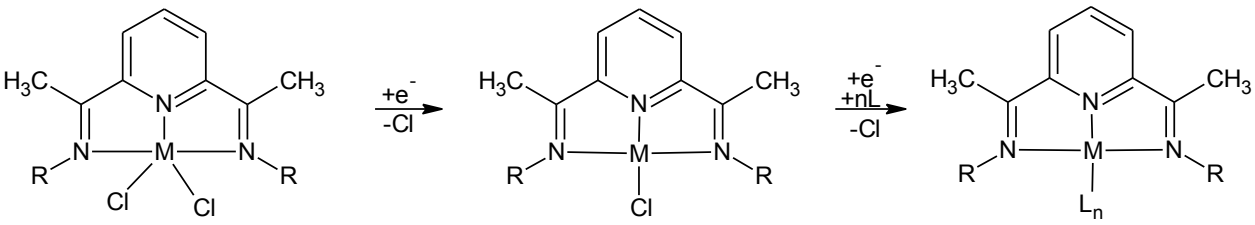

Scheme 18. Redox non-innocence of the bis-(imino)pyridine ligand (R = Me, Ph and M= Co, Ru) [4].

Ruthenium, tridentate nitrogen donor ligands based on the pyrazolylpyridine moieties have a C-N inter-ring bond [5, 6] and the stability of the metal complex containing 2,6-bis-(pyrazolyl)pyridine is due to the back-bonding of π*-orbitals in the pyridine ring. In 2,6-bis-(pyrazolyl)pyridine based ligands for example; pyridine ring is a good π-acceptor because it has insufficient π-electrons while pyrazole is a π-donor because it has

excess π-electrons [7, 8]. The ligands of tridentate polyamine donor ligands have the ability to bind the metal center with two nitrogen donor atoms [9].

3.2 Synthesis of Co(II) and Ru(II) complexes

The Co(II) and Ru(II) complexes of bis-(imino)pyridine and bis-(pyrazolyl)pyridine ligands were prepared by addition of corresponding metal chloride in aqueous solution to the tridentate ligand in DMF or methanol in a 1:1 stoichiometric ratio [10]. The proposed structures are shown in Figures 12 and 13.

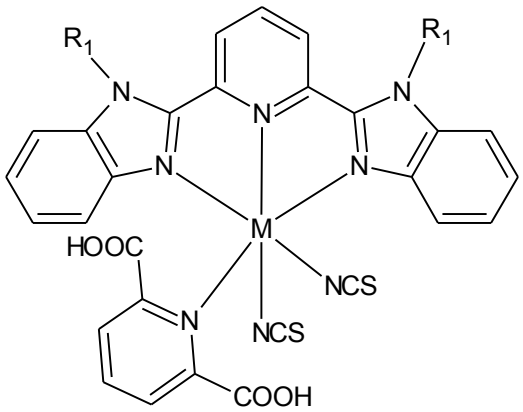

Figure 12. Proposed structure of complexes with bis-(imino)pyridine ligands. (M= Ru or Co and R_1 = H, C_4H_9 or Bz)

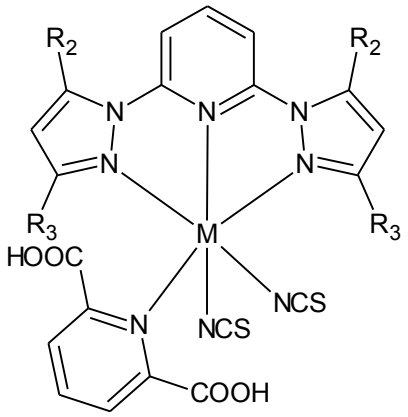

Figure 13. Proposed structure of complexes with bis-(pyrazolyl)pyridine ligands. (M = Ru or Co, R_2 = H and R_3 = CH_3)

3.3 Solubility test

The solubility of ligands and complexes in different solvents is presented in Table 2. The ligands and complexes are substantially soluble in both water and DMSO but their solubility greatly varied in all other solvents.

Table 2. Solubility test for ligands and complexes

	H_2O	MeOH	EtOH	$CHCl_3$	CH_2Cl_2	THF	Hexane	Toluene	DMF	DMSO
L_1	✓	✓	✓	x	x	x	x	x	✓	✓
L_2	✓	✓	✓	✓	x	x	x	x	✓	✓
L_3	✓	✓	✓	✓	x	x	x	x	✓	✓
L_4	✓	✓	✓	x	x	x	x	x	✓	✓
L_5	✓	✓	✓	x	x	x	x	x	✓	✓
C_1	✓	x	x	x	x	x	x	x	✓	✓
C_2	✓	x	x	x	x	x	x	x	✓	✓
C_3	✓	x	x	x	x	x	x	x	✓	✓
C_4	✓	x	x	x	x	x	x	x	✓	✓
C_5	✓	x	x	x	x	x	x	x	✓	✓
C_6	✓	✓	✓	x	x	x	x	x	x	✓
C_7	✓	✓	✓	x	x	x	x	x	x	✓
C_8	✓	✓	✓	x	x	x	x	x	x	✓
C_9	✓	✓	✓	x	x	x	x	x	x	✓
C_{10}	✓	✓	✓	x	x	x	x	x	x	✓

Key: x – Insoluble

✓ - Soluble

3.4 Conductivity measurements

All the ligands and complexes were dissolved in water to measure their molar conductance. The results are as presented in Table 3, the values of molar conductivity of ligands and complexes fall in the range of 0.1-28.5 $\mu Scm^2/mol$. This shows that they are non-electrolyte in solution, and thus support the formulation of the complexes.

Table 3. Molar conductance of ligands and complexes.

Component	**Conductivity ($\mu Scm^2/mol$)**
L_1	7.63
L_2	26.2
L_3	28.5
L_4	11.28
L_5	22.7
C_1	4.48
C_2	4.77
C_3	7.40
C_4	7.47
C_5	3.82
C_6	0.1
C_7	9.49
C_8	1.70
C_9	8.07
C_{10}	6.19

3.5 The FTIR spectra studies

The FTIR spectra of the ligands and their corresponding complexes were compared and assigned in comparison with relevant literatures. Relevant IR data are presented in Table 4.

Table 4. Relevant FTIR data of ligands and complexes

	ν(OH) cm^{-1}	ν(N-H) cm^{-1}	ν(N=C=S) cm^{-1}	ν(C=O) cm^{-1}	ν(C=C) cm^{-1}	ν(C=N) cm^{-1}	ν(C-O) cm^{-1}	ν(C-N) cm^{-1}	ν(M-N) cm^{-1}
L_1	-	3205	-	-	1542	1425	-	1206	-
L_2	-	3235	-	-	1622	1542	-	1091	-
L_3	-	3237	-	-	1623	1570	-	1069	-
L_4	-	3365	-	-	1666	1580	-	1048	-
L_5	-	3410	-	-	1608	1543	-	1161	-
C_1	3409	3244	2084	1620	1600	1400	1397	1109	622
C_2	3424	-	2068	1641	1598	1459	1400	1117	618
C_3	3429	-	2069	1646	1599	1510	1397	1116	618
C_4	3417	-	2067	1638	1547	1454	1397	1121	619
C_5	3424	-	2069	1646	1577	1457	1398	1113	619
C_6	3415	3235	2122	1634	1560	1464	1398	1075	540
C_7	3418	-	2170	1623	1597	1427	1304	1102	442
C_8	3414	-	2368	1622	1555	1394	1283	1075	541
C_9	3409	-	2034	1624	1609	1497	1396	1109	455
C_{10}	3490	-	2070	1622	1540	1433	1397	1112	533

3.6 Infrared spectra of 2,6-bis-(imino)pyridine ligands, Ru(II) and Co(II) complexes.

3.6.1 Infrared spectra of 2,6-bis-(imino)pyridine ligands

The infrared spectra of the **L_1**, **L_2** and **L_3** in figure 14, exhibits medium bands (Table 4) due to υ(N-H) stretching vibration at 3205 cm^{-1} for **L_1**, 3235 cm^{-1} for **L_2** and 3237 cm^{-1} for **L_3**. The presence of a weak vibration in **L_2** spectrum at 3105 cm^{-1} is due to υ(C-H) asymmetric stretching vibration, confirms the presence of butyl group. The strong absorption band at 2922 and 2858 cm^{-1} in the spectra of **L_1** and **L_2** is due to υ(C-H) symmetric and asymmetric stretching vibrations. The weak absorption bands between 1542 and 1623 cm^{-1} in the spectra of intra-ligands is due to υ(C=C) stretching vibrations. The C=N strong stretching vibrations was observed as prominent band at 1462, 1542 and 1570 cm^{-1} for **L_1**, **L_2** and **L_3** respectively.

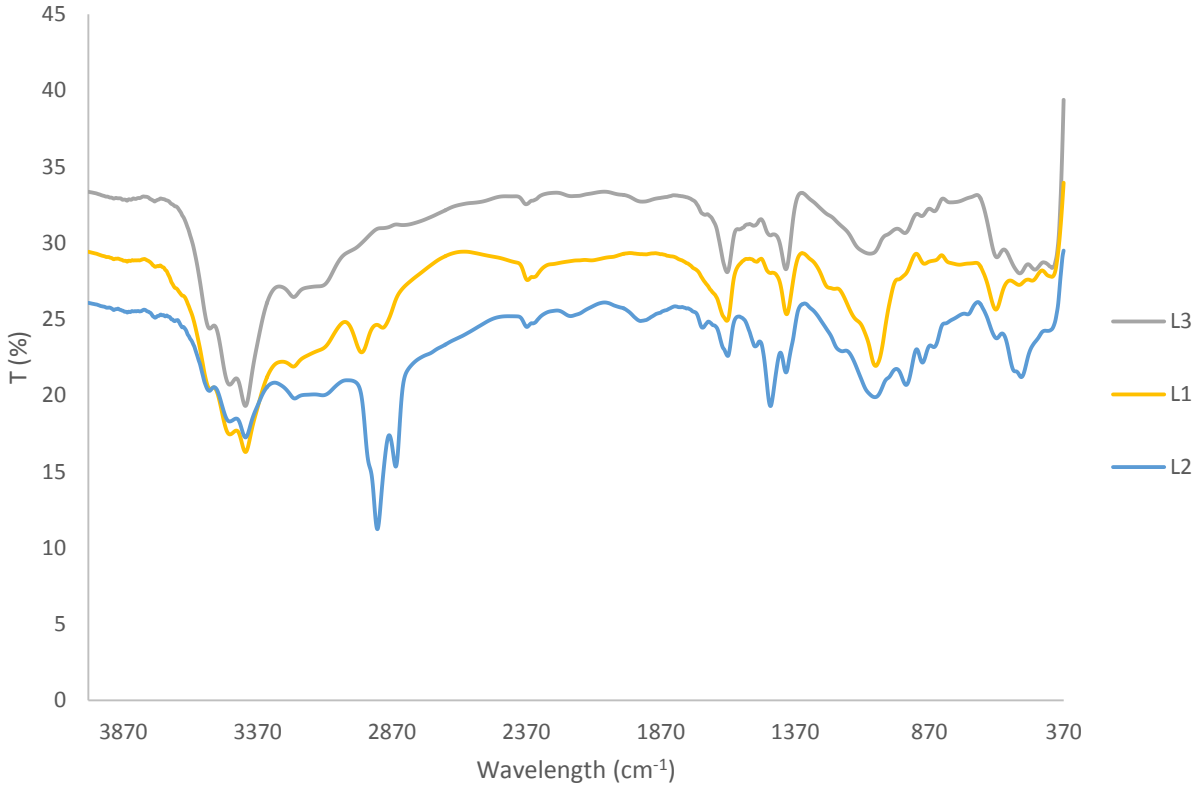

Figure 14. FTIR spectra of bis-(imino)pyridine ligands (**L_1**, **L_2** and **L_3**)

3.6.2 Infrared spectra of Ru(II) and Co(II) complexes of 2,6-bis-(imino)pyridine ligands.

In Figure 15a and 15b, strong and broad vibrational bands (Table 4) were observed between 3429 and 3209 cm^{-1} due to υ(O-H) bending vibrations. This is due to O-H presence in 2,6-pyridinecarboxylic acid (**L_0**) containing carboxylic group introduced during complexation of ruthenium(II) metal ion [6]. The υ(N-H) stretching vibrations band in **C_1** and **C_6** spectrum was observed at 3244 and 3235 cm^{-1} shifted to higher frequency. The redshift is due to uncoordinated NH group of benzimidazole [7].

The vibrational bands around 2100 cm^{-1} are due to υ(N=C=S) stretching vibrations of the thiocynate moiety. The υ(N=C=S) vibrations for cobalt complex were observed at higher wavelength relative to ruthenium complexes (**C_6**, **C_7**, **C_8**), and the peaks were not prominent as it was reported in literature [10]. The presence of medium vibrational band between 1646 and 1620 cm^{-1} ascribe to the *v*(C=O) asymmetric stretching vibrations. This is evident that carboxylic group of pyridine-2,6-dicarboxylic acid (**L_0**) undergoes deprotonation [10], similar observation were obtained in literature [10,5]. The weak absorption band around 1600 cm^{-1} in the spectra of complexes is due to υ(C=C) stretching vibrations. The υ(C=N) stretching vibrations between 1510 and 1400 cm^{-1} on the spectra of the complexes are observed to shift to lower frequency compared to the free ligands, blue-shift is due to the coordination of the amine to metal ion [12]. The presence of υ(C-O) vibration between 1291 and 1113 cm^{-1} is due to carbonyl group

of pyridine-2,6-dicarboxylic acid ($\mathbf{L_0}$). The C-N stretching bands of the complexes were observed to shift to the higher frequency region.

Some of the weak vibrational bands due to N-H stretching vibration disappear in the finger print region in the metal complexes except for that of $\mathbf{C_1}$ and $\mathbf{C_6}$ because contains a secondary amine that is not directly bonded to the metal ions [11]. The presence of new medium vibrational bands between 618 and 622 cm^{-1} assigned to Ru-N bond for Ru(II) complexes [11], and for Co(II) around 540 cm^{-1}confirms covalent bond formation between the metal center and the N atoms of the ligands [11].

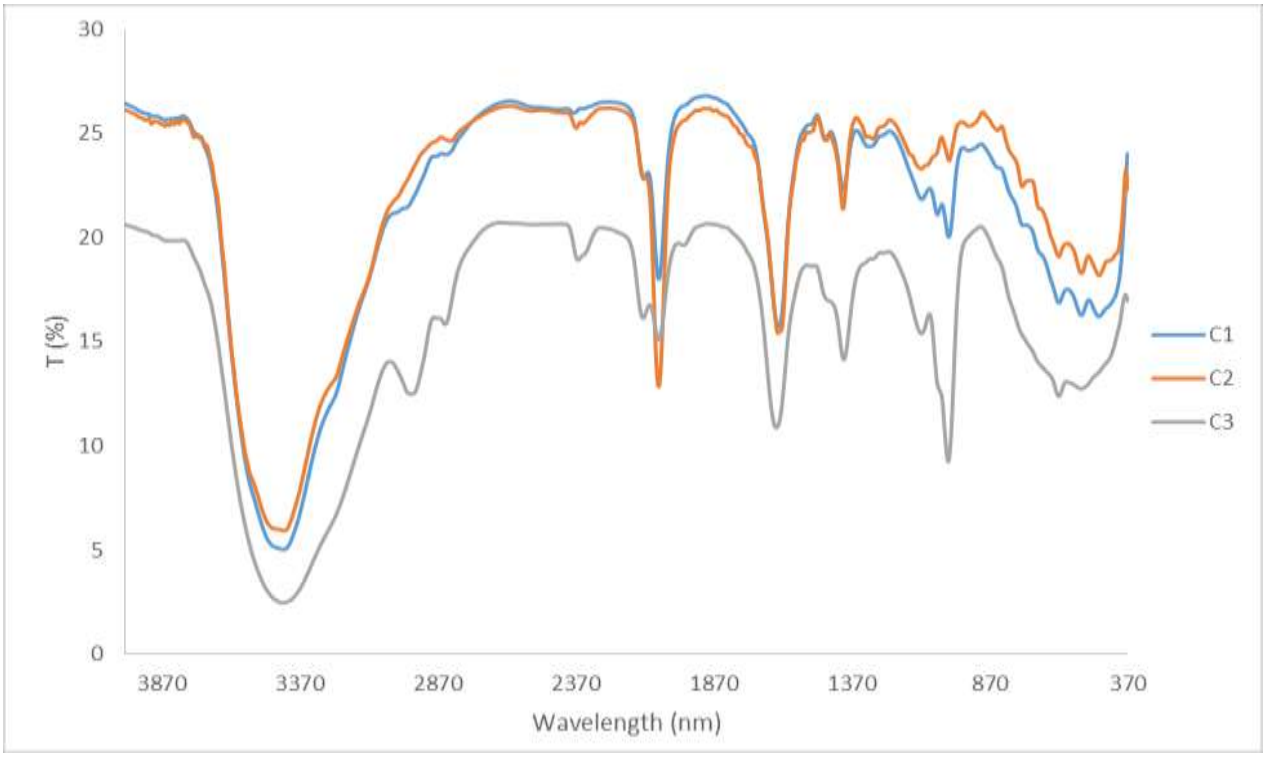

Figure 15a. FTIR spectra of Ru(II) and Co(II) complexes of bis-(imino)pyridine ligands ($\mathbf{C_1}$, $\mathbf{C_2}$ and $\mathbf{C_3}$)

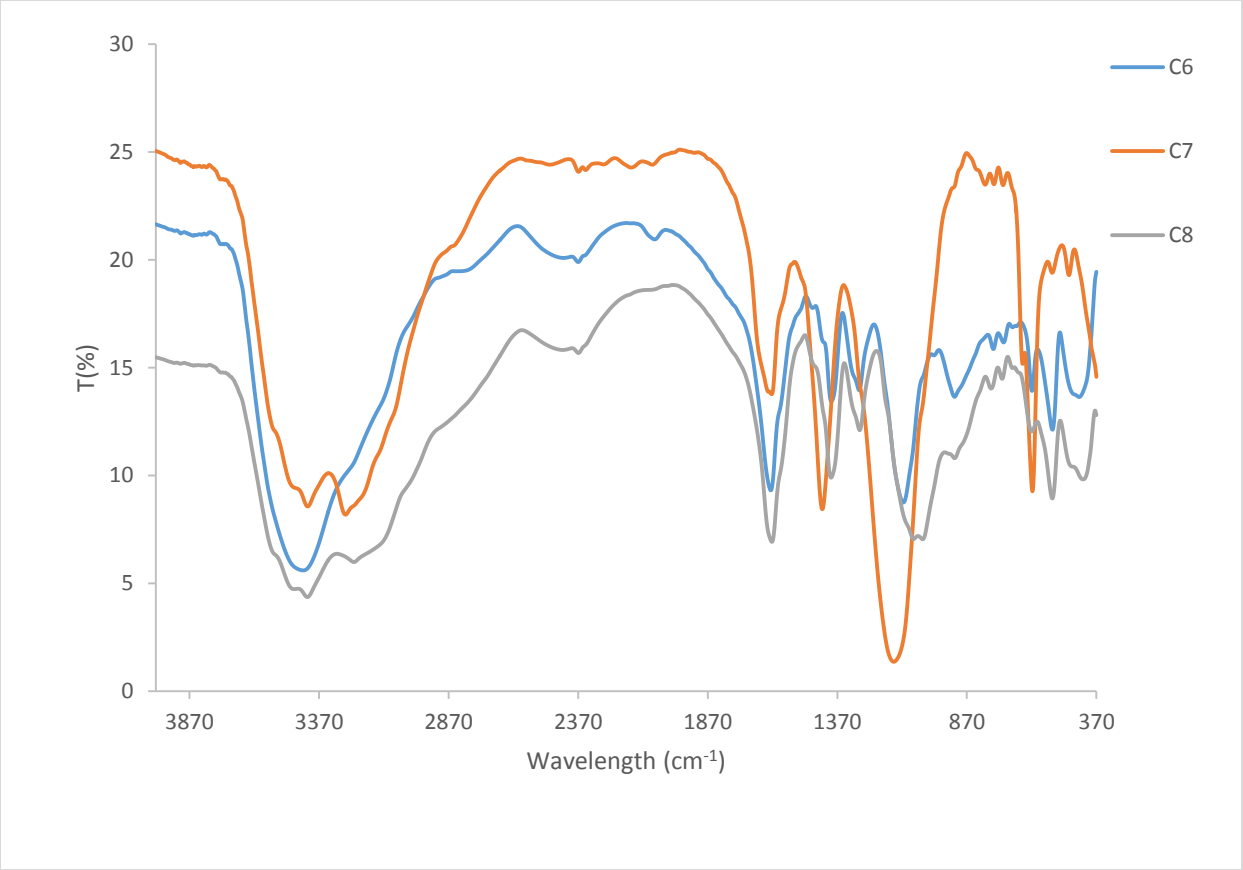

Figure 15b. FTIR spectra of Ru(II) and Co(II) complexes of bis-(imino)pyridine ligands (**C_6**, **C_7** and **C_8**,)

3.7 Infrared spectra of 2,6-bis-(pyrazolyl)pyridine ligands, Ru(II) and Co(II) complexes.

3.7.1 FTIR spectroscopy of 2,6-bis-(pyrazolyl)pyridine ligands

The infrared spectra of **L_4** and **L_5** (Figure 16) showed weak absorption band (Table 4) due to υ(N-H) stretching vibration at 3365 and 3410 cm^{-1} respectively. The two ligands

exhibit medium vibrational bands at 2976 and 2981 cm^{-1} for **L_4** and **L_5** respectively due to υ(C-H) stretching vibrations. A new weak band appeared at 2903 cm^{-1} due to υ(C-H) stretching vibrations for the methyl group. The strong bands at 1646 and 1638 cm^{-1} are assigned to the υ(C=N) stretching vibrations. The spectra of **L_4** and **L_5** appeared to be very similar but differ in intensity, this is because they difference in molar mass [12].

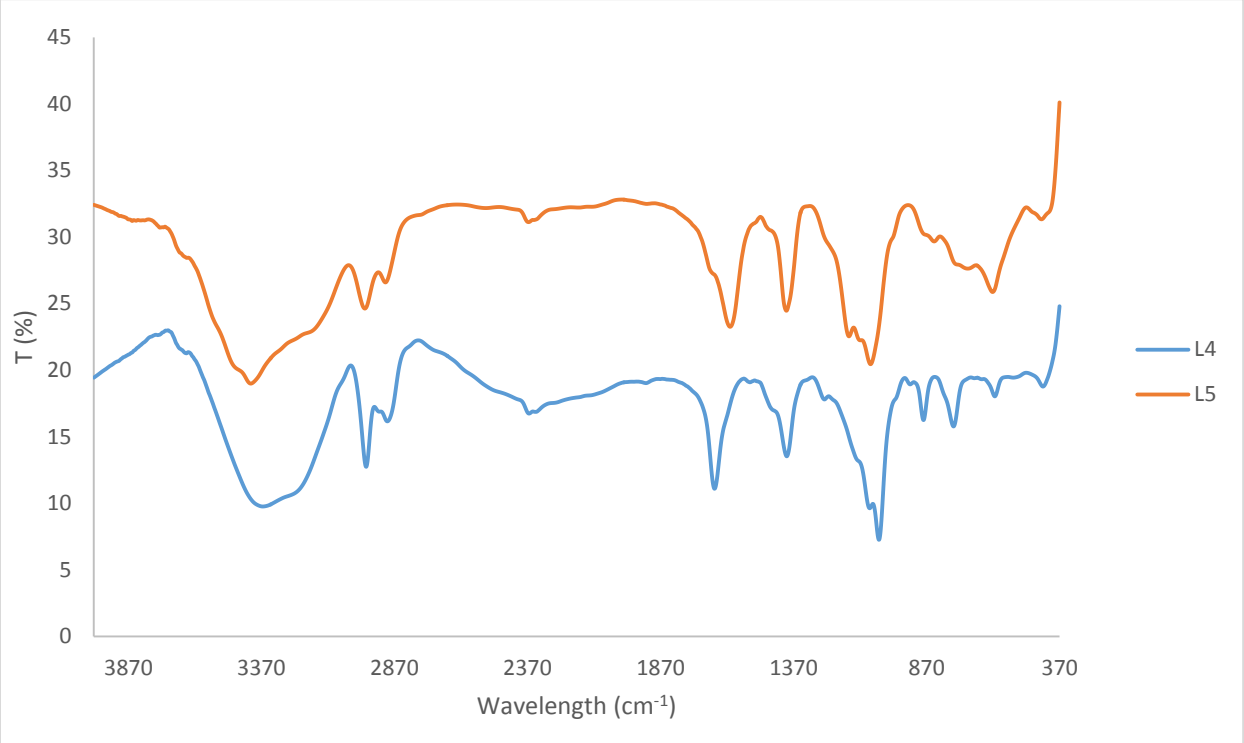

Figure 16. FTIR spectra of bis-(pyrazolyl)pyridine ligands (**L_4** and **L_5**)

3.7.2 FTIR spectroscopy of Ru(II) and Co(II) complexes of 2,6-bis-(pyrazolyl)pyridine ligands.

The broad vibrational bands (Table 4) observed between 3490 and 3409 cm^{-1} assigned for υ(O-H) bending vibrations are due to O-H present in **L_0** containing carboxylic group

introduced during complexation of ruthenium(II) metal ion as shown in Figure 17. The strong vibrational bands observed between 2034 to 2070 cm^{-1}, corresponding to ν(N=C=S) stretching vibrations of thiocynate moiety. The presence of medium band between 1638 and 1646 cm^{-1} assigned to ν(C=O) asymmetric stretching vibrations is due to deprotonated carboxylate of **L_0** [10]. The weak band observed between 1540 and 1666 cm^{-1} assigned for ν(C=C) vibration. The ν(C=N) stretching vibrational bands observed between 1454 and 1329 cm^{-1}. The ν(C=N) and ν(C-N) stretching vibrational bands of the complexes are observed at lower frequency compared to the free ligands, attributed to coordination metal ion and N atom present in pyrazole [12].The C=N band for **L_4** was observed at lower frequency compared to the complex with the same ligand in the literature [12] where it was observed at 1481 cm^{-1} in a metal complex. The presence of ν(C-O) vibrations is due to carbonyl group of pryridine-2,6-dicarboxylic acid (**L_0**). The spectra of **C_4** and **C_5** show similar stretching vibrations but at different intensity because of their molar weight are different [10]. The presence of new medium vibrational bands at 619 cm^{-1} for both **C_4** and **C_5** assigned for ν(Ru-N) vibration, confirms covalent bonding of Ru-N [13], **C_9** and **C_{10}** around 455 cm^{-1} assigned for ν(Co-N) confirms covalent bonding [11].

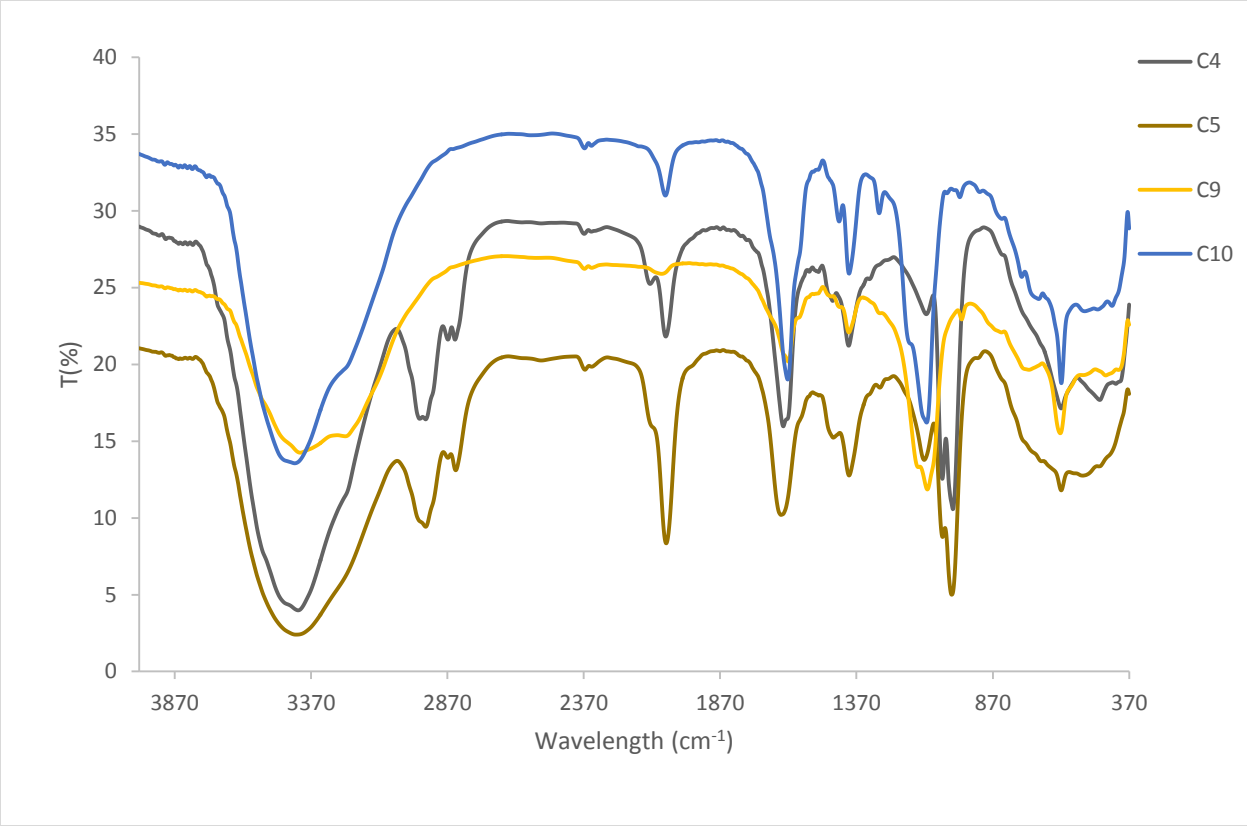

Figure 17. FTIR spectra of Ru(II) and Co(II) complexes of bis-(pyrazolyl)pyridine ligands (**C_4**, **C_5**, **C_9** and **C_{10}**)

3.8 NMR spectroscopic studies of ligands and complexes.

3.8.1 NMR spectroscopic studies of bis-(imino)pyridine ligands

The ^{1}H-NMR and ^{13}C-NMR for **L_1**-**L_3** could not be recorded due to poor solubility of the ligands in all deuterated solvents.

3.8.2 NMR spectroscopy of bis-(pyrazolyl)pyridine ligands

3.8.2.1 NMR spectroscopic studies of 2,6-bis-(pyrazolyl)pyridine.

The ^{1}H NMR ^{13}C NMR were performed to establish the formation of the ligands, **L_4** in deuterated water (D_2O) show five signals at δ 8.4 (2H, d, Pyr), 8.1 (1H, t, Py), 7.9 (2H, d, Py), 7.8 (2H, d, Py) and 6.4 (2H, t, Pyr) as shown in Figure 18. The spectra showed one set of signal for the pyrazole rings indicating that they are equivalent. The number of peaks observed are similar to the ^{1}H-NMR obtained in literature [12] for the same ligand, but the peak position are slightly different. The ^{13}C-NMR spectra for **L_4** showed all expected six peaks and this confirms that the desired ligand was synthesized as shown in Figure 19. The peaks observed were similar to ^{1}H-NMR.

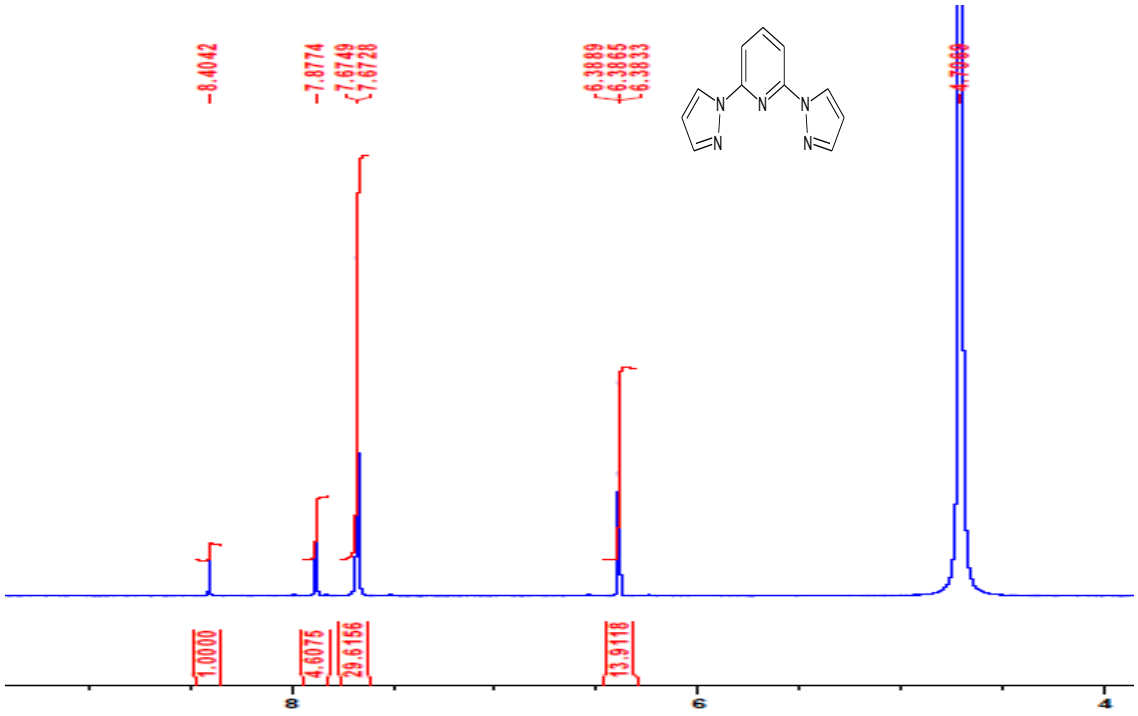

Figure 18. ^{1}H-NMR spectrum of 2,6-bis-(pyrazolyl)pyridine ligands (**L_4**)

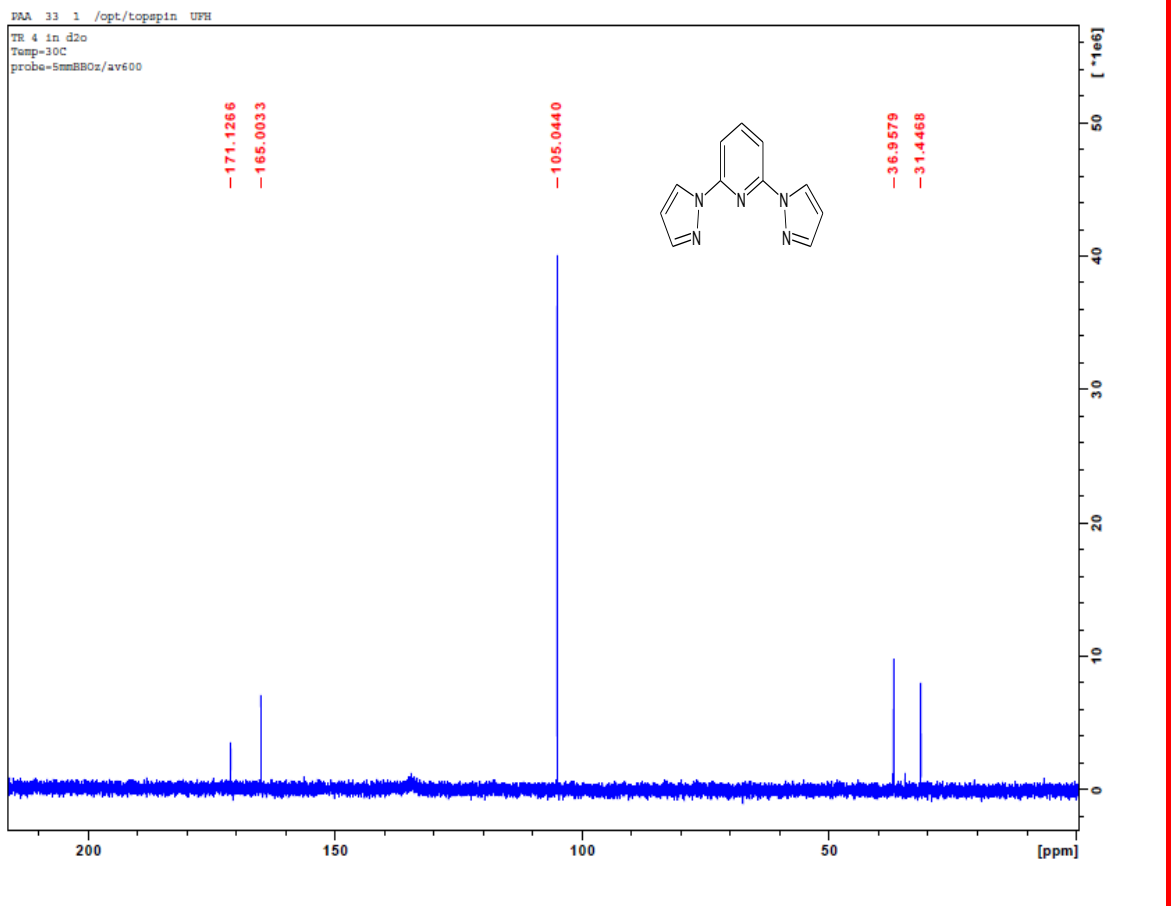

Figure 19. ^{13}C-NMR spectrum of bis-(pyrazolyl)pyridine ligands (**L_4**)

3.8.2.2 NMR spectroscopic studies of bis-(3,5-dimethylpyrazolyl)pyridine ligand.

The ^{1}H-NMR spectra for **L_5** in figure 20, was similar to the spectra for **L_4** but **L_5** contains additional peaks assigned to methyl groups. The spectra of **L_5** in D_2O solution showed four peaks at δ 8.4 (1H, t, Py), 8.2 (2H, d, Py). In comparison with the spectrum of **L_4**, the pyrazole ring show three peaks a triple and two doublet while in **L_5** one peak was expected at the aromatic region around 6 ppm, the singlet at that region and the peaks at upfield assigned to CH_3 were not obtained which may be due to poor solubility that

make resolving the spectrum difficult. ^{13}C-NMR for **L_5** could not be recorded due to poor solubility in solvents.

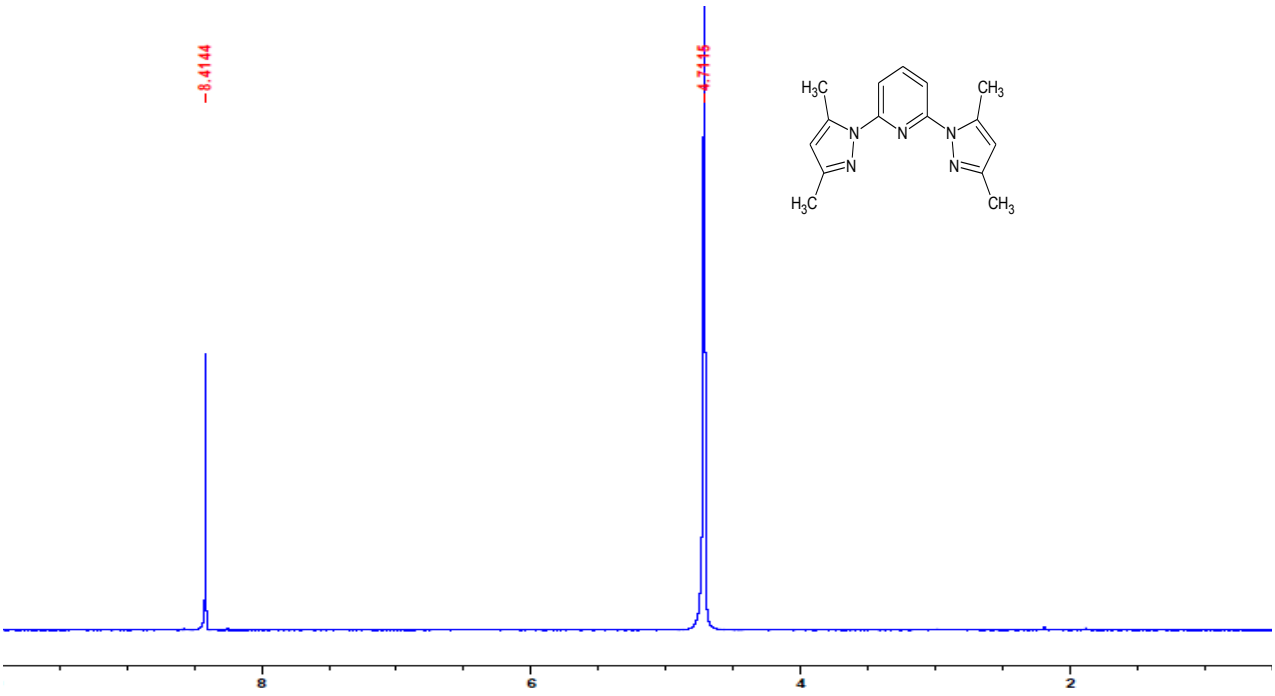

Figure 20. ^{1}H-NMR spectrum of bis-(3,5-dimethylpyrazolyl)pyridine ligands (**L_5**)

3.8.3 NMR spectroscopy of Ru(II) complexes.

3.8.3.1 NMR spectroscopic studies for Ru(II) of bis-(imino)pyridine ligands.

The ^{1}H NMR and ^{13}C NMR of the complexes were observed in D_2O solution. The ^{1}H-NMR spectrum of **C_1** D_2O solution presented in Figure 21, shows four signals at δ 8.57 (2H, s, Pdca), 8.38 (1H, s, Py), 8.10 (1H, s, Py) and 7.93 (4H, m, Py). The spectrum showed one set of signal for the benzimidazole rings indicating that are equivalent [14]. Three peaks observed for 2,6-bis-(benzimidazolyl)pyridine are similar to the ^{1}H-NMR of the same ligand reported in literature [15, 13] for benzimidazole, but the

peak position are slightly different but from the expected peak around δ 13 ppm assigned for N-H singlet and peak around δ 7.30 ppm assigned for Ph-H (4H) multiplet were not observed. The peaks observed at upfield are due to traces of diethyl ether which was used to wash the product. . The ^{13}C-NMR spectra for **C_1** showed all the expected 14 peaks and this confirms that the desired ligand was synthesized as shown in Figure 22.

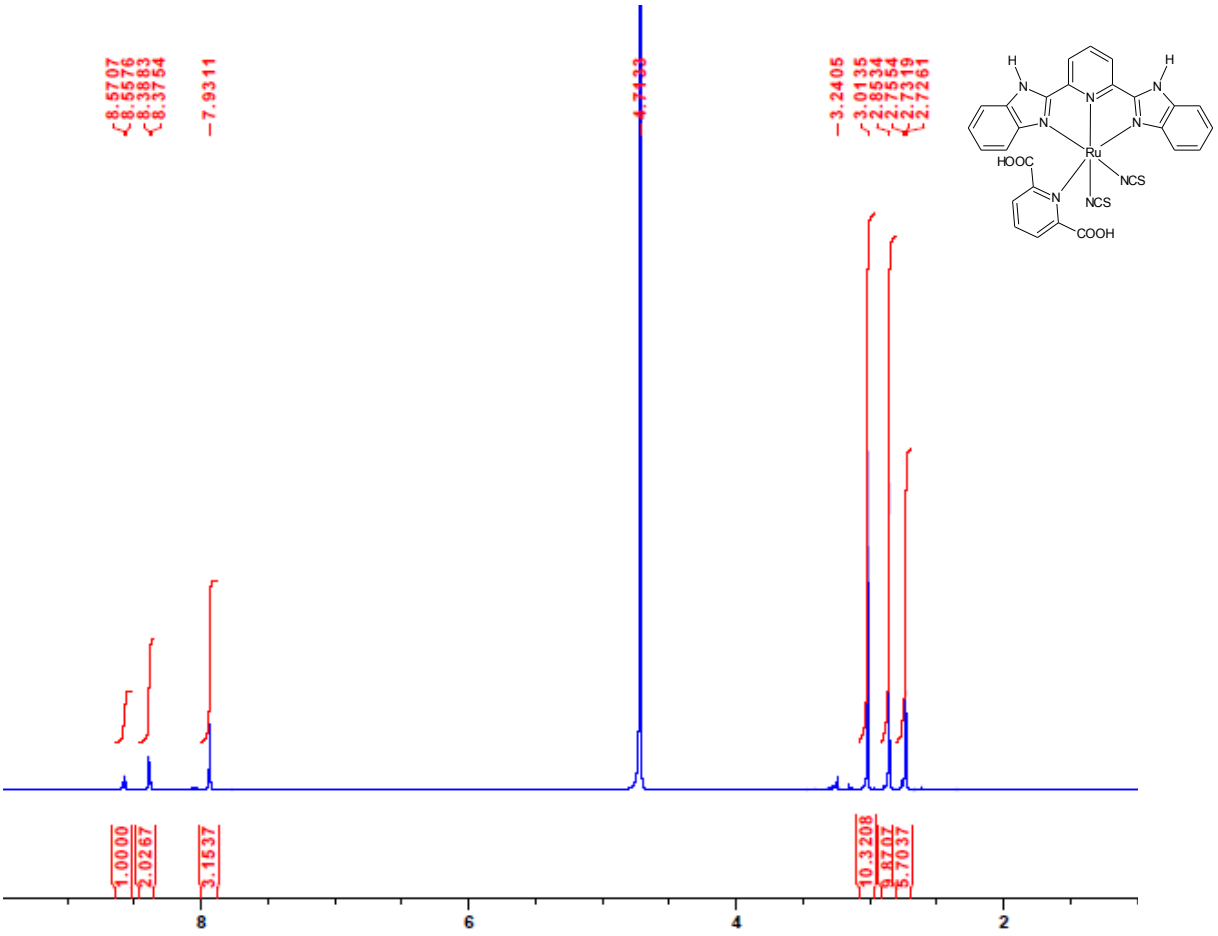

Figure 21. ^{1}H-NMR spectrum for Ru(II) complex of bis-(benzimidazolyl)pyridine ligands (**C_1**)

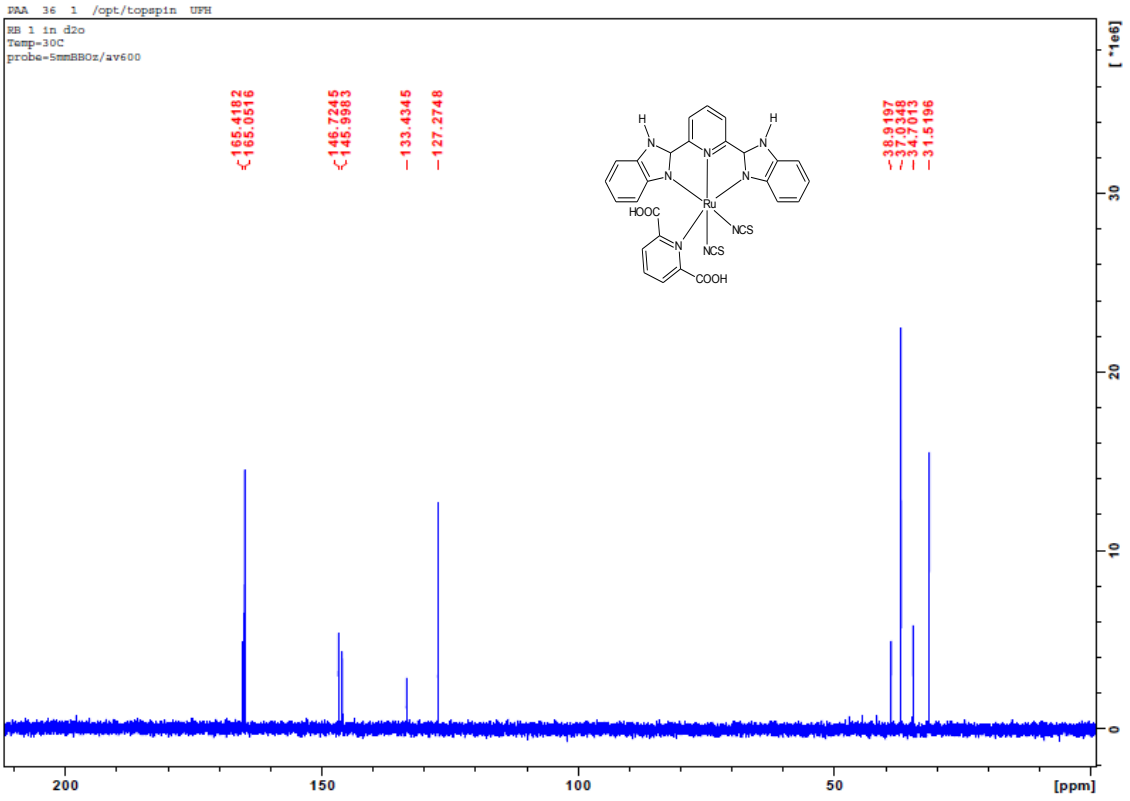

Figure 22. ^{13}C-NMR spectrum for Ru(II) complex of bis-(benzimidazolyl)pyridine ligand (**C_1**)

The ^{1}H-NMR spectrum for **C_2** was similar to the spectrum for **C_1** but **C_2** contains additional peaks that are assigned to butyl groups. The spectrum of **C_2** in D_2O solution showed 10 peaks at δ 8.57 (2H, d, Pdca), 8.39 (1H, s, Py), 8.10 (1H, s, Py), 7.94 (4H, m, Py), 3.25-2.87 (18H, s, butyl) and 3.02-2.75 (18H, s, butyl) as shown in Figure 23. The expected peak around δ 9.00 ppm assigned for 2H, t, Pdca and peak around δ 7.30 ppm assigned for Ph-H (4H) multiplet were not observed. The ^{13}C-NMR spectrum for **C_2**

showed all expected peaks represented in Figure 24 and this confirms that the desired complex was synthesized.

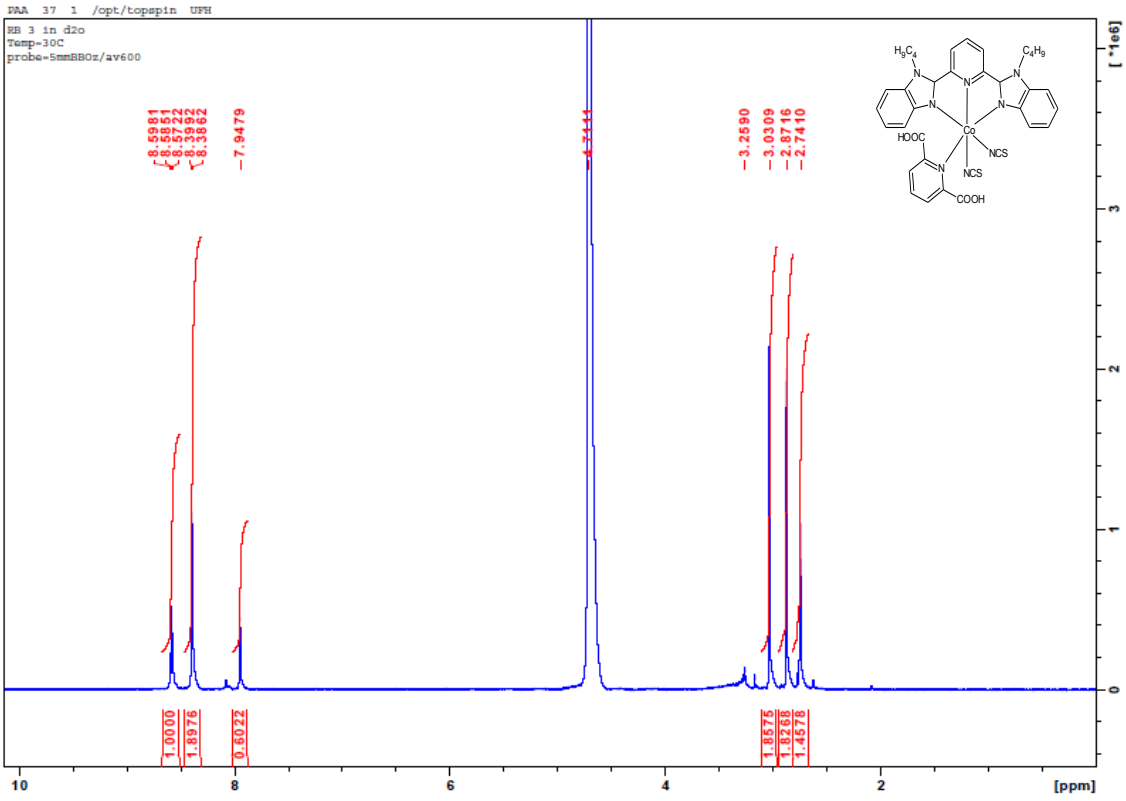

Figure 23. ^{1}H-NMR spectrum of Ru(II) complex of 2,6-bis-(butylbenzimidazolyl)pyridine ligand (**C_2**)

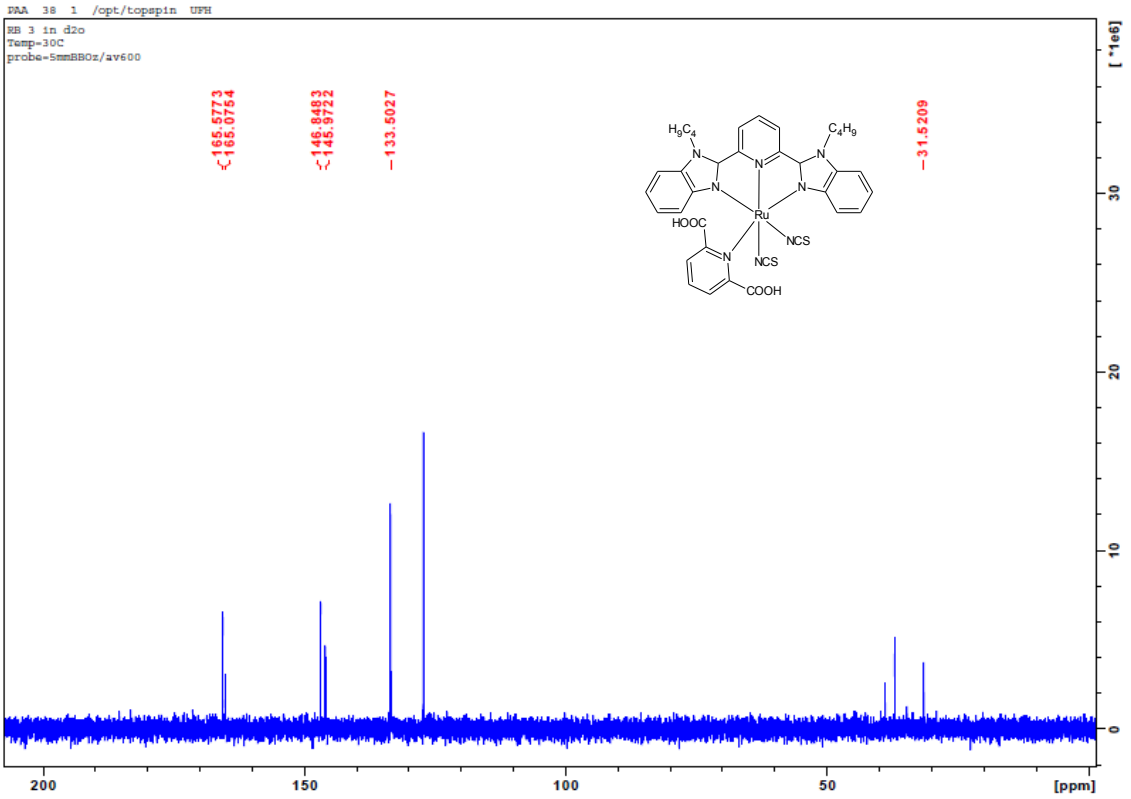

Figure 24. ^{13}C-NMR spectrum of Ru(II) of bis-(butylbenzamidazolyl)pyridine ligands (**C_2**)

The ^{1}H-NMR and ^{13}C-NMR for **C_5** could not be recorded due to poor solubility of the complexes.

3.8.3.2 NMR spectroscopic studies of Ru(II) complexes of bis-(pyrazolyl)pyridine.

The ^{1}H-NMR and ^{13}C-NMR for **C_4** and **C_5** could not be recorded due to poor solubility of the complexes in all deuterated solvents.

3.8.4 NMR spectroscopic studies of Cobalt(II) complexes.

The ^{1}H-NMR and ^{13}C-NMR for cobalt(II) complexes could not be recorded due to poor solubility of the complex.

References

[1] Turkoglu, G.; Heinemann, F. W.; Burzlaff, N. Transition metal complexes bearing a 2,2-bis-(3,5-dimethylpyrazol-1-yl)propionate ligand: One methyl more matters. *Dalton Transitions*, **2011**, *40*, 4678-4686.

[2] Thompson, J. R. J.; Ovens, J. S.; Williams, V. E.; Leznoff, D. B.; Thompson, J. R. Supramolecular assembly of bis-(benzimidazole)pyridine: An extended anisotropic ligand for highly birefringent materials. *Chemistry: A. European Journal*, **2013**, *19*, 16572-16578.

[3] Mukherjee, R. Coordination chemistry with pyrazole-based chelating ligands: Molecular structural aspects. *Coordination Chemistry Reviews*, **2000**, *203*, 151-218.

[4] Chirik, P. J.; Wieghardt, K. Radical ligands confer nobility on base-metal catalysts. *Science*, **2010**, *327*, 794-795.

[5] Singh, A.; Chetia, B.; Mobin, S. M.; Das, G.; Iyer, P. K.; Mondal, B. Ruthenium monoterpyridine complexes with 2,6-bis-(benzimidazol-2-yl)pyridine: Synthesis, spectral properties and structure. *Polyhedron*, **2008**, *271*, 983-1988.

[6] Abu-Surrah, A. S.; Lappalainen, K.; Piironen, U.; Lehmus, P.; Repo, T.; Leskela, M. New bis-(imino)pyridine-iron- and cobalt(II)-based catalysts: Synthesis, characterization and activity towards polymerization of ethylene. *Journal of Organometallic Chemistry*, **2002**, *648*, 55-61.

[7] Halcrow, M. A. Iron(II) complexes of 2,6-di(pyrazol-1-yl)pyridines-A versatile system for spin-crossover research. *Coordination Chemistry Reviews*, **2009**, *253*, 2493-2514

[8] Bart, S. C.; Chlopek, K.; Bill, E.; Bouwkamp, M. W.; Lobkovsky, E.; Neese, F.; Wieghardt, K.; Chirik, P. J. Electronic structure of bis(imino)pyridine iron dichloride,

monochloride, and neutral ligand complexes: A combined structural, spectroscopic and computational study. *Journal of the American Chemical Society*, **2006**, *128*, 13901-13912.

[9] Sairem, G.; Anna, V. R., Wang, P.; Das, B.; Kollipara, M. R. η^5 and η^6-cyclic π-perimeter hydrocarbon platinum group metal complexes of 3-(2-pyridyl)pyrazole derived ligands with a pendant nitrile group: Syntheses, spectral and structural studies. *Journal of Chemical Science*, **2012**, *124*, 411-419.

[10] Adeloye, A. O.; Ajibade, P. A.; Synthesis and characterization of a Ru(II) complex with functionalized phenanthroline ligands having single-double linked anthracenyl and 1-methoxy-1-buten-3-yne moieties. *Molecules*, **2010**, *15*, 7570-7581.

[11] Nazeeruddin, M. K.; Zakeeruddin, S. M.; Humphry-Baker, R.; Jirousek, N.; Liska, P.; Vlachopoulos, N.; Shklover, V.; Fischer, C. H.; Gratzel, M. Acid-base equilibria of (2,2′-bipyridyl-4,4′-dicarboxylic acid)ruthenium(II) complexes and the effect of protonation on charge-transfer sensitization of nanocrystalline titania. *Inorganic Chemistry*, **1999**, *38*, 6298-6305.

[12] Philippopoulos, A. I.; Terzis, A.; Raptopoulou, C. P.; Catalano, V. J.; Falaras, P. Synthesis, characterization, and sensitizing properties of heteroleptic Ru(II) complexes based on 2,6-bis-(1-pyrazolyl)pyridine and 2,2-Bipyridine-4,4-dicarboxylic acid ligands. *European Journal of Inorganic Chemistry*, **2007**, *2007*, 5633-5644.

[13] Rodriguez, A. M. G.; Garcia de Torres, A.; Pavon, J. M. C.; Ojeda, C. B. Simultaneous determination of iron, cobalt, nickel and copper by UV-visible spectrophotometry with multivariate calibration. *Talanta*, **1998**, *47*, 463-470.

[14] Ajibade, P. A.; Kolawole, G. A. Synthesis, characterization and antiprotozoal studies of some complexes of antimalarial drugs. *Transition Metal Chemistry*, **2008**, *33*, 493-497

[15] Wu, H.; Huang, X.; Yuan, J.; Kou, F.; Jia, F.; Liu, B.; Wang, K. A V-shaped ligand 2,6-bis(2-benzimidazolyl)pyridine and its picrate Mn(II) complex: Synthesis, crystal structure and DNA-binding properties. *European Journal of Medicinal Chemistry,* **2010**, *45*, 5324-5330

CHAPTER 4

4.0 PHOTOELECTROCHEMISTRY OF THE METAL COMPLEXES AND THEIR EVALUATION AS SENSITIZERS FOR DSSCS.

4.1 Introduction

Metal complexes containing polypyridine ligands complexes have attracted significant interest in recent years in the study of molecular electronics [1], photochemical conversion of solar energy [2] and photoluminescence biosensor [3] due to their remarkable photophysical and electrochemical properties [4]. In the study of photochemical solar energy conversions systems using metal complexes as dyes for light harvesting, the solar cells use photo generated charge transfer states on the metal complex to inject electrons into the band gap of a semiconductor such as TiO_2 [5].

In order for the metal complexes to be effective light-harvesting materials, the compounds should possess electronic properties such as low energy metal-to-ligand charge transfer (MLCT) transitions [6]. In sensitizers based on coordination compounds photon emission usually exhibits a singlet metal-to-ligand charge transfer states [7]. MLCT is also capable of charge injection to conduction band of the semiconductor and triplet MLCT state can occur; however this process causes a decrease in emission and the excited state undergoes deactivation through both non-radiative and radiative decay pathways with an emission quantum yield [8].

The fastest injection times are observed for dyes with suitable anchoring groups, such as carboxylic and phosphonic moieties [9]. The carboxylic groups are used for

anchoring the metal complex to the surface of the semiconductor and ultimately improves electronic coupling between the π* orbital of the ligand, which is the lowest LUMO of the complex [10]. A strong electron-withdrawing group can be attached onto carboxylate group to control the oxidation potential in electrochemical studies [11]. The rate and nature of a polypyridine complexes is coupled to the electron transfer step. The electrochemistry of polypyridine metal complex can be useful in the selection of the proper oxidizing agent to oxidize the dye sensitizer to an intermediate oxidation state [12].

In this chapter, photophysical properties of 10 nitrogen chelating ligands containing five ruthenium(II) and cobalt(II) complexes were evaluated by electronic absorption spectroscopy and emission spectroscopy in solution. The redox potential of these complexes was obtained from cyclic voltammetry. The 8 sensitizers consists of 4 ruthenium(II), 3 cobalt(II) complexes and **N719** were fabricated. TiO_2 electrode was used as a semiconductor and their photovoltaic performance was measured by solar stimulator.

4.2 UV-Vis absorption studies of synthesized ligands and complexes.

Table 5 shows the electronic absorption bands for the ligands in DMSO solution. The electronic spectra (Figure 23-27) of the ligands in DMSO show one prominent band which is assigned to the π-π* transitions (near UV region) [13]. The electronic spectra of complexes in DMSO exhibits band assigned to MLCT (Metal to Ligand Charge

Transfer) transitions and d-d transitions [14]. In the electronic spectra of the complexes d-d transitions are observed at lower intensity than the MLCT [15]. In the visible region of ruthenium(II) complexes two bands are observed as shown in Table 6, these bands are assigned to $^4T_{2g} \rightarrow {}^2T_{2g}$ and $^4T_{1g}(F) \rightarrow {}^4T_1(P)$ transitions of an octahedral complex [16]. In the electronic spectra of cobalt(II) complexes, two bands of weak intensity are observed in the visible region as shown in Table 6. These bands are assigned to $^4T_{1g}(F) \rightarrow {}^4T_{2g}(F)$ and $^4T_{1g}(F) \rightarrow {}^4T_1(P)$ of an octahedral Co(II) complexes [16].

Table 5. UV-Vis absorption bands for ligands

Ligands	**π-π* (nm)**
L_1	314, 355
L_2	236
L_3	239
L_4	240
L_5	238

Table 6. UV-Vis absorption bands for cobalt(II) complexes.

Complexes	MLCT (nm)	$^4T_{2g}(F) \rightarrow {}^2T_{2g}(P)$ (nm)	$^4T_{1g}(F) \rightarrow {}^4T_{2g}(F)$ (nm)	$^4T_{1g}(F) \rightarrow {}^4T_{2g}(F)$ (nm)
C1	268, 338	446	578	-
C2	277, 365	632	720	-
C3	269, 338	588	588	-
C4	274, 368	577	577	-

C5	266, 343	437	437	-
C6	257, 375	470	-	552-638
C7	266, 361	-	-	-
C8	257, 306	435	-	526
C9	259, 306	443	-	694
C10	269, 365	568	-	657

4.2.1 UV-Vis spectroscopy of metal complexes of bis-(benzimidazolyl)pyridine (L_1)

In the spectrum of $\mathbf{L_1}$ presented in Figure 25, two intense bands are observed at 313 nm and 343 nm assigned to π- π* transitions of the intra-ligand transitions, similar observations were reported in literature [17]. The complexes showed intense absorption in the UV region with two bands at 268 and 338 nm for $\mathbf{C_1}$ and at 265 and 358 nm for $\mathbf{C_6}$ assigned to MLCT transitions due to dπ(M) to π(ligand) [17]. In the electronic spectrum of $\mathbf{C_1}$, two bands at lower intensity are observed at 446 nm and assigned to $^4T_{2g} \rightarrow {}^2T_{2g}$ and 580 nm assigned to $^4T_{1g}(F) \rightarrow {}^4T_1(P)$ to transitions in an octahedral complex [18]. The spectrum of $\mathbf{C_6}$ showed two bands at 447 nm assigned to $^4T_{1g}(F) \rightarrow {}^4T_1(P)$ and a multiple band between 552 and 638 assigned to $^4T_{1g}(F) \rightarrow {}^4T_{2g}(P)$ transitions, these bands confirm that the geometry around the metal Co^{2+} ion is octahedral [16].

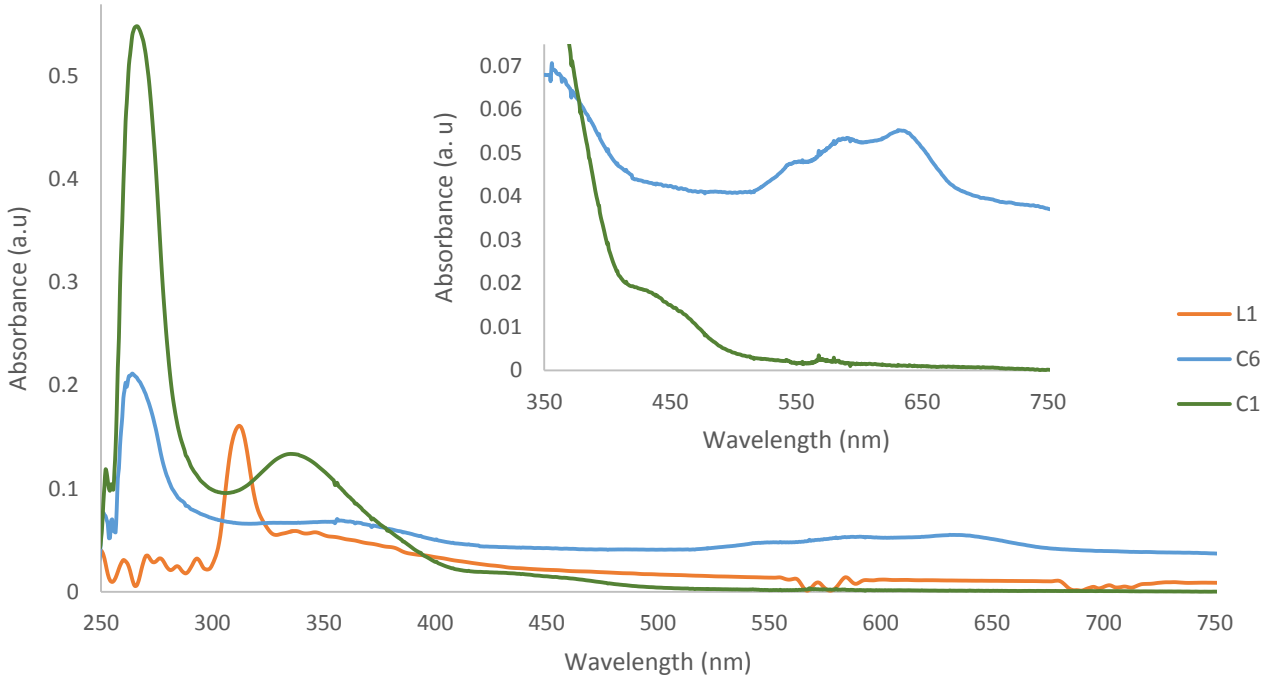

Figure 25. UV-Vis spectra of $\mathbf{L_1}$ and its Ru(II) ($\mathbf{C_1}$) and Co(II) ($\mathbf{C_6}$) complexes.

4.2.2 UV-Vis spectroscopy of metal complexes of bis-(butylbenzimidazolyl)pyridine (L_2)

The electronic spectrum of $\mathbf{L_2}$ (Figure 26), shows a band in the UV region at 236 nm assigned to π- π* transitions. In the electronic spectra of the complexes, these bands were observed as two intense bands at 277 and 365 nm for $\mathbf{C_2}$ and at 266 and 361 nm for $\mathbf{C_7}$ assigned to MLCT transitions. The spectrum of ruthenium(II) complex, $\mathbf{C_2}$ was observed to show two bands at 632 and 720 nm assigned to $^4T_{2g} \rightarrow {}^2T_{2g}$ and $^4T_{1g}(F) \rightarrow {}^4T_1(P)$ respectively transitions of an octahedral Ru(II) complex [19]. The electronic spectrum of $\mathbf{C_7}$ does not show any observable d-d transition the reason for

this could be the reaction was stopped before the ligands were coordinated to the metal ion was complete or the complex is soluble in the solvent that was used for synthesis.

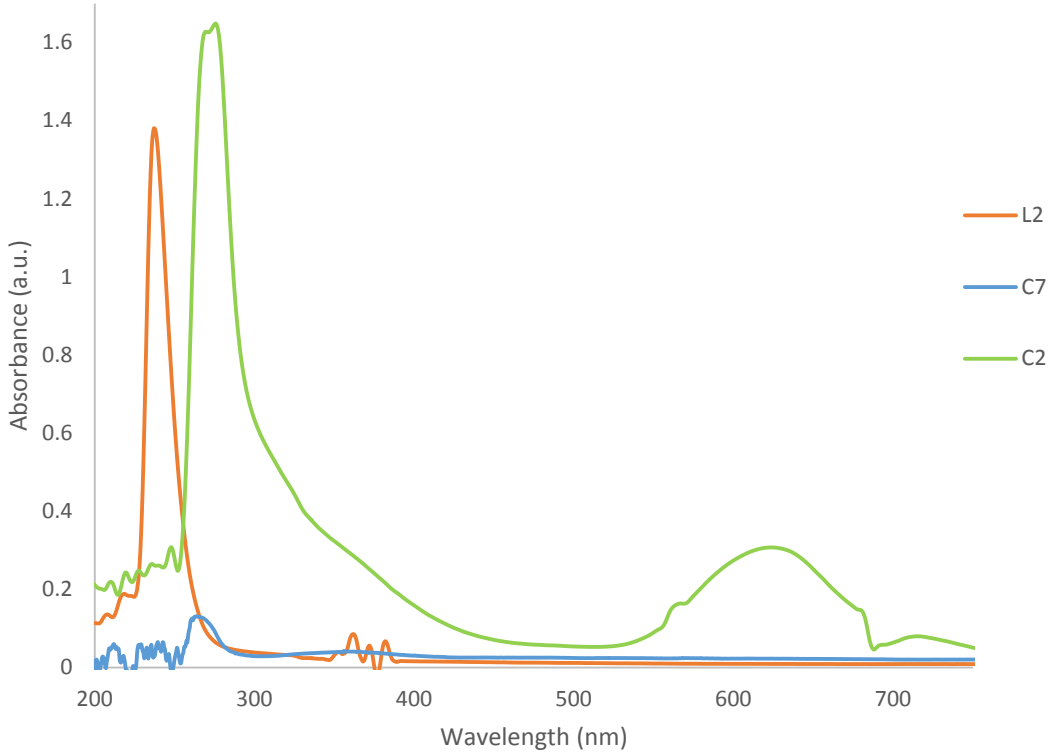

Figure 26. UV-Vis spectra of **L_2** and its Ru(II) (**C_2**) and Co(II) (**C_7**) complexes.

4.2.3 UV-Vis spectroscopy of metal complexes of bis-(benzylbenzimidazolyl)pyridine (L_3)

Figure 27 shows the electronic spectra of **L_3** and its corresponding metal complexes. In the spectrum of **L_3**, intense band is observed at 239 nm assigned to π- π* transitions in the UV region. The complexes showed two bands in the UV region at 269 and 338 nm for **C_3** and at 257 and 306 nm for **C_8** assigned to MLCT. In the electronic spectrum of **C_3**, a broad band with hyperfine splitting at lower intensity is observed in the range 452-

588 nm assigned to $^4T_{2g} \rightarrow {}^2T_{2g}$ and $^4T_{1g}(F) \rightarrow {}^4T_1(P)$ transitions [19]. The electronic spectrum of **C_8** showed two bands at 435nm assigned to $^4T_{1g}(F) \rightarrow {}^4T_1(P)$ and 526 nm assigned for $^4T_{1g}(F) \rightarrow {}^4T_{2g}(P)$, the bands in the visible region confirms the structure of Co(II) complex to be octahedral [18].

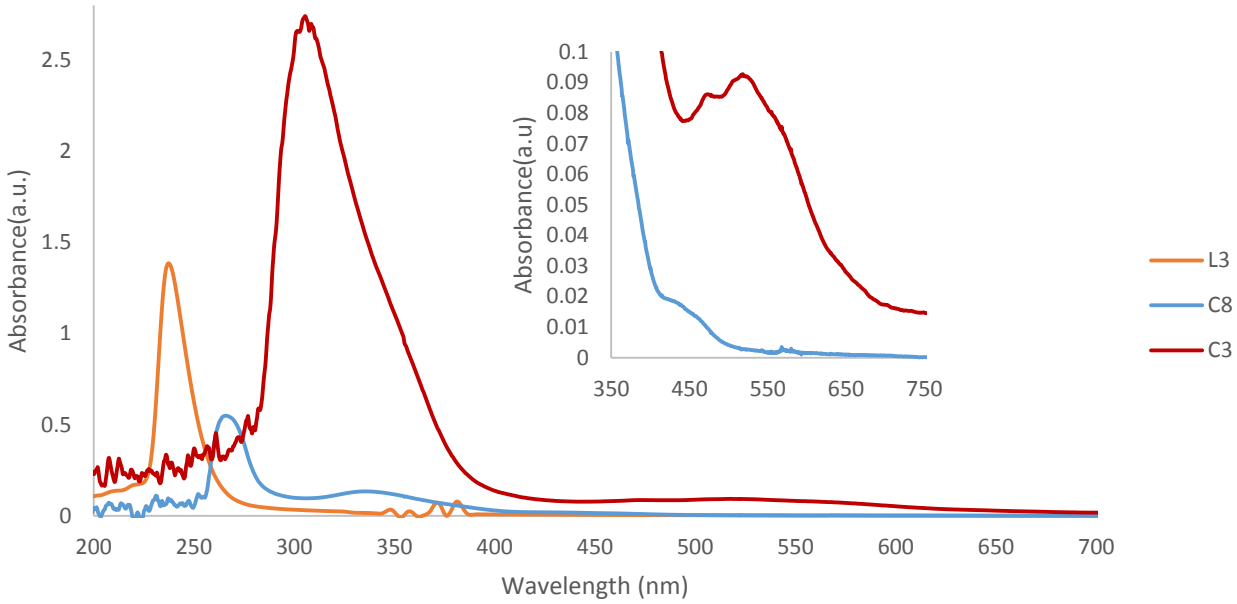

Figure 27. UV-Vis spectra of **L_3** and its Ru(II) (**C_3**) and Co(II) (**C_8**) complexes.

4.2.4 UV-Vis spectroscopy of metal complexes of bis-(pyrazolyl)pyridine (L_4)

The electronic spectrum of **L_4** shown in Figure 28, with intense bands at 240 nm assigned to π- π* transitions in the UV region. The complexes show two bands in the UV region at 259 and 306 nm for **C_4** and at 257 and 306 nm for **C_9** assigned to MLCT. In the electronic spectrum of **C_4,** a broad band is observed at 588 nm assigned to $^4T_{2g} \rightarrow {}^2T_{2g}$ transition [15,16]. The electronic spectrum of **C_9** showed two bands at 443 nm

assigned to $^4T_{1g}(F) \rightarrow {}^4T_1(P)$ and 694 nm assigned for $^4T_{1g}(F) \rightarrow {}^4T_{2g}(P)$ transitions, the electronic spectrum of Co(II) complex confirms the compound to be octahedral [18].

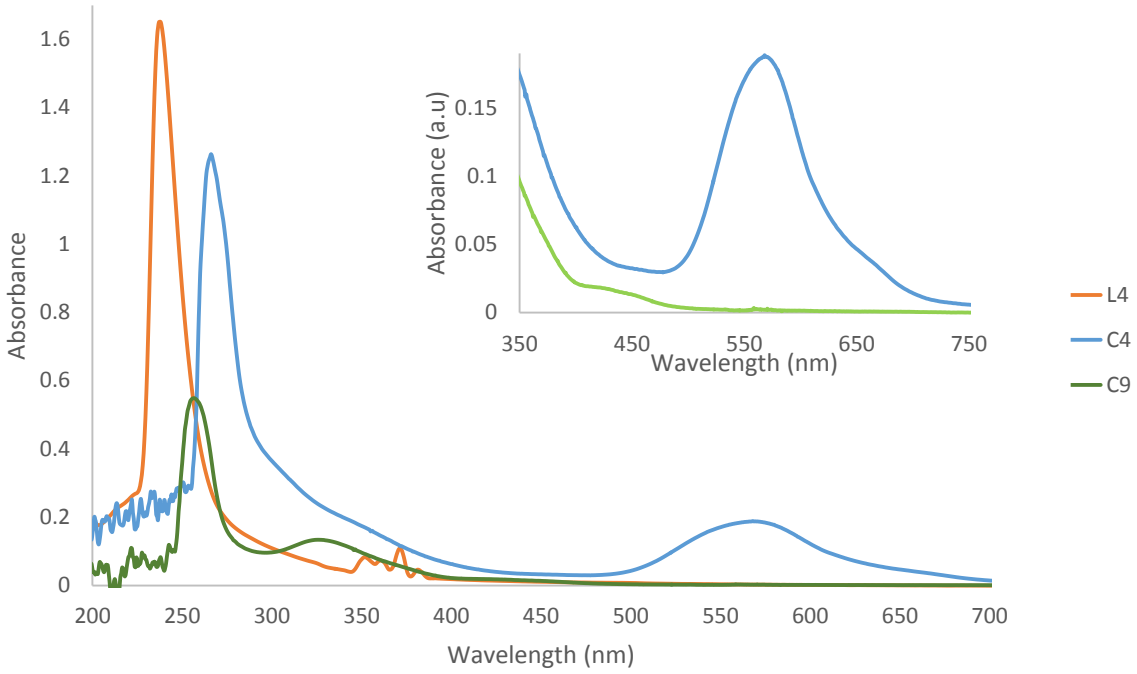

Figure 28. UV-Vis spectra of **L_4** and its Ru(II) (**C_4**) and Co(II) (**C_9**) complexes.

4.2.5 UV-Vis spectroscopy of metal complexes of bis-(3,5-dimethylpyrazolyl)pyridine (L_5).

In Figure 29, the electronic spectrum of **L_5** show a band at 238 nm assigned to π-π* transitions in the UV region. Each of the complexes showed two bands in this region at 269 and 338 nm for **C_5** and at 257 and 306 nm for **C_{10}** assigned to MLCT. In the UV region the complexes were observed at lower intensity and at higher frequency when

compared to the ligands. The electronic spectrum of **C_5** shows two bands at 437 nm assigned to $^4T_{2g} \rightarrow {}^2T_{2g}$ and 575 nm assigned to $^4T_{1g}(F) \rightarrow {}^4T_1(P)$ transitions [21]. The electronic spectrum of **C_{10}** also shows two bands at 568 nm assigned to $^4T_{1g}(F) \rightarrow {}^4T_1(P)$ and 657 nm assigned for $^4T_{1g}(F) \rightarrow {}^4T_{2g}(P)$ [18].

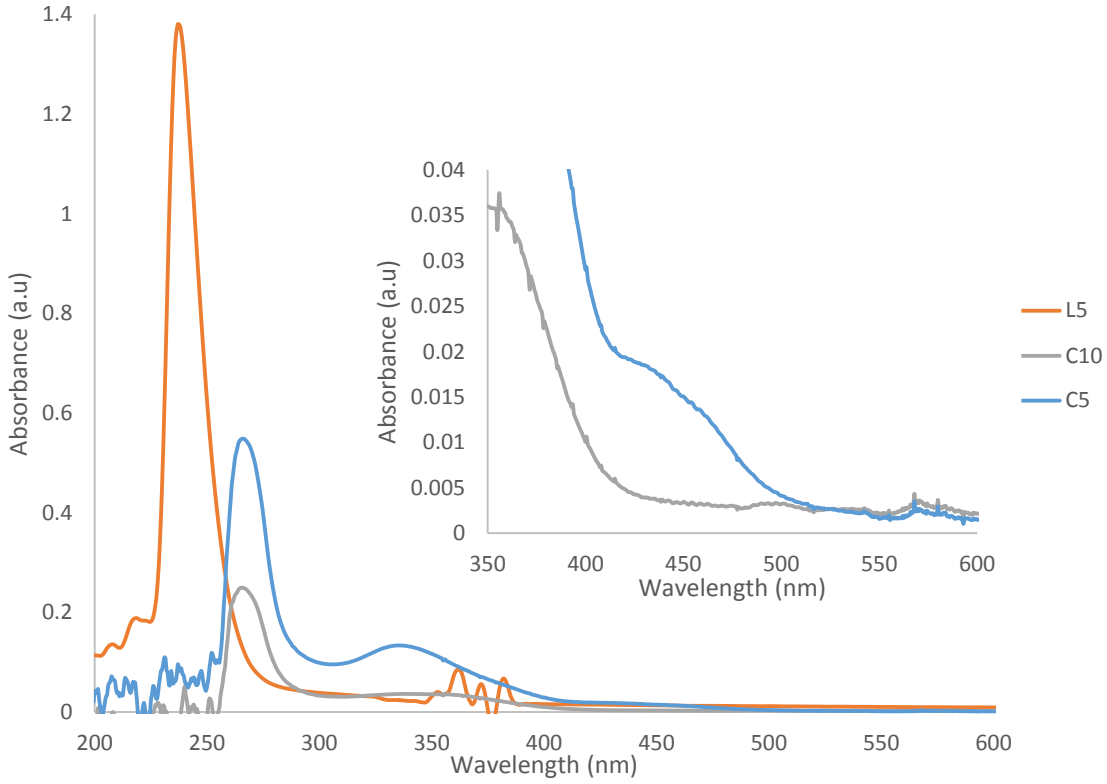

Figure 29. UV-Vis spectra of **L_5** and its Ru(II) (**C_5**) and Co(II) (**C_{10}**) complexes

4.3 Emission spectroscopy of the complexes.

The emission spectra measurements of Ru(II) and Co(II) complexes recorded in DMSO solutions were carried out in order to determine the emission properties of cobalt(II) and

ruthenium(II) complexes in a range of 200-900 nm. The complexes show photo excitation above 400 nm similar to those reported by Chen *et al.*[21]. The emission of ruthenium(II) complexes were observed to have a common broad emission bands above 400 nm with different emission intensities due to electronic transition from the ground state to the excited state of the metal ions [22].

4.3.1 Emission spectroscopy of Ru(II) complexes

The emission of ruthenium(II) complexes were observed to have a broad emission band at 703, 703, 705,703 and 704 for $\mathbf{C_1}$, $\mathbf{C_2}$, $\mathbf{C_3}$, $\mathbf{C_4}$ and $\mathbf{C_5}$ respectively. $\mathbf{C_1}$ relative to $\mathbf{C_2}$ and $\mathbf{C_3}$ red-shifted by 1nm, the red-shift emission is due to the stability of ^{3}MLCT state by the π-conjugation of $\mathbf{L_3}$ [23]. While in $\mathbf{C_5}$ blue-shifted by 2nm compared to $\mathbf{C_4}$, the blue-shift is ascribed to lowering of intraligand charge transfer originated from the LUMO [23, 24] due to electron donating group present in intraligand of $\mathbf{C_5}$ [25]. The emission intensity showed gradual increase with decrease in the molar weight of the complexes of bis-(imino)pyridine in the order $\mathbf{C_1}$>$\mathbf{C_2}$>$\mathbf{C_3}$ while in the complexes of bis-(pyrazolyl)pyridine increase in emission intensity was observed with increase in molar weight of the complexes in the order $\mathbf{C_5}$>$\mathbf{C_4}$ as shown in Figure 30. The emission of $\mathbf{C_3}$ is observed at lower intensity compared to $\mathbf{C_1}$ and $\mathbf{C_2}$ this is due to while the intensity of $\mathbf{C_4}$ is low compared to $\mathbf{C_5}$ is due to molecular weight [26]. The emission for complexes of bis-(pyrazoly)pyridine is observed at low intensity compared those of bis-(imino)pyridine, this is due low ligand field excitation state ligands [30]. All the complexes were observed to show a broad emission ascribed to ^{3}MLCT emission [24]

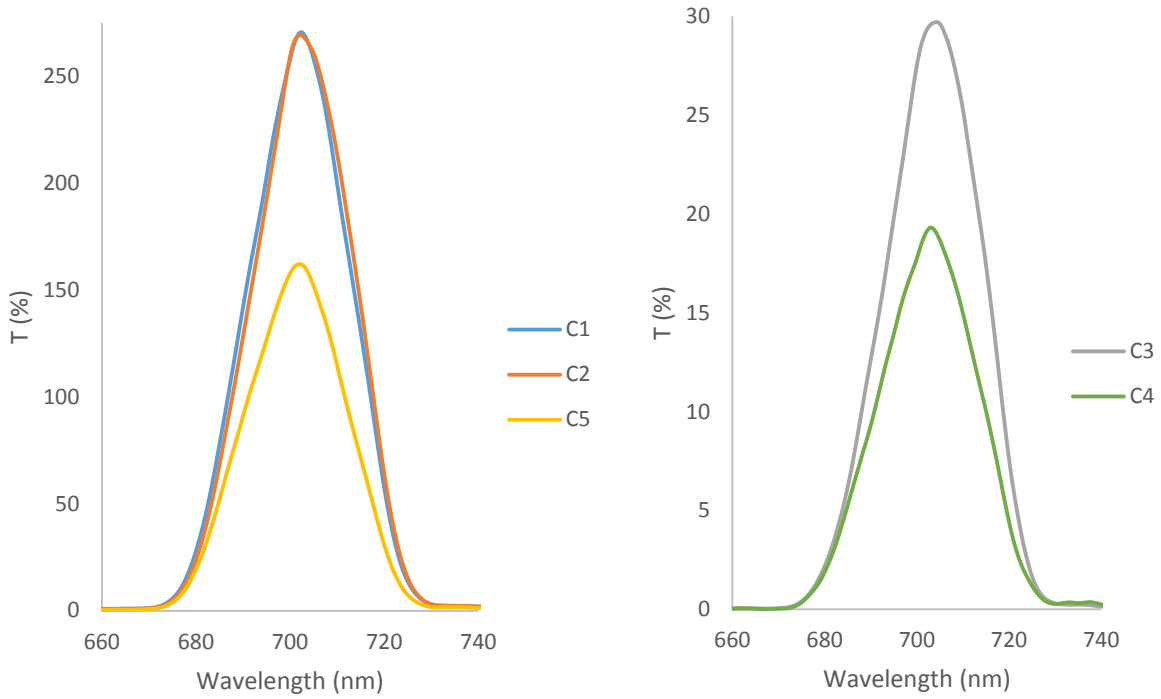

Figure 30. Emission spectra of Ru(II) complexes ($\mathbf{C_1}$, $\mathbf{C_2}$, $\mathbf{C_3}$, $\mathbf{C_4}$ and $\mathbf{C_5}$)

4.3.2 Photoluminesce (PL) spectroscopy of Co(II) complexes

The photoluminescence emission spectra of cobalt(II) complexes in DMSO solution were shown in Figure 31. The complexes were observed to exhibit strong photo emission maxima, $\mathbf{C_6}$, $\mathbf{C_7}$, $\mathbf{C_8}$, $\mathbf{C_9}$ and $\mathbf{C_{10}}$ were observed to show excitation at 705, 664, 708, 704 and 705 nm respectively. The complex, $\mathbf{C_7}$ relative to $\mathbf{C_6}$ and $\mathbf{C_8}$ blue-shifted by 41 nm relative to $\mathbf{C_6}$ the blue-shift emission is due to the introduction of alkyl groups [31]. In the electronic absorption of $\mathbf{C_7}$ d-d transition was not observed therefore $\mathbf{C_7}$ has high π* orbital energy hence the lower emission is obtained compared to $\mathbf{C_6}$ and $\mathbf{C_8}$ [32]. While $\mathbf{C_8}$ red-shifted by 3nm, the π-conjugated substituent present on $\mathbf{L_3}$ enhanced the electronic stabilization of the ^{3}MLCT excitation state of the complex [31, 33]. The

complex, C_{10} relative to C_9 experience a red-shift by 1nm, the red-shift is due to the alkly substituent on pyrazole that enhanced the π-accepting properties of pyrazole and caused increase in HOMO-LUMO [34].

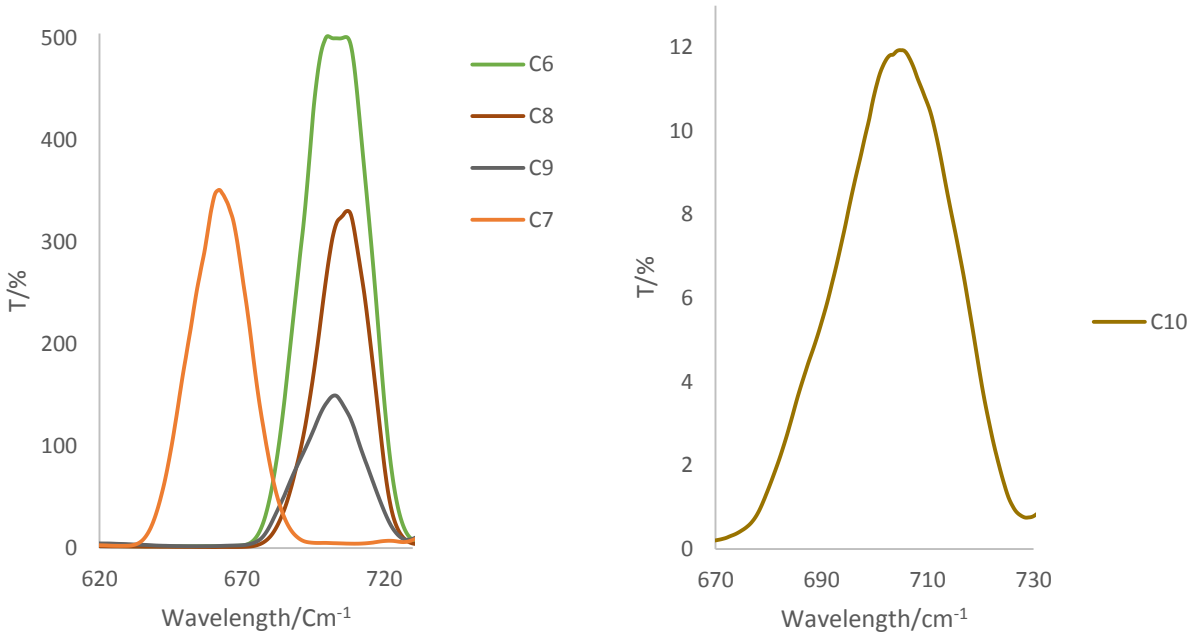

Figure 31. Emission spectra of Co(II) complexes (C_1, C_2, C_3, C_4 and C_5)

4.4 Electrochemistry of metal complexes.

4.4.1 Electrochemistry of ruthenium(II) complexes.

4.4.1.1 Electrochemistry of ruthenium(II) complexes of bis-(imino)pyridine.

The cyclic voltammogram of ruthenium(II) complexes (Figures 32-34) show the Ru(II)/Ru(III) redox couple at positive and negative potentials. The oxidation peaks were not visible in the cyclic voltammogram of **C_1**, **C_2** and **C_3**. At the cathodic potential, irreversible peak was observed at –1.01 V. The high negative potential is due to reduction of ligands [35]. While the complexes containing derivatives of bis-(imino)pyridine showed irreversible reduction peak at -1.00 and -0.99 V for **C_2** an **C_7** respectively. The reduction potential ascribed to the presence of a protection group on the N-atoms of the benzimidazole ring [36]. The high values observed for reduction potential is ascribed to reduction of ligand [37].

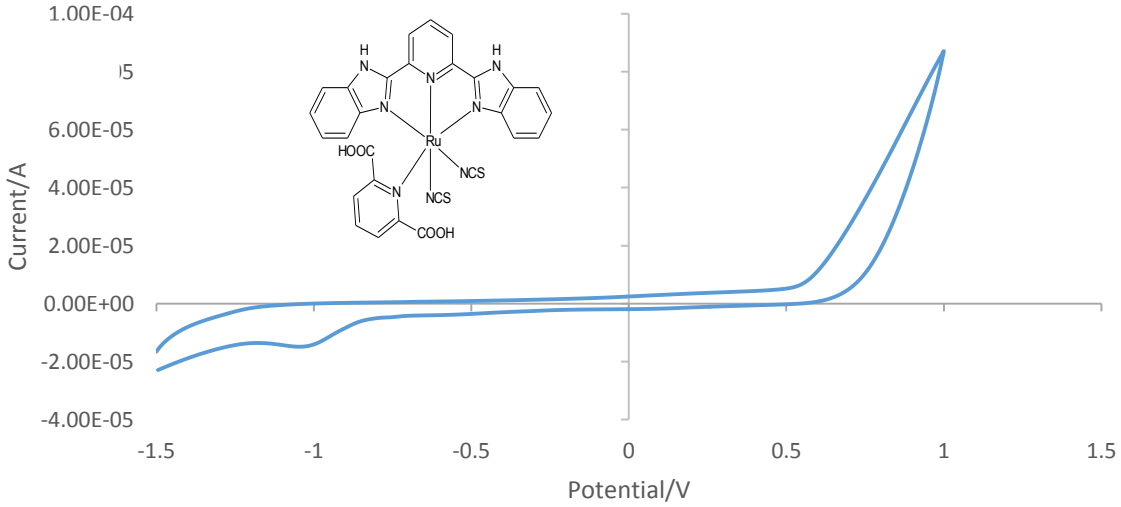

Figure 32. Cyclic voltammetry of **C_1**

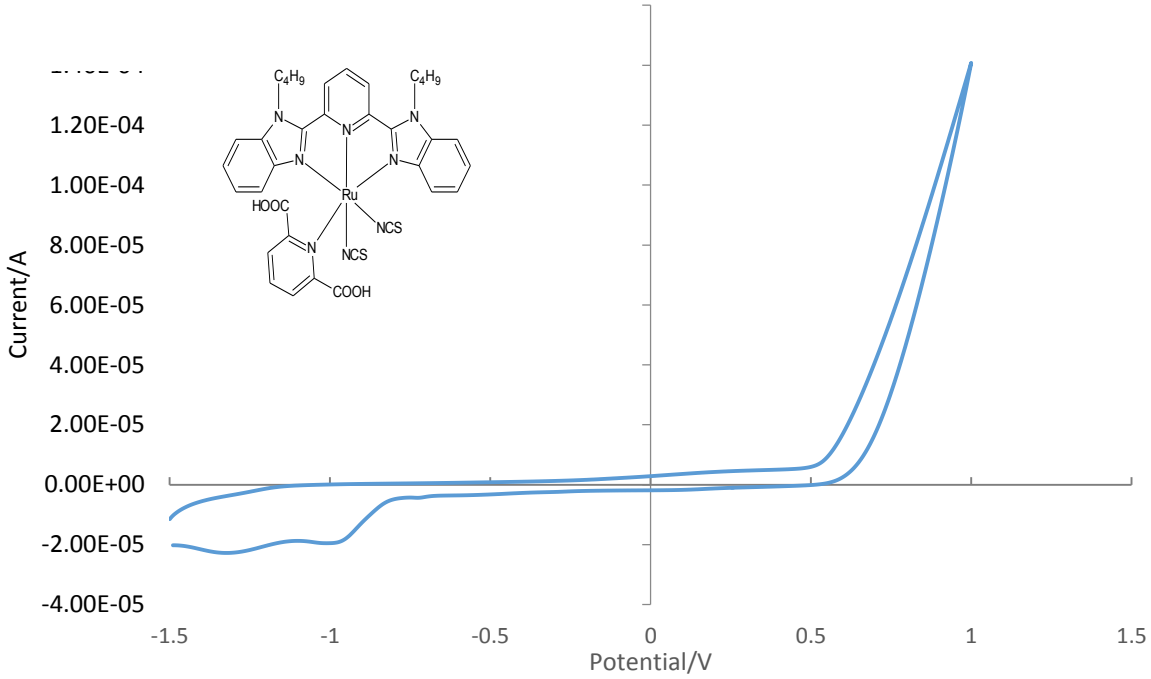

Figure 33. Cyclic voltammetry of **C_2**

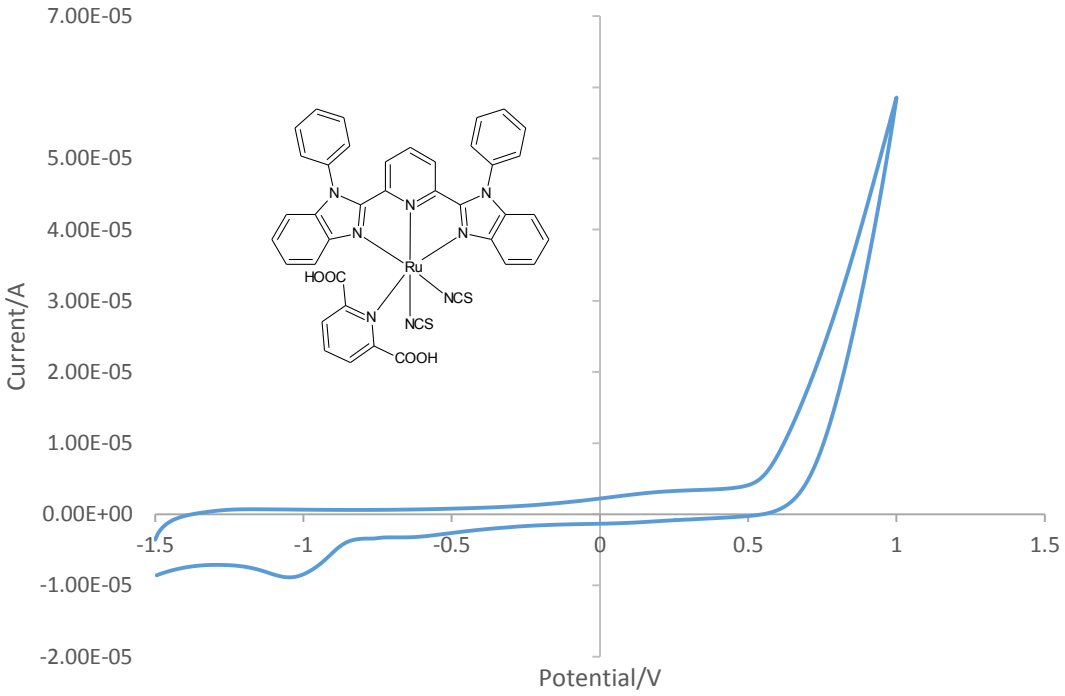

Figure 34. Cyclic voltammetry of **C_3**

4.4.1.2 Electrochemistry of ruthenium(II) complexes of bis-(pyrazoly)pyridine

Irreversible oxidation peak in the cyclic voltammogram of **C_4** and **C_5** was observed at 0.23V and 0.24V respectively as shown in Figures 35 and 36. The low oxidation potentials for the complexes attribute to σ-donor ligand that stabilize the oxidized Ru(II) metal ion [38]. At the anodic potential irreversible reduction peaks were observed at –1.01 V for both **C_4** and **C_5**. The negative irreversible peak for both **C_4** and **C_5** may be assigned to the contribution of ligands containing pyrazole ring [38, 39]. The irreversible process involved is reduction of ligand [39].

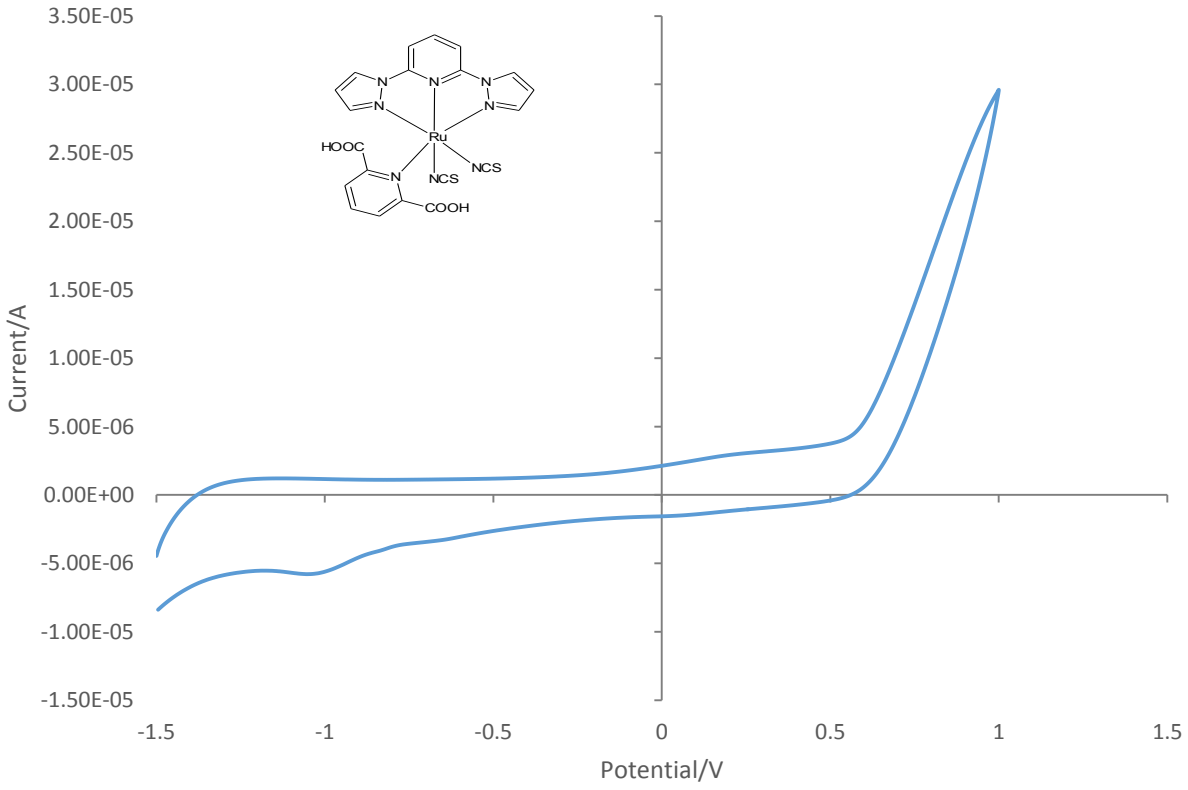

Figure 35. Cyclic voltammetry of **C_4**

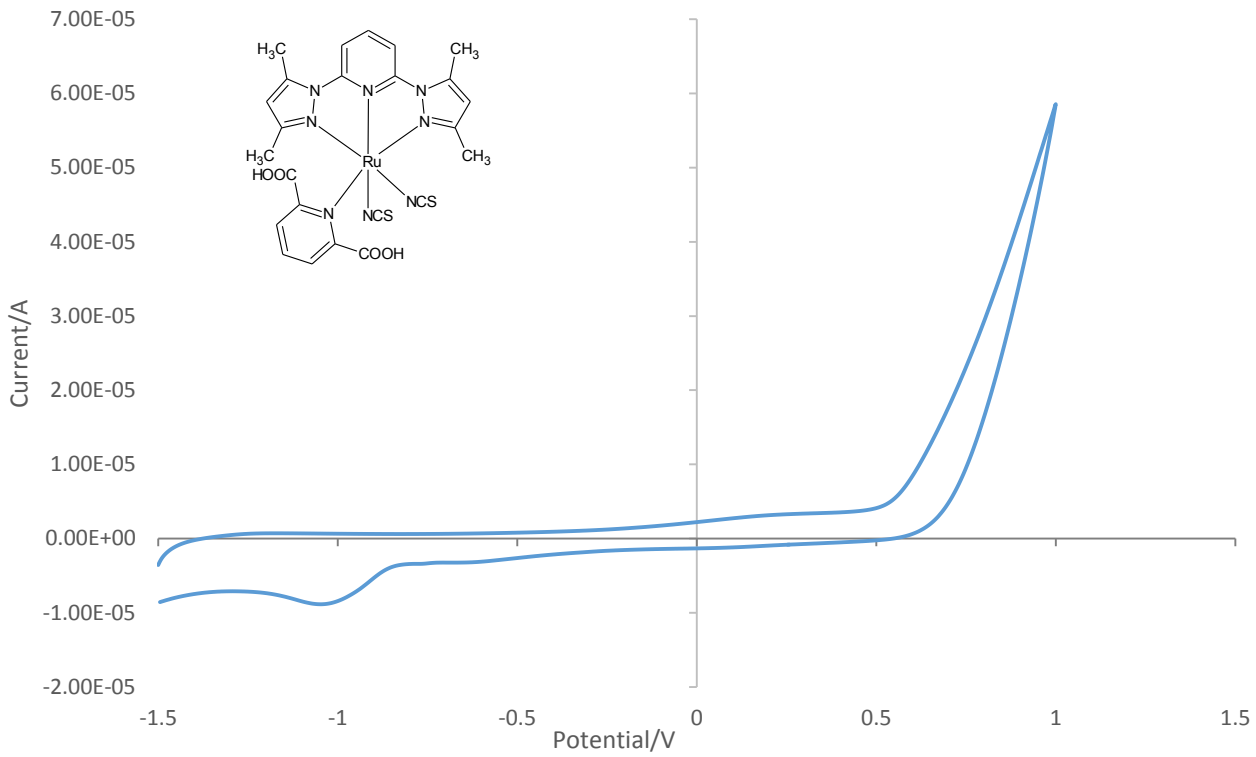

Figure 36. Cyclic voltammetry of **C_5**

4.4.2 Electrochemistry of cobalt(II) complexes

4.4.2.1 Electrochemistry of cobalt(II) complexes of bis-(imino)pyridine.

Cyclic voltammogram of cobalt(II) complexes show the Co(II)/Co(III) redox couple at oxidation and reduction potentials. In the cyclic voltammogram of **C_6** shown in Figure 33, irreversible oxidation peak was observed at -0.42 V ascribed to oxidation of electron withdrawing group from uncoordinated NH group of benzimidazole [40], while the reversible oxidation for **C_7** and **C_8** (Figures 37 and 39) was observed at -0.38 and -0.29 respectively attribute to the oxidation of ligand. The irreversible oxidation peaks

observed at +0.55, +0.12V for **C_6**, +0.58, 0.10V for **C_7** and +0.83, +0.17 for **C_8**, the more positive oxidation potentials attribute to .The positive reduction peaks observed at 0.46, +0.46 and +0.48V for **C_6**, **C_7** and C8 respectively, the potentials are assigned to assigned ancillary group that result in reduction of the cobalt(II) metal ion [41]. The negative potential at -0.48 is due to the ligand-based reduction [35]. The high reduction potentials observed at -1.11, -1.09 and -1.02 V for **C_6**, **C_7** and **C_8** assigned to the reduction of the metal due to electron transfer to the π-LUMO of the anchoring ligand (2,6-pyridinedicarboxylic acid) resulting in coordination of the metal ion and the anchoring ligand [42].

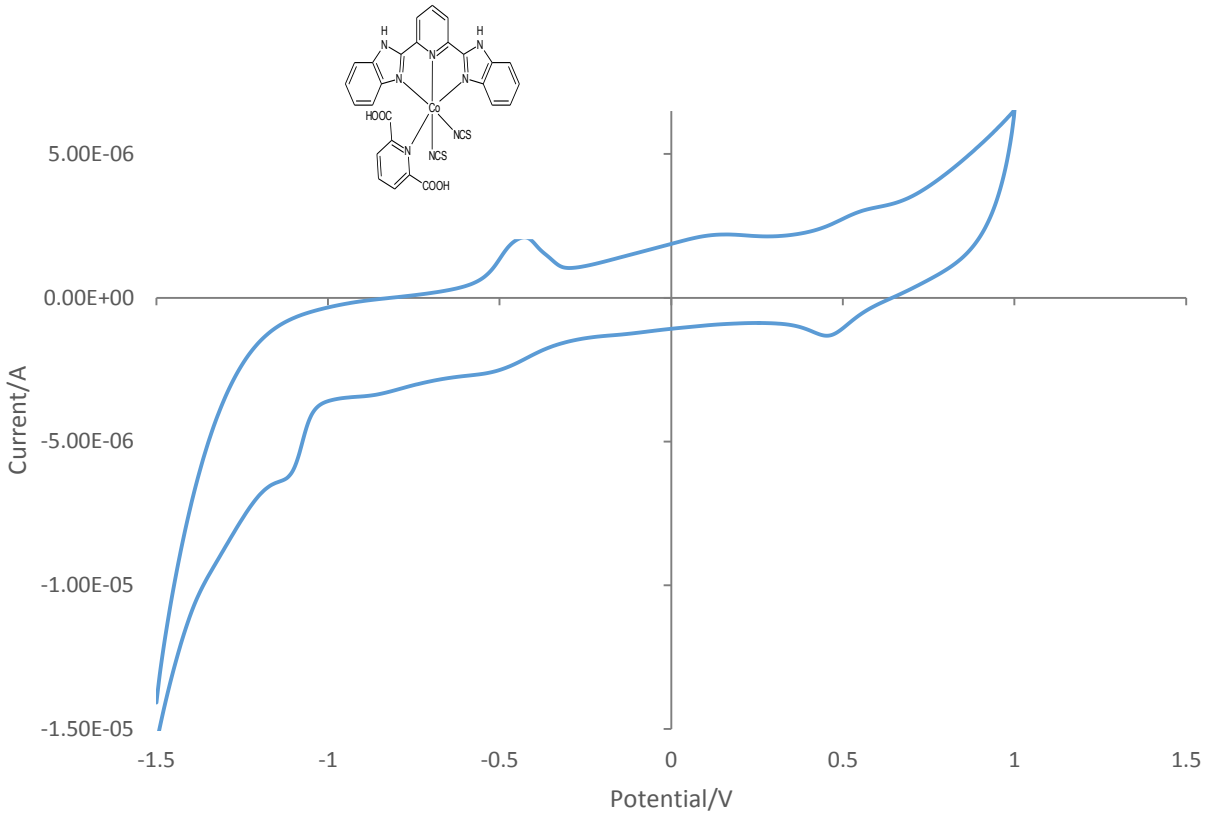

Figure 37. Cyclic voltammetry of **C_6**

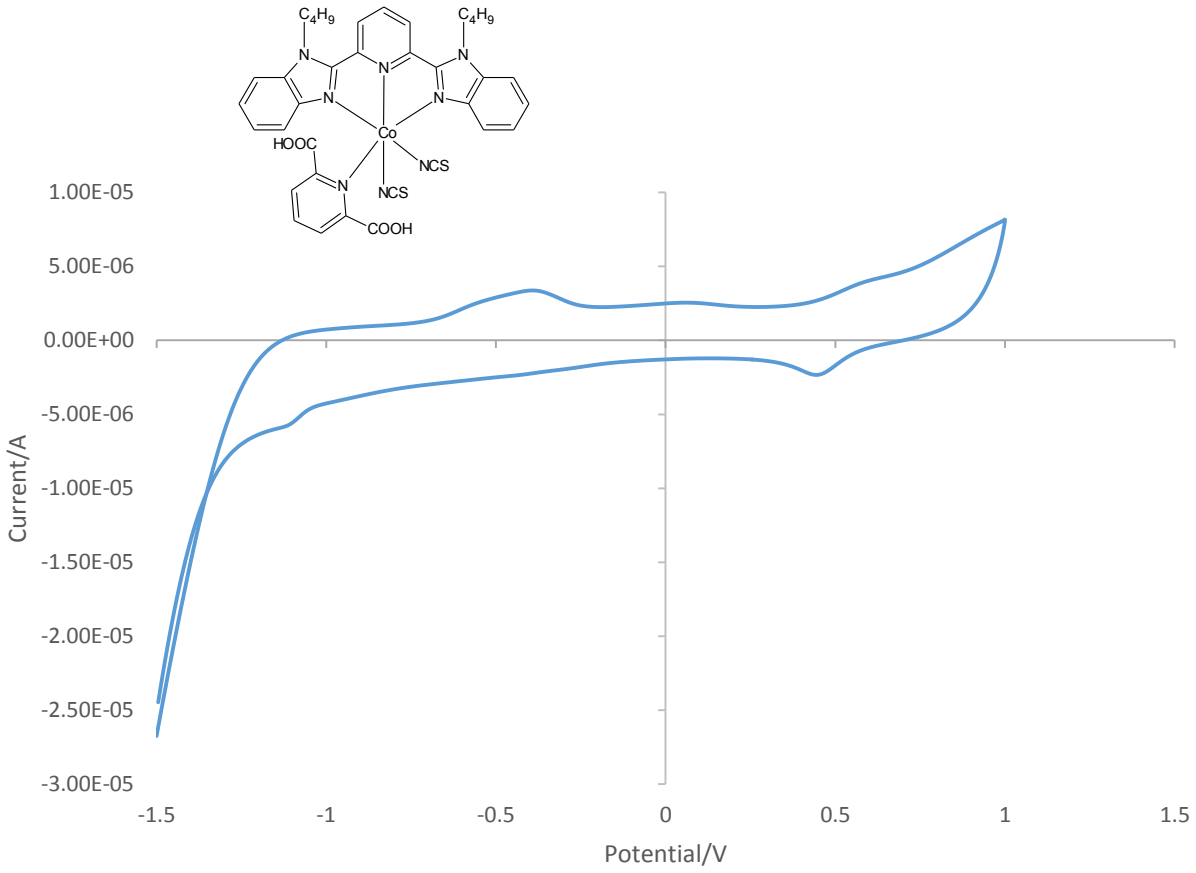

Figure 38. Cyclic voltammetry of $\mathbf{C_7}$

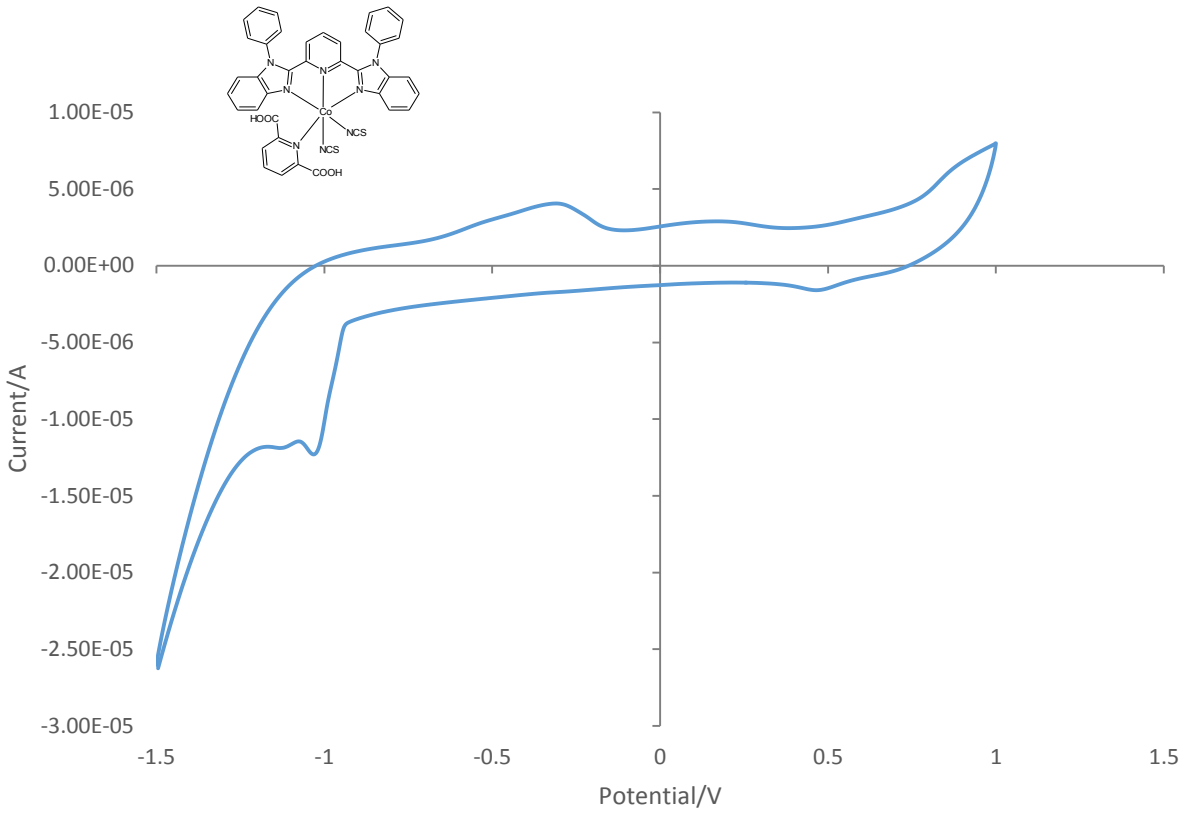

Figure 39. Cyclic voltammetry of $\mathbf{C_8}$

4.4.2.2 Electrochemistry of cobalt(II) complexes of bis-(pyrazolyl)pyridine.

In the cyclic voltammogram of $\mathbf{C_9}$ and $\mathbf{C_{10}}$ (Figures 40 and 41) irreversible oxidation peaks were found at 0.41 and 0.77 V respectively, the increase in potential of $\mathbf{C_{10}}$ is due to electron withdrawing group ($-CH_3$) present on the pyrazole causing the insufficient electrons in the ligand [42]. The reversible potentials were observed at -1.20 V for $\mathbf{C_9}$ and -0.41, -120 V for $\mathbf{C_{10}}$. The high reversible peak ascribed to the oxidation of the metal [22], in all metal-based oxidation reversible oxidation is experienced [43]. At the negative reduction peaks were observed at -1.11V for $\mathbf{C_9}$ and 0.48,-1.03V for C10. The

high reduction potentials is due to the presence of a pyrazole ring [22, 44] causing the reduction to take place in the metal ion [41]. The positive reduction observed in the voltammogram of C_{10} is related to the red-shift observed in the visible region of $\mathbf{C_{10}}$ spectrum (Figure 33), it can also be ascribed to the ancillary ligand (thiocynate) [41].

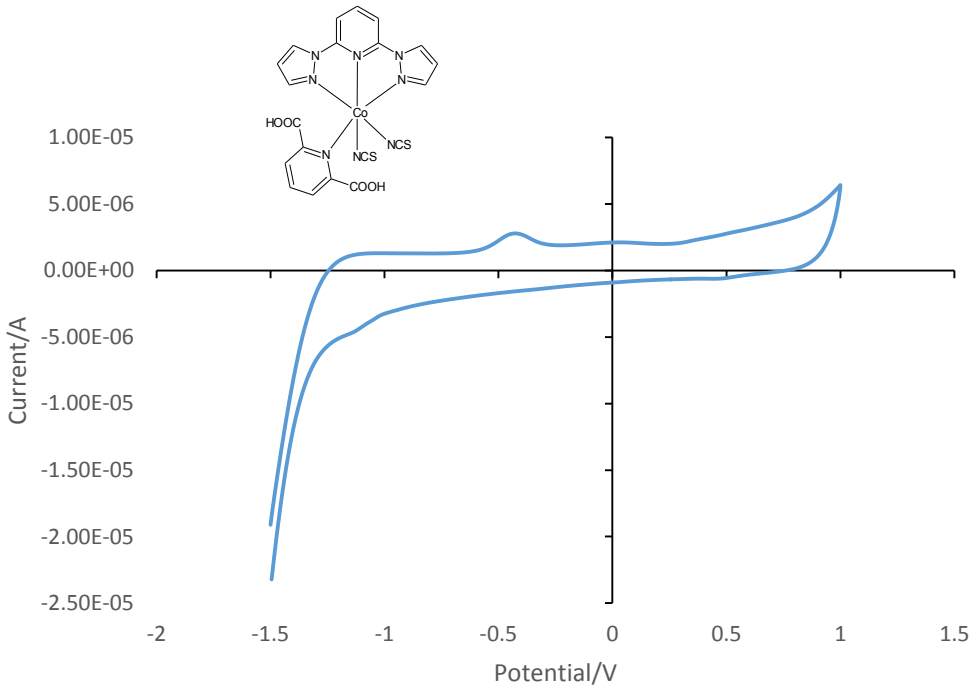

Figure 40. Cyclic voltammetry of $\mathbf{C_9}$

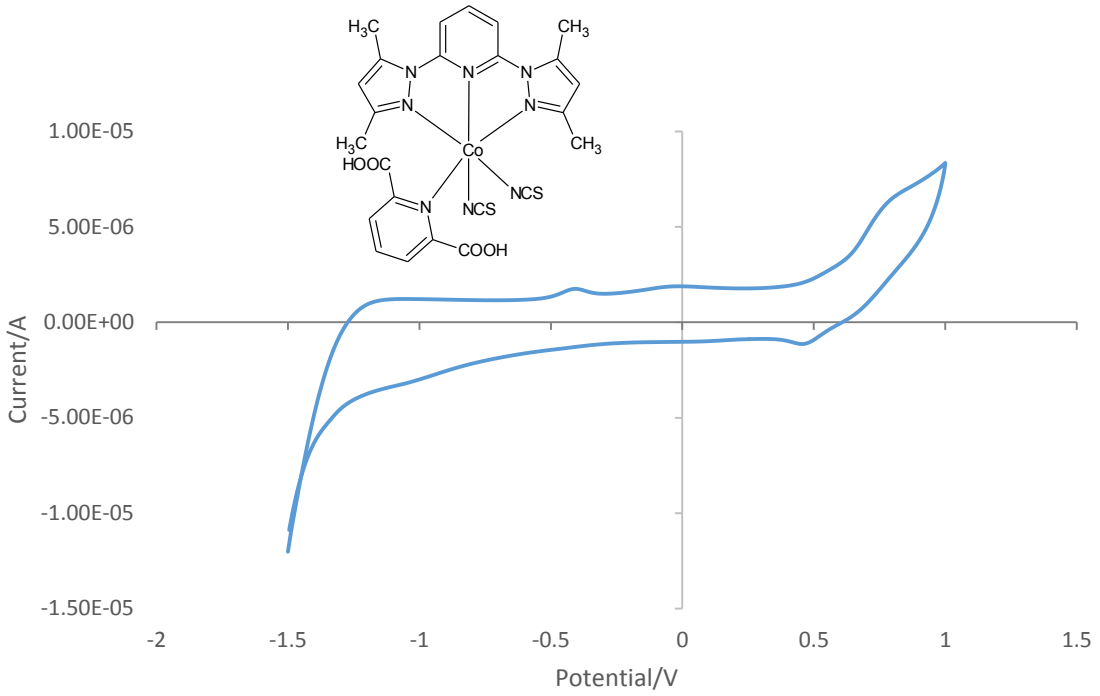

Figure 41. Cyclic voltammetry of $\mathbf{C_{10}}$

4.5 Solar cell fabrication and current-voltage characterization of N719, and some synthesized Ru(II) and Co(II) complexes.

The I-V characterization of the cells was performed using semiconductor parameter analyzer. The results of the cells are obtained from the I-V curves were used to determine the conversion efficiency of the DSSC of N719, ruthenium(II) and cobalt(II) complexes, where the solar cell efficiency using the following equation [46]:

$$\eta = \frac{Jsc \times Voc \times FF}{P}$$

$$FF = \frac{Pmax}{Jsc\,Voc}$$

$$Jsc = \frac{Isc}{A}$$

Where η is the conversion efficiency, J_{sc} is the short circuit current, FF is the fill factor and P is the incident light which equals to 0.08 W for **N719**, **C_1**, **C_2**, **C_4** and equals to 0.04 W for **C_5** and **C_8**-**C_{10}**.

Photographic picture of fabricated solar cells using some ruthenium(II), cobalt(II) and N719 is presented in Figure 42.

Figure 42. Photographic picture of fabricated solar cells.

4.5.1 Current-voltage characterization of N719 dye.

The results of the dye-sensitized solar cell obtained from I-V curve of **N719** shown in Figure 39 were used to determine the efficiency of the cell. The efficiency obtained was 8.85% which was similar to that reported literature [46] where **N719** was used in dye-sensitized solar cell.

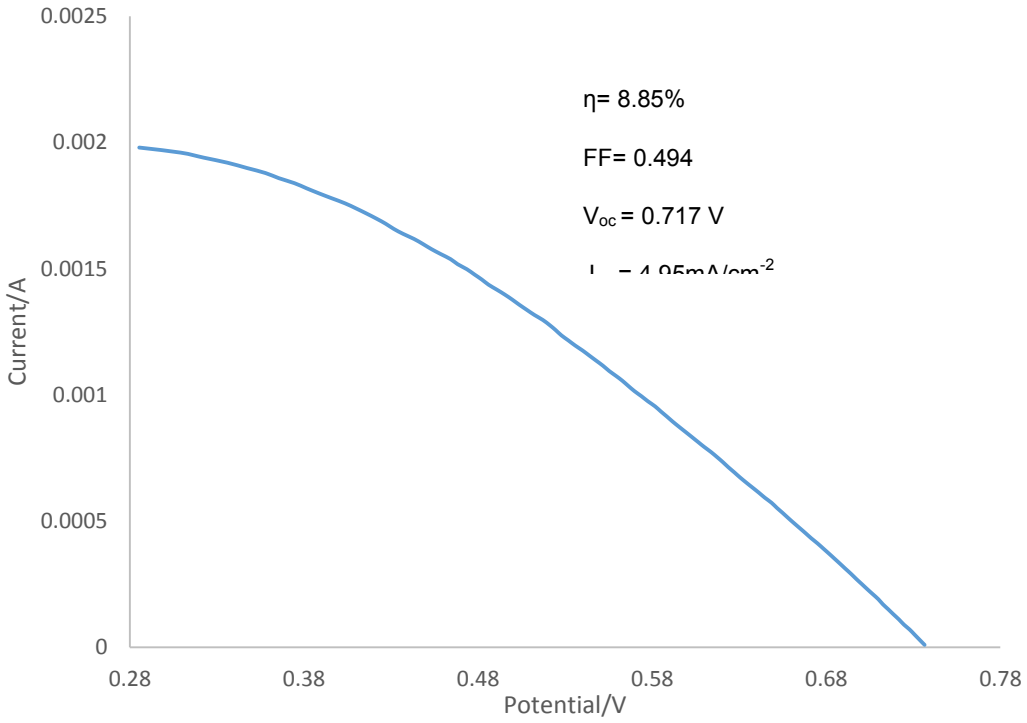

Figure 43. I-V curve of N719 dye-sensitized solar cell using I^-_3/I^- electrolyte

4.5.2 Current-voltage characterization of ruthenium(II) complexes.

The solar conversion efficiencies of the ruthenium dyes, $\mathbf{C_1}$, $\mathbf{C_2}$, $\mathbf{C_4}$ and $\mathbf{C_5}$ presented in Table 8, were obtained from the I-V curves shown in Figures 44-47. Complex, $\mathbf{C_3}$ was not characterized because of its low yield. The efficiencies of the ruthenium complexes

were very low compared to the **N719**, dye which was used as the standard dye in solar cell characterization. Complexes that consist of bis-(pyrazolyl)pyridine, **C_5**, showed the highest efficiency (1. 01×10^{-3} %).

Table 7 I-V characterization of ruthenium complexes

Complex	J_{sc}/ mAcm^{-2}	V_{oc}/ mV	P_{max}	FF	(η)
C_1	0.191	5.93 × 10^{-3}	0.09 × 10^{-3}	0.787	9.8 x10^{-5}
C_2	0.0176	14.3 × 10^{-3}	0.0171 × 10^{-3}	0.679	19.0x10^{-5}
C_4	0.199	37.0 × 10^{-3}	0.0442 × 10^{-3}	0.598	49.1 x10^{-5}
C_5	0.022	87.3 × 10^{-3}	0.0908 × 10^{-3}	0.517	101.0x10^{-5}

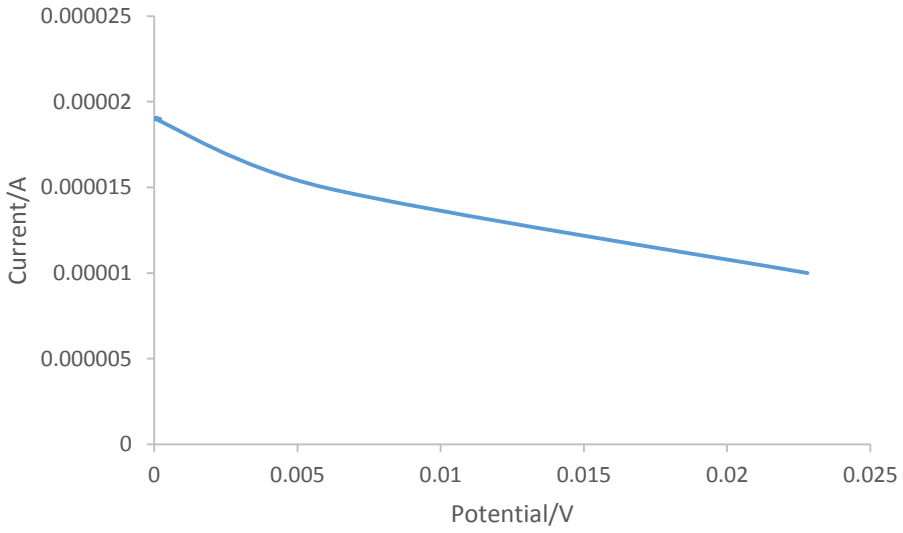

Figure 44. I-V curve **C_1** dye-sensitized solar cell using I^-_3/I^- electrolyte

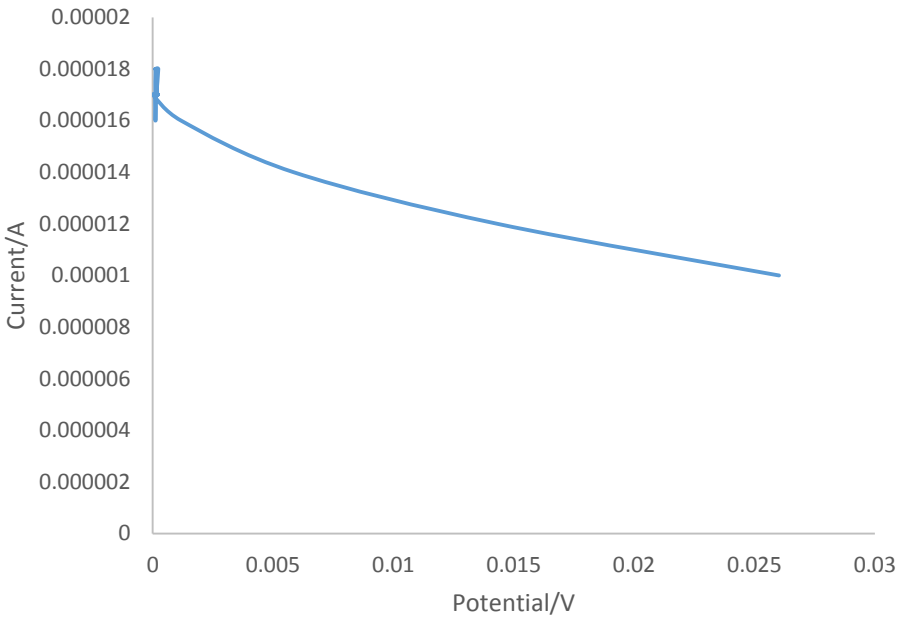

Figure 45. I-V curve of **C_2** dye-sensitized solar cell using I^-_3/I^- electrolyte

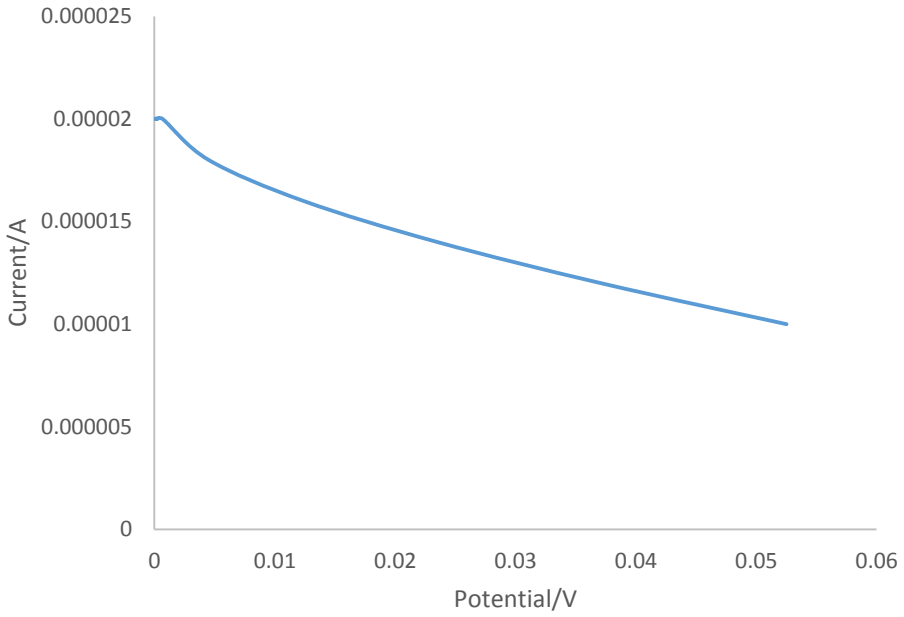

Figure 46. I-V curve of **C_3** dye-sensitized solar cell using I^-_3/I^- electrolyte

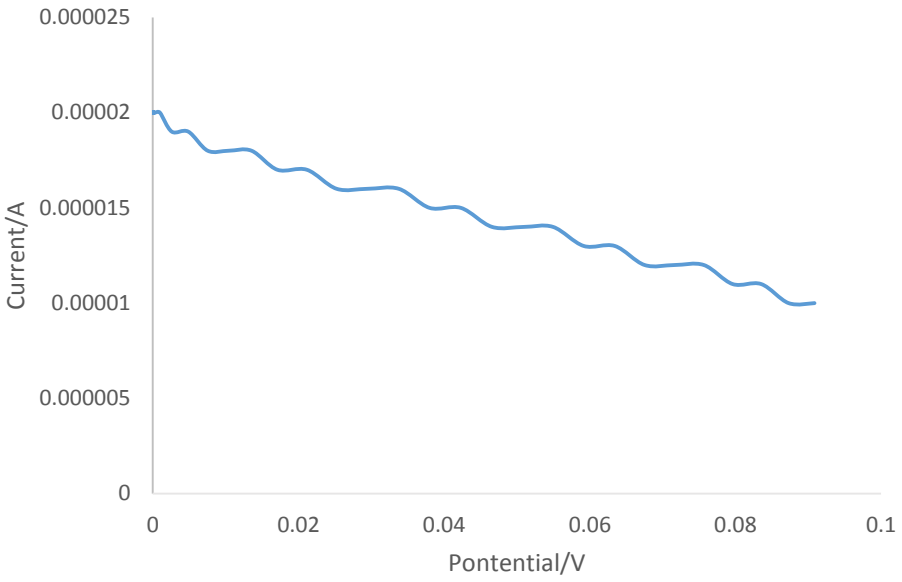

Figure 47. I-V curve of $\mathbf{C_5}$ dye-sensitized solar cell using I^-_3/I^- electrolyte

4.5.2 Current-voltage characterization of cobalt(II) complexes.

Table 9 show the solar conversion efficiencies of cobalt(II) dyes, $\mathbf{C_8}$, $\mathbf{C_9}$, and $\mathbf{C_{10}}$ obtained from the I-V curves represented in Figures 48-50. The solar conversion efficiency of cobalt(II) complexes were very low when compared to **N719** and the Ru(II) complexes. The efficiency of the complexes was between 0.60 $x10^{-5}$ and 1.5 $x10^{-5}$.The I-V characterization complex $\mathbf{C_6}$ was not done because it was lighter in colour and also $\mathbf{C_7}$ was not characterized because the d-d transition was not obtained in the electronic spectroscopy. The I-V curves were showing unusual results with coiled graphs which might be due to freshly prepared solar cells.

Table 8. I-V characterization of cobalt complexes

Complex	Jsc	Voc	Pmax	FF	(η)
C_8	0.00283	0.049×10^{-3}	0	2.93	1.0×10^{-5}
C_9	0.00347	0.016×10^{-3}	0.001×10^{-3}	11.35	1.5×10^{-5}
C_{10}	0.00119	0.161×10^{-3}	0.005×10^{-3}	1.64	0.60×10^{-5}

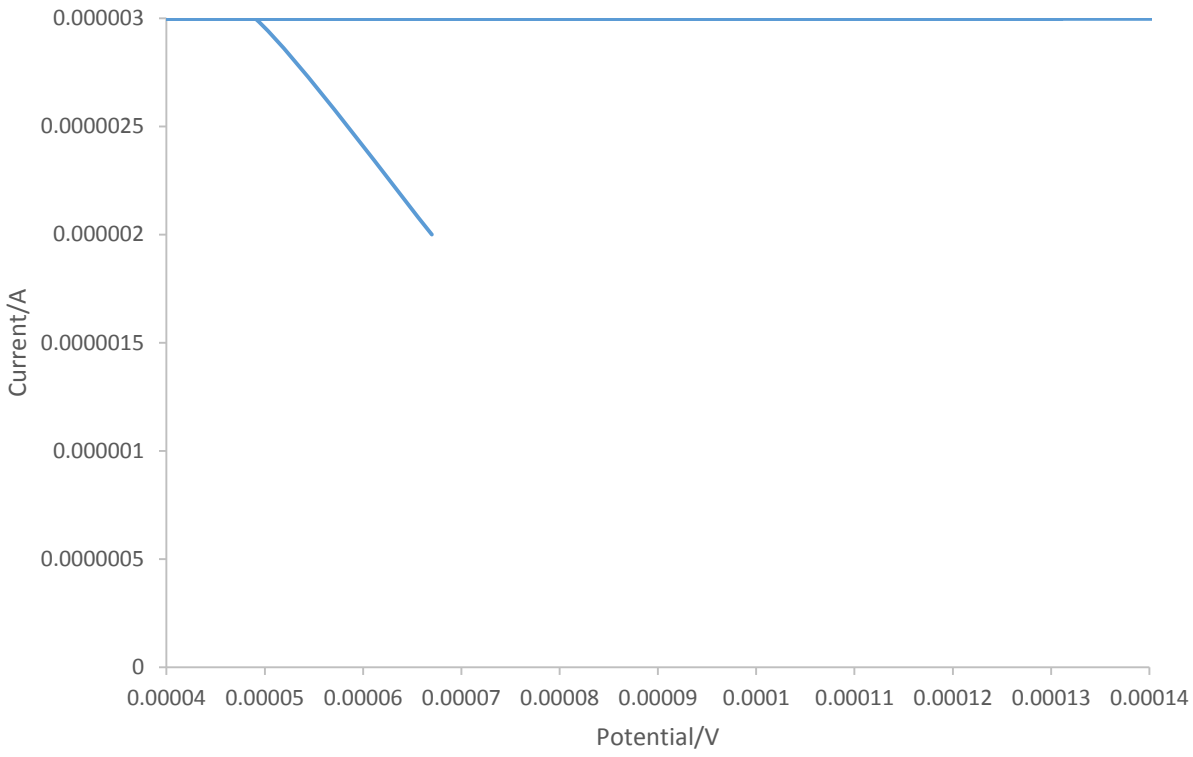

Figure 48. I-V curve of **C_8** dye-sensitized solar cell using I^-_3/I^- electrolyte

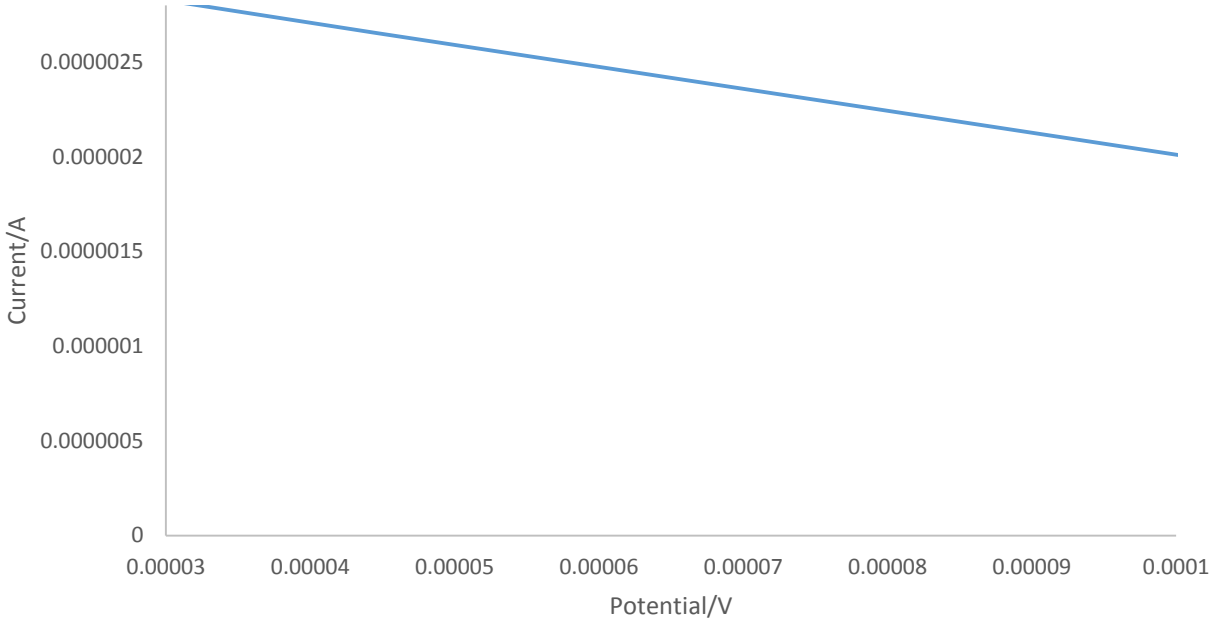

Figure 49. I-V curve of $\mathbf{C_9}$ dye-sensitized solar cell using I^-_3/I^- electrolyte

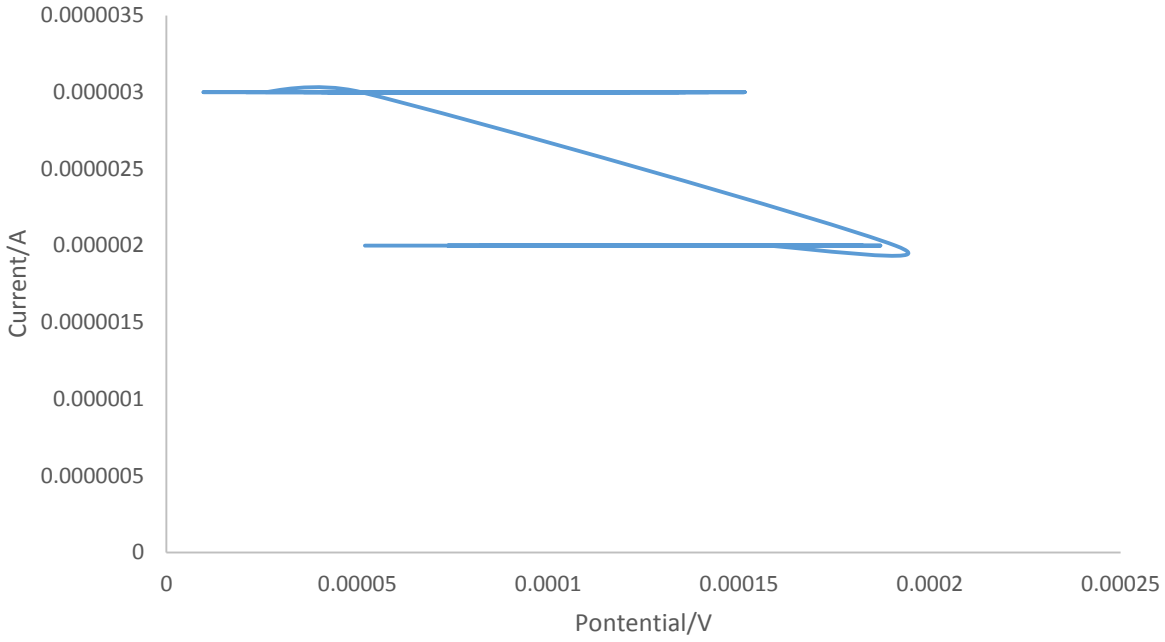

Figure 50. I-V curve of $\mathbf{C_{10}}$ dye-sensitized solar cell using I^-_3/I^- electrolyte

The efficiency of ruthenium(II) and cobalt(II) complexes was very low compared to the standard dye. The V_{oc} and J_{sc} were very low and the solar conversion efficiency is dependent on the two factors [47]. The poor values of these factors tend to decrease efficiency of cells and the decrease in efficiency is probably due to poor adsorption of the dye onto the surface of the TiO_2 semiconductor. The reason for poor adsorption might be the anchoring ligand, the carboxylic groups were not strong enough to attach onto the surface of the semiconductor. Moreover, the other reason might be the carboxylic groups are too close to the metal ion and the electrons could not freely move through the dye to the semiconductor. The structure of the dye strongly affects the efficiency of the DSSC [25, 46].

The electrolyte is also the most important component in dye-sensitized solar cells [20, 25]. During fabrication of solar cells there was a discharge of electrolyte from the cells. It was difficult to fill the TiO_2 semiconductor area properly with the electrolyte, which could also be the reason for low efficiency. The dye sensitizer regeneration depends on the electrolyte and the role of the electrolyte is to sustain redox cycle of dye for continuous performance in light for a longer time [20]. The results obtained show the correlation between photophysical and electrochemical properties of the complexes used for DSSCs. The ruthenium complex, **C_5** obtained the highest energy efficiency compared to other complexes, this is due to properties of pyrazolyl ligands [47].

References

[1] Ashraful, A.; Hironori, A. Molecular design of ruthenium(II) polypyridyl photosensitizer for efficient nanocrystalline TiO_2 solar cells. *Journal of Photochemistry and Photobiology A: Chemistry*, **2003**, *158*, 131-138.

[2] Wang, G. L.; Jiao, H. J.; Liu, K. L.; Wu, X. M.; Dong, Y. M.; Li, Z. J.; Zhang, J. A novel strategy for the construction of photoelectrochemical sensors based on quantum dots and electron acceptor: The case of dopamine detection. *Electrochemistry Communications*, **2014,** *41*, 47-50.

[3] Kuchison, A. M.; Wolf, M. O.; Patrick, B. O. Photophysical and electrochemical properties of Ru(II) complexes containing tridentate bis-(phosphino-oligothiophene) ligands. *Dalton Transactions*, **2011**, *40*, 6912-6921.

[4] Ding, J.; Li, Y.; Hu, H.; Bai, L.; Zhang, S.; Yuan, N. The influence of anatase-rutile mixed phase and ZnO blocking layer on dye-sensitized solar cells based on TiO_2 nanofiber photoanodes*. Nanoscale Research Letters, **2013***, *8*, 1-9.

[5] Cheng M. H.; Hsieh, W. F. High-efficiency metal-free organic-dye-sensitized solar cells with hierarchical ZnO photoelectrode, *Energy and Environmental Sciences*, **2010**, *3*, 442-447.

[6] Kuang, D.; Ito, S.; Wenger, B.; Klein, C.; Moser, J. E.; Humphry-Baker, R.; Zakeeruddin, S. M.; Gratzel, M. High molar extinction coefficient heteroleptic ruthenium complexes for thin film dye-sensitized solar cells. *Journal of the American Chemistry Society***, 2006**, *128*, 4146-4154.

[7] Amlan K. Pal, A. K.; Serroni, S.; Zaccheroni, N.; Campagna, S.; Hanan, G. S. Near infra-red emitting Ru(II) complexes of tridentate ligands: Electrochemical and photophysical consequences of a strong donor ligand with large bite angles. *Journal of Chemical Science*, **2014**, *5*, 4800-4811

[8] DeRosa, M. C.; Crutchley, R. J. Photosensitized singlet oxygen and its applications. *Coordination Chemistry Reviews*, **2002**, *233-234*, 351-371.

[9] Pellegrin, Y.; Pleux, L. E.; Blart, L.; Renaud, A.; Chavillon, B.; Szuwarski, N.; Boujtita, M.; Cario, L.; Jobic, S.; Jacquemin, D.; Odobel, F. Ruthenium polypyridine complexes as sensitizers in NiO based p-type dye-sensitized solar cells: Effects of the anchoring groups. *Journal Photochemistry and Photobiology A: Chemistry*, **2011**, *219*, 235-242.

[10] Wu, Y.; Zhu, W. Organic dye sensitizers from D-π-A to D-A-π-A: Effects of internal electron-withdrawing units on molecular absorption, energy level and photovoltaic performance. *Chemical Society Reviews*, **2013**, *12*, 2039-2058.

[11] Lobello, M. G.; Wu, K. L.; Reddy, A. M.; Marotta, G.; Gratzel, M.; Nazeeruddin. M. K., Chi, Y.; Chandrasekharam, M.; Vitillaro, G.; De Angelis, F. Engineering of Ru(II) dyes for interfacial and light-harvesting optimization. *Dalton Transactions*, **2014**, *43*, 2726-2732.

[12] Adeloye, A. O.; Olomola, T. O.; Adebayo, A. I.; Ajibade, P. A. A high molar extinction coefficient bisterpyridyl homoleptic Ru(II) complex with *trans*-2-methyl-2-butenoic acid functionality: Potential dye for dye-sensitized solar cells**,** *International Journal of Molecular Science*, **2012**, *13*, 3511-3526.

[13] Liu, J.; Li, J. Electrochemical analysis of dye adsorption on aligned carbon nanofiber arrays coated with TiO_2 nanoneedles for dye-sensitized solar cell. *Frontiers of Optoelectronics in China*, **2011**, *4*, 53-58.

[14] Jamson, D. L.; Goldsby, K. A. 6-bis-(N-pyrazolyl)pyridines: the convenient synthesis of a family of planar tridentate N3 ligands that are terpyridine analogs. *Journal of Organic Chemistry*, **1990**, *55*, 4992-4994.

[15] Ajibade, P. A.; Kolawole, G. A. O'Brien, P.; Helliwell, M.; Raftery, J. Cobalt(II) complexes of the antibiotic sulfadiazine, the X-ray single crystal structure of $[Co(C_{10}H_9N_4O_2S)_2(CH_3OH)_2]$. *Inorganica Chimica Acta*, **2006**, 359, 3111-3116.

[16] Ajibade, P. A., Kolawole, G. A. Synthesis, characterization, antiplasmodial and antitrypanosomal activity of some metal(III) complexes of sulfadiazine. *Bulletin of the Chemical Society of Ethiopia*, **2008**, *22*, 261-268.

[17] Ahmadi, R. A.; Hasanvand, F.; Bruno, G.; Rudbari, H. A.; Amani, S. Synthesis, spectroscopy, and magnetic characterization of copper(II) and cobalt(II) complexes with 2-amino-5-bromopyridine as ligand. *ISRN Inorganic Chemistry,* **2013,** 426, 712-720.

[18] Alsindi, W. Z.; Sun, X-Z.; George, M. W. Excited state dynamics of metal-bipyrimidine complexes studied by time-resolved infrared spectroscopy. *Central Laser Facility Annual Report*, **2005/2006**, 169-171.

[19] Deng, H.; Yu, Z.; Dong, J.; Wu, S. 2,6-Bis(3,5-dimethylpyrazol-1-yl)pyridine: A useful pseudo-N3 ligand in efficient ruthenium(II)-catalyzed transfer hydrogenation of ketones , *Organometallics,* **2005,** *24,* 4110-4112.

[20] Adeloye, A. O.; Ajibade, P. A.; Cummings, F. R.; Le Roux, L. J.; Mamphweli, S. N.; Meyer E. L. Synthesis, photophysical and preliminary investigation of the dye-sensitized solar cells properties of functionalized anthracenyl-based bipyridyl and phenanthrolyl Ru(II) complexes. *Journal of Chemical Sciences,* **2013**, 125, 17-27.

[21] Elise, D.; Buriez, O.; Labbe, E.; Verpeaux, J. N.; Amatore, C. Design and electrochemical characterization of a new cobalt(II)–cyclodextrin complex. Evidence for a supramolecular stabilization of the Co(I) state. *Electrochemistry Communications,* **2009**, *11*, 114-117.

[22] Cheng, F.; Tang, N. A new family of dinuclear Ru(II) polypyridyl complexes containing dibenzo-14-crown-4. *Inorganic Chemistry Communications,* **2008,** 11, 939-942.

[23] Tyson, D. S.; Luman, R. C.; Zhou, X.; Castellano. F. N. New Ru(II) chromophores with extended excited-state lifetimes. *Inorganic Chemistry, **2001**, 40, 4063-4071.*

[24] Ji, S.; Wu, W.; Wu, W.; Song, P.; Han, K.; Wang, Z.; Liu, S.; Guo, H.; Zhao, J. Tuning the luminescence lifetimes of ruthenium(II) polypyridine complexes and its application in luminescent oxygen sensing. ***Journal of Material Chemistry***, **2010**, **20**, 1953-1963.

[25] Adeloye, O. A; Ajibade, P. A. Synthesis, characterization and preliminary investigation of electro redox properties of anthracenyl-functionalizes terpyridyl ligands. *Tedrahrdron letters.* **2011,** 52, 274-277.

[26] Adeloye, A. O.; Ajibade, P. A. Synthesis and characterization of a Ru(II) complex with functionalized phenanthroline ligands having single-double linked anthracenyl and 1-methoxy-1-buten-3-yne moieties. *Molecules,* **2010**, *15*, 7570-758.

[27] Machura, B.; Switlicka, A.; Penkala, M. N- and S-bonded thiocyanate copper(II) complexes of 2,6-bis-(benzimidazolyl)pyridine. Synthesis, spectroscopic characterization, X-ray structure and DFT calculations. *Polyhedron*, **2012,** 45, 221–228

[28] Tripathi, P. N.; Verma, S.; Singh, R. P. Photochemical and electrochemical properties of tetranuclear Ru (II) complexes. *Recent Research in Science and Technology**, 2012***,** 21-27.

[29] Moehl, T.; Tsao, N. H.; Wu, K.L.; Hsu, H. C.; Chi, Y. L.; Ronca, E.; De Angelis, F.; Nazeeruddin, M. K.; Gratzel, M. High open-circuit voltages: Evidence for a sensitizer-induced TiO_2 conduction band shift in Ru(II)-dye sensitized solar cells. *Chemistry of Materials*, **2013**, *25*, 4497−4502.

[30] Muller, G.; Riehl, J. P.; Schenk, K. J. S.; K. J.; Hopfgartner, G.; Piguet, C.; Bunzli, J. C. B. Lanthanide triple helical complexes with a chiral bis(benzimidazole)pyridine derivative. *European Journal of Inorganic Chemistry,* **2002**, 5, 3101-3110.

[31] Baitalik, S.; Dutta, S.; Biswas, P.; Florke, U.; Bothe, E.; Nag, K. Structural, Spectroscopic, and proton-coupled electron-transfer behavior of pyrazolyl-3,5-bis(benzimidazole)-bridged HOMO- and heterochiral Ru(II)Ru(II), Os(II)Os(II), and Os(II)Ru(II)2,2-Bipyridine Complexes. *European Journal of Inorganic Chemistry,* **2010**, 570–588

[32] Zhang, X.; Chen, L.; Li, L.; Mao, J.; Wu, W.; Agren, H.; Hua, J. Photovoltaic properties of bis-(octyloxy)benzo-[c][1,2,5]thiadiazole sensitizers based on *N*,*N*-diphenylthiophen-2-amine donor. *Journal of Materials Chemistry,* **2014**, *2*, 4063-4072.

[33] Kim, J. J.; Yoon, J. A new ruthenium containing dipyridylamine ligand for effective nanocrystalline dye-sensitized solar cells. *Inorganic Chimica Acta,* **2013***, 394,* 506-511.

[34] Xun Jin Zhu, X. J.; Holliday, B. J. Electropolymerization of a ruthenium(ii) bis(pyrazolyl)pyridine complex to form a novel ru-containing conducting metallopolymer. *Macromolecular Rapid Communications*, **2010**, 31, 904–909.

[35] Petoud, S.; Buinzli, J. C. G.; Schenk, K. J.; Piguet, C. Luminescent properties of lanthanide nitrato complexes with substituted bis(benzimidazolyl)pyridines. *Inorganic Chemistry,* **1997,** *36,* 1345-1353

[36] Wu, H, L.; Yuan, J. K.; Huang,X. C.; Kou, F.; Liu, B.; Jia, F.; Wang, K. T.; Bai. Y. Two zinc(II) and cadmium(II) complexes based on the V-shaped ligand 2,6-bis(2-benzimidazolyl)pyridine: Synthesis, crystal structure, DNA-binding properties and antioxidant activities. *Inorganica Chimica Acta*, **2012**,390, 12–21.

[37] Yum, J.; Baranoff, E.; Kessler, F.; Moehl, T.; Ahmad, S.; Bessho, T.; Marchioro, A.; Ghadiri, E.; Moser, J. E.; Yi, C.; Nazeeruddin, M. K.; Gratzel, M. A cobalt complex redox shuttle for dye-sensitized solar cells with high open-circuit potentials. *Nature communications,* **2012**, 3, 631-638.

[38] Jamson, D. L.; Goldsby, K. A. 6-bis(N-pyrazolyl)pyridines: The convenient synthesis of a family of planar tridentate N3 ligands that are terpyridine analogs. *Journal of Organic Chemistry*, **1990**, *55*, 4992-4994.

[39] Gong, D.; Jia, X.; Wang, B.; Zhang, X.; Jiang, L. Synthesis, characterization, and butadiene polymerization of iron(III),iron(II) and cobalt(II) chlorides bearing 2,6-bis-(2-benzimidazolyl)pyridyl or 2,6-bis-(pyrazol)pyridine ligand. *Journal of Organometallic Chemistry,* **2012**, *702*, 10-18.

[40] Ole, A. F.; Santos, G. N. C, Quiroga, R. V. Fabrication and characterization of dye sensitized solar cells using nanostructured TiO_2 photoelectrode. *International Journal of Scientific and Engineering Research*, **2012**, *8*, 1-7.

[41] Baheti, A.; Singh, P.; Lee, P. C.; Thomas, K. R. J.; Ho, K. C. 2,7-Diaminofluorene-based organic dyes for dye-sensitized solar cells: Effect of auxiliary donor on optical and electrochemical properties. *Journal of Organic Chemistry*, **2011**, *76*, 4910-4920

11222.

[42] Yu Chen, Y.; Xu, W. H. ; Kou, K. J.; Yu, B. L.; Wei, X. H.; Chao, H.; Ji, H. N. Aggregation-induced emission of ruthenium(II) polypyridyl complex $[Ru(bpy)_2(pzta)]^{2+}$. *Journal of Inorganic Chemistry Communications*, **2010**, *13*, 1140-1143

[43] Andre, S. P.; Melina, K. I.; Yukie, M. I. N. Metal complex sensitizers in dye sensitized solar cells. *Coordination Chemistry Reviews*, **2004**, *48*, 1343-136.

[44] Vougioukalakis, G. C.; Stergiopoulos, T.; Kantonis G.; Kontos, A. T.; Papadopoulos, K.; Arta Stublla. A.; Pierre G.; Potvin. P. G.; Falaras, P. Terpyridine- and 2,6-dipyrazinylpyridine-coordinated ruthenium(II) complexes: Synthesis, characterization and application in TiO_2-based dye-sensitized solar cells. *Journal of Photochemistry and Photobiology A: Chemistry*, **2010**, *214*, 22-32.

[45] Wang, Z. H.; Kawauchi, H.; Kashima, T.; Arakawa, H. Significant influence of TiO_2 photo electroctrode morphology on the energy conversion efficiency of N719 dye-sensitized solar cell. *Journal of Coordination Chemistry*, **2004**, *248*, 1381-1389.

[46] Wu, K. L.; Li, C. H.; Chi, Y.; Clifford, J. N.; Cabau, L.; Palomares, E.; Cheng, Y. M.; Pan, H. A.; Chou, T. P. Dye molecular structure device open-circuit voltage correlation in Ru(II) sensitizers with heteroleptic tridentate chelates for dye-sensitized solar cells. *Journal of the American Chemical Society*, **2012**, *134*, 7488-96.

[47] Kim, D. H.; Lesego, M. D.; Hanson, K.; Alibabaei, L.; Lee, K.; Meyer, T. J.; Parsons, G. N. Stabilizing chromophore binding on TiO_2 for long-term stability of dye-sensitized solar cells using multicomponent atomic layer deposition. *Physical chemistry*, **2014**, *16*, 8615-8622.

Chapter 5

5.0 Conclusions and future work.

5.1 Conclusions

Five ligands consisting of 2,6-bis-(benzimidazolyl)pyridine (**L_1**) and its two derivatives (**L_2** and **L_3**), 2,6-bis-(pyrazoly)pyridine (**L_4** and **L_5**) and their corresponding ten complexes containing five ruthenium(II) and five cobalt(II) complexes were successfully synthesized. All the compounds were characterized by elemental analysis, conductivity measurements, melting point, FTIR and NMR spectroscopy. All the ligands and complexes are soluble in water and DMSO, and are non-electrolyte in solution. Spectroscopic studies were used to confirm successful synthesis of the ligands and the metal complexes. FTIR spectra of the complexes confirmed the coordination of the metal ions through the nitrogen atoms. NMR spectroscopy was used to confirm the structure of the ligands and complexes but characterization of **L_1**-**L_3** and some complexes using NMR was not possible due to poor solubility in almost all the solvents.

The photophysical and electrochemical studies of the ruthenium(II) and cobalt(II) complexes were carried out using UV-Vis, PL and cyclic voltammogram. The electronic spectroscopy confirmed the stereochemistry of the complexes to be octahedral, except for **C_7** as d-d transition was not visible. Photoluminescence of the complexes was observed at different wavelengths and appeared similar in all the compounds, the intensity was found to increase with decreasing molar mass of ruthenium(II) and cobalt(II) complexes. The complexes show good electrochemical properties except for

some ruthenium(II) complex (**C_1**) in which the oxidation potential was not visible in the cyclic voltammograms. The photophysical and electrochemical properties of the complexes show that they can be employed as light-harvesting materials for the fabrication of dyes sensitized solar cells.

Seven complexes containing four ruthenium(II) and three cobalt(II) complexes of 2,6-bis-(benzimidazolyl)pyridine and 2,6-bis-(pyrazolyl)pyridine ligands were used for solar cell fabrication and **N719** dye was used as the standard dye. The dye-sensitized solar cells were characterized with solar stimulator. The solar cell efficiency of ruthenium(II) and cobalt(II) complexes was calculated from the I-V curves of DSSCs. The efficiency of the complexes was observed to increase with increasing molar weight depending on the nature of the ligand. Complex, **C_5** showed the highest efficiency (1.01×10^{-3} %) in all the complexes that were examined.

The performance of these complexes was very low compared to that of **N719** dye which was used as the standard for this study. The low efficiency of the complexes was due to low values of V_{oc} and J_{sc}. The low efficiency of cells can be ascribed to poor electron injection into the TiO_2 semiconductor. This might have been caused by poorly adsorbed anchoring ligands in which may be link to the orientation of the carboxylic anchoring group on the metal complexes.

5.2 Future Work

Further work needs to be done to modify the ligands and the complexes after synthesis because some of the ligands were poorly soluble. This can be done by introducing substituents that will make them more soluble. In electrochemical studies, the use of different support electrolyte such as tetrabutylammonium hexafluorophosphate (TBAH) instead of using phosphate buffer solution (PBS) is required especially in electrochemistry of ruthenium, and use of other solvents instead of water.

Replacement of the anchoring ligands with tridentate (bis-(pyrazolyl)pyridine and bis-(benzimidazolyl)pyridine) containing a carboxylic acid or phosphonic acid and then try to compare the efficiency of the complexes. The tridentate ligands with carboxylic or phosphonic group together with thiocynate ligand could result to higher efficiency. The use of tridentate ligands will enhance the adsorption of dye onto the surface of the TiO_2 semiconductor.

It is necessary to do the current-voltage characterization against time as to observe the efficiency with time, the results of freshly prepared dye-sensitized solar cells sometimes give strange I-V curves. To minimize the discharge of electrolyte from the cell, requires an increase in temperature during the sealing of the cells. This would prevent the possibility of the cell losing the electrons during characterization. The results must be taken into account in the design of cobalt complexes as a sensitizer for DSSCs as to replace ruthenium with most relatively cheaper metal.